E.O. Paton Electric Welding Institute of the National Academy of Sciences of Ukraine

International Scientific-Technical and Production Journal

The Paton WELDING JOURNAL

September 2013
No.9

Published since 2000

English translation of the monthly «Avtomaticheskaya Svarka» (Automatic Welding) journal published in Russian since 1948

Founders
E.O. Paton Electric Welding Institute of the NAS of Ukraine, International Association «Welding»

Publisher
International Association «Welding»

Translators:
A.A. Fomin, O.S. Kurochko, I.N. Kutianova
Editor
N.G. Khomenko
Electron galley
D.I. Sereda, T.Yu. Snegiryova

Address
E.O. Paton Electric Welding Institute, International Association «Welding»
11, Bozhenko Str., 03680, Kyiv, Ukraine
Tel.: (38044) 200 60 16, 200 82 77
Fax: (38044) 200 82 77, 200 81 45
E-mail: journal@paton.kiev.ua
www.patonpublishinghouse.com
URL: www.rucont.ru

State Registration Certificate
KV 4790 of 09.01.2001
ISSN 0957-798X

Subscriptions
$348, 12 issues per year, air postage and packaging included.
Back issues available.

CONTENTS

«The Paton Welding Journal» abstracted and indexed in Ukrainian refereed journal «Source», RJ VINITI «Welding» (Russia), INSPEC, «Welding Abstracts», ProQuest (UK), EBSCO Research Database, CSA Materials Research Database with METADEX (USA), Questel Orbit Inc. Weldasearch Select (France); presented in Russian Science Citation Index & «Google Scholar»; abstracted in «Welding Institute Bulletin» (Poland) & «Rivista Italiana della Saldatura» (Italy); covered in the review of the Japanese journals «Journal of Light Metal Welding», «Journal of the Japan Welding Society», «Quarterly Journal of the Japan Welding Society», «Journal of Japan Institute of Metals», «Welding Technology».

DEFECTS OF JOINTS OF HIGH-STRENGTH RAILS PRODUCED USING FLASH-BUTT WELDING

S.I. KUCHUK-YATSENKO, V.I. SHVETS, A.V. DIDKOVSKY, E.V. ANTIPIN and **L.M. KAPITANCHUK**
E.O. Paton Electric Welding Institute, NASU
11 Bozhenko Str., 03680, Kiev, Ukraine. E-mail: office@paton.kiev.ua

The investigations of defects of structure of rail joints, made by flash-butt welding, were carried out. The defects were detected at the fracture surface of joints during static bending tests and also after fracture under the operation conditions. The analysis of microstructure and chemical heterogeneity of the fracture surface was performed using Auger-microprobe JAMP 9500F of the JEOL company (Japan). The defects formed as a result of deviation from the standard welding conditions include lacks of penetration and inclusions of iron-manganese silicates which considerably decrease the values at mechanical tests of welded joints. Their presence in the welded joints is not admissible. Clusters of inclusions of aluminium silicates, the so-called dead spots, and oxide films of the more complicated composition are formed in the joint on the basis of non-uniformly distributed non-metallic inclusions of rail metal. The dead spots of small area do not influence the values at mechanical tests of welded joints. Their total area on the fracture should not exceed 15 mm^2. On the basis of carried out investigations the criteria of quality evaluation of the high-strength steel joints, made by flash-butt welding using modern control systems, were determined. 9 Ref., 2 Tables, 11 Figures.

Keywords: *flash-butt welding, rail steels, static bending, fracture surface, defects of welded joints, lack of penetration, iron-manganese silicates, aluminium silicates*

In the last five years the large-scale laying of high-strength rails in the main Ukrainian and Russian rail roads is performed. The rails are mainly joined by flash-butt welding (FBW) using equipment and technology developed by the E.O. Paton Electric Welding Institute [1]. The quality control of welded rails is performed directly after welding using in-process and non-destructive ultrasonic testing. Moreover, in accordance with the standard requirements, at the beginning of each working shift the static bending tests of the reference specimens are carried out.

At the E.O. Paton Electric Welding Institute the large volume of data on all the kinds of tests of joints of high-strength rails in combination with investigation of fractures and data of mechanical tests was accumulated. It was found that at the same area of defects revealed in the joints of high-strength rails of converter melting, the values of mechanical tests are decreased to a greater extent than those in the rails of open-hearth production.

The aim of this paper is the study of defects in joints of high-strength rails of converter melting, made using FSW.

The specimens for investigations were selected at the rail welding enterprises on the basis of results of in-process and non-destructive ultrasonic testing. The defects of structure were detected on the surface of fractures after bending tests of welded butts. The tests were carried out according to the procedure accepted at the rail roads of Ukraine and Russia [2].

The metallographic investigations of microstructure of rail joints were carried out in the

Table 1. Chemical composition of rail steels of different production, wt.% (GOST R 51685–2000)

Steel grade	C	Mn	Si	P	S	V	Ti	Cr	Al	Cu
M76	0.71–0.82	0.75–1.05	0.25–0.45	<0.035	<0.040	–	–	–	0.02	–
E76F K76F				<0.025	<0.030	0.03–0.15	–	–	0.02	≤ 0.15
E76T K76T				<0.030	<0.035	–	0.007–0.025	–	0.02	
KF	0.78–0.81	0.89–0.91	0.30–0.39	0.013–0.02	0.003–0.01	0.057–0.061	–	0.03–0.04	–	0.02–0.04

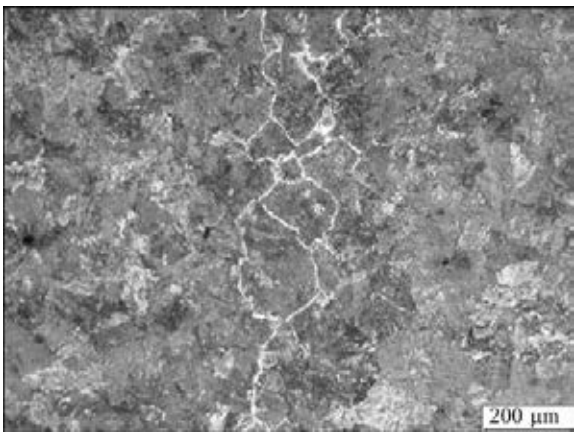

Figure 1. Microstructure of weld center of rail welded joint

light microscope «Neophot 32» and fractographic examinations with X-ray spectral microanalysis of the fracture surface were performed using Auger-microprobe JAMP 9500F of the JEOL company (Japan). The chemical composition of rail steels is given in Table 1.

The typical microstructure of rail weld metal produced at the optimal conditions, represents a sorbitic perlite (Figure 1). Along the joint line the band of about 200 μm width with precipitations of hypoeutectoid ferrite along the boundaries of the primary austenite grains is observed, the size of which is equal to the point 2–3 according to ASTM. Depending on the gradient of the temperature field in welding the amount of hypoeutectoid ferrite can change. At the optimal rigid conditions, characterized by the high gradient of temperature field, the thickness of ferrite fringe is minimum, and it can be interrupted. Such joints are characterized by the highest plastic properties.

The fracture of rail joints welded at the optimal conditions has a crystalline structure. The surface of fracture consists mainly of cleavage facets with a stream-like pattern and tongues, tear crests are also present (Figure 2).

At the fracture surface the refractory inclusions of titanium carbonitrides, calcium alumi-

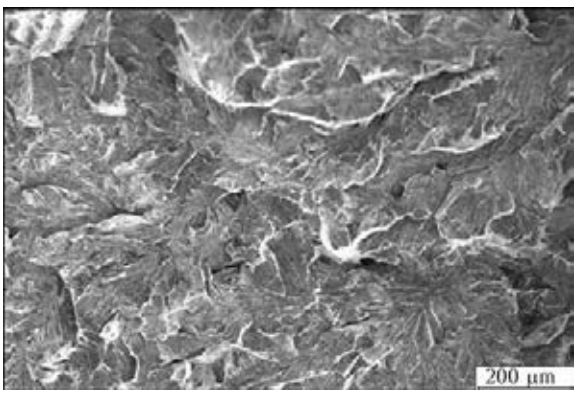

Figure 2. Fracture surface of rail welded joint

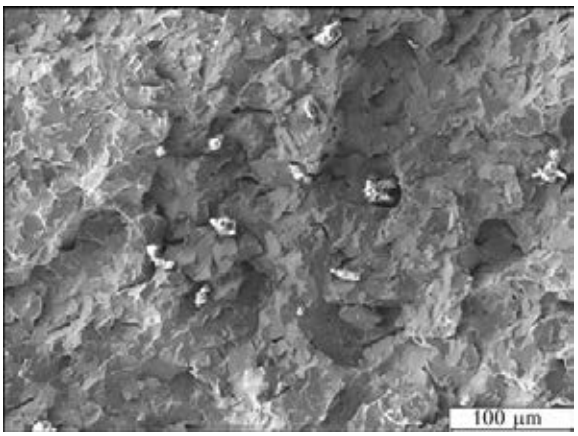

Figure 3. Refractory of non-metallic inclusions on fracture surface of rail welded joint

nates, manganese oxysulfides can be found (Figure 3). The size of these non-metallic inclusions is not more than dozens of micrometers. The presence of such inclusions gives a reliex shape to fracture. Their presence is not critical for strength characteristics of a joint.

The defects which sufficiently influence the strength properties of the joints arise as violation of homogeneity of crystalline structure of a fracture.

One of such defects is lack of penetration. In FBW the lack of penetration is formed under the conditions when the metal of rail edge is in solid or solid-liquid state before upsetting. At the fracture it has an appearance of a plane bright area (Figure 4). It was established that microstructure of surface of the analyzed lack of penetration represents plane areas of rail metal matrix (Figure 5, spectrum No.1), divided by a structural

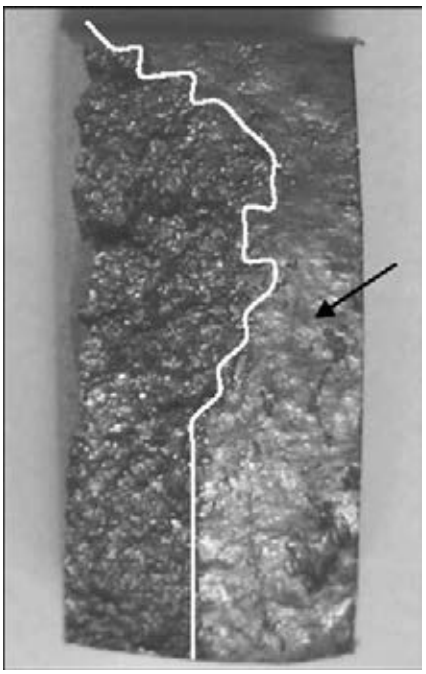

Figure 4. Lack of penetration on fracture surface of rail welded joint

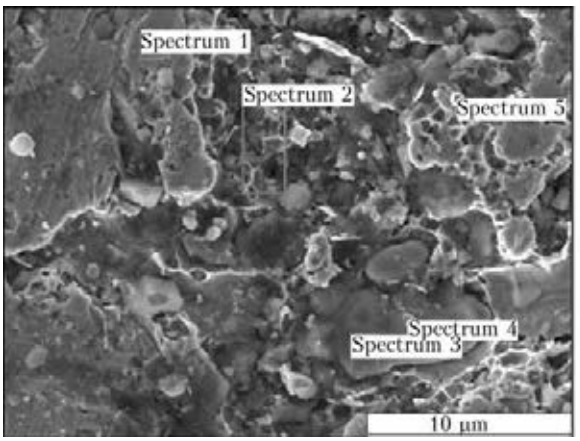

Number of spectrum	Element content, at.%							Note
	C*	O	Na	Si	Ca	Mn	Fe**	
1	5.90	3.23	0.18	0.00	0.00	0.00	90.68	Matrix
2	28.77	22.60	1.61	3.20	1.24	0.74	41.83	Inclusions
3	3.00	53.06	0.08	0.16	0.08	4.19	39.44	Same
4	5.96	68.24	0.09	18.32	0.00	0.51	6.89	»
5	7.01	53.36	0.37	0.61	0.08	0.35	38.22	»

* — distribution of carbon in steel in during welding requires separate study which is beyond the scope of this article. ** — value of iron concentration depends on correlation of sizes of analyzed object and diameter of electron probe.

Figure 5. Microstrucutre of fracture surface and chemical heterogeneity on the area of lack of penetration in rail welded joint

component, composed of oxides and silicates (Figure 5, spectra Nos. 2–5). Obviously, this structure component is formed of non-metallic inclusions of base metal and oxidation products of rail metal fused along the boundaries.

The presence of defects of this type even of small area (1–2 mm^2) detected using modern means of ultrasonic testing, is not admissible in welded joints as far as they reduce the values at static and impact tests and provoke fatigue fractures of welded butts.

Another type of defects represents spots with a non-developed relief in the range of which the bright and dead spots are combined (Figure 6). The analysis of microstructure of fracture surface showed that bright spots represent a layer of iron-manganese silicates (Figure 7, *a*). Dead spots, adjacent to a monolithic layer, are the area of clustering the particles of iron-manganese silicates (Figure 7, *b*). The fracture occurs as a result of delamination along the film at the area of monolithic layer and along the pit mechanism in the places of inclusions clustering.

The iron-manganese silicates are formed in the process of welding at the oxidation of fused metal. It is supposed [3] that formation of oxide structures in the plane of a joint is determined by the presence of oxygen in the spark gap during the period of fusion, preceding the upsetting. It is shown in work [4] that the main factor influencing the formation of defects in the plane of a joint is the state of melt at the fused ends of parts during the period, preceding the upsetting. If the melt is preserved, then it is squeezed out during deformation from the butt together with oxides, forming at its surface, independently of oxygen content in the spark gap. The duration of existence of melt layer on edges depends on its thickness, gradient of temperature field in the near-contact area of edges and speed of parts fusion [5].

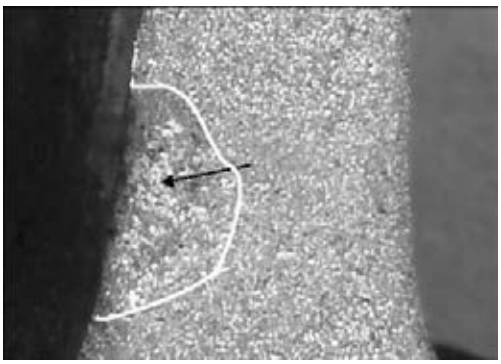

Figure 6. Iron-manganese silicates on the fracture surface of rail welded joint

The described defects are observed in the joints of rails welded with deviations from the preset values of welding parameters. They are reliably detected using modern methods of ultrasonic testing even at a small area (1–2 mm^2). Their presence in welded joints is not admissible as far as they decrease the values of mechanical properties at static and impact tests and provoke fatigue fractures of welded butts.

The particular place relates to the defects which are defined in the standard documents as «dead» (DS) or «grey» spots. At the surface of fracture they are observed as the areas of dark color with a non-developed relief (Figure 8). These are the defects which are most often observed during tests of welded joints of different metals produced using FBW.

The comparative analysis of chemical composition from the defect area showed that DS are enriched with aluminium, manganese, silicon as compared to the surrounding surface of crystalline structure (Figure 9, *a*). During the more detailed investigations it was established that DS represents the clusters of particles of manganese aluminium silicates, arranged in the metallic matrix (Figure 9, *b*). The particles have a fused

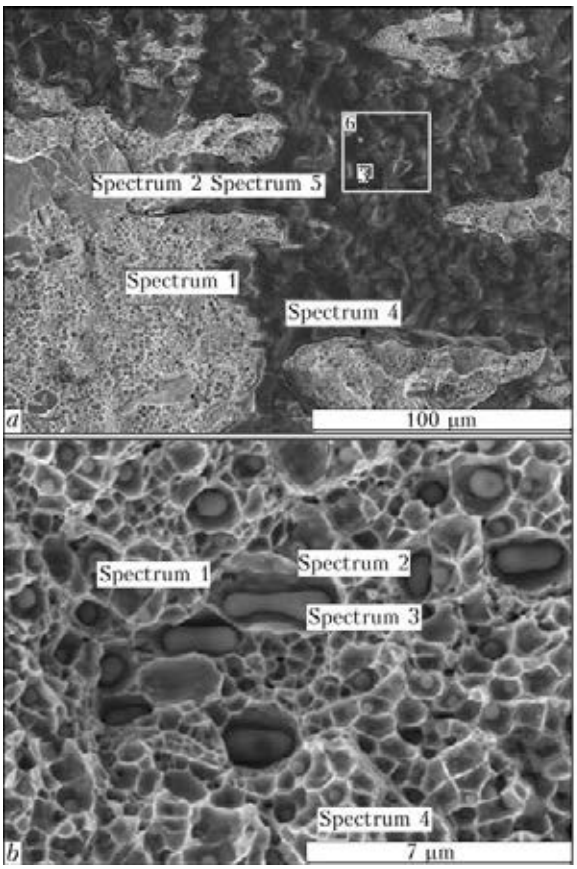

Number of spectrum	Element content, at.%					Note
	C	O	Si	Mn	Fe	
1	8.96	5.59	0.95	0.76	83.74	Clustering of silicate particles
2	5.42	3.16	0.00	0.10	91.31	Cleavage facet
3	2.24	56.41	12.63	8.87	19.85	Monolithic layer of silicates
4	0.74	58.67	12.69	7.46	20.44	Same
5	2.43	52.69	4.70	7.40	32.78	»
6	2.40	55.97	9.64	8.59	23.40	»

Number of spectrum	Element content, at.%					Note
	C	O	Si	Mn	Fe	
1	5.99	54.25	14.49	15.53	9.74	Silicate particles
2	7.22	48.70	15.58	10.01	18.49	Same
3	3.20	59.61	14.73	18.37	4.09	»
4	10.03	4.53	0.52	0.00	84.92	Matrix (without inclusions)

Figure 7. Microstructure and results of analysis of chemical composition heterogeneity on the area of fracture with iron-manganese silicates in the form of film (*a*) and inclusions (*b*)

shape and are characterized by a weak adhesion to iron.

It should be noted that at the fracture both the particles of aluminium silicates and also the spots of location of these particles, removed during fracture, are observed. The haze defect of fracture is predetermined by a pit relief of the surface after fracture along the inclusions.

The characteristic feature of inclusions of aluminium silicates is a negligible amount of iron in their composition (0.86–0.99 at.%). It evidences of the fact that their formation is not connected with the flashing of edges. They are formed in the layer adjacent to the fused metal on the base of inclusions of base metal (see Table 2). The saturation with manganese occurs during its transition from the matrix into the forming fusible silicate, which is possible due to the high diffusion mobility and surface activity of manganese in iron. The location of aluminium silicates in the layer adjacent to the fused metal impedes their squeezing out into the flash during upsetting.

It is known that fusible aluminium silicates are formed during underoxidation of silicon in presence of aluminium [6]. As the source of silicon the silicocalcium can be, used as deoxidizer during manufacture of rails, that is indirectly confirmed by presence of calcium in the composition of aluminium silicates. The aluminium gets to the steel from ferroalloys and, possibly, the ladle slag [7].

In the course of investigation of a large number of defects of the DS type in the rail joints of different manufacture it was established that they are considerably differed from the defects,

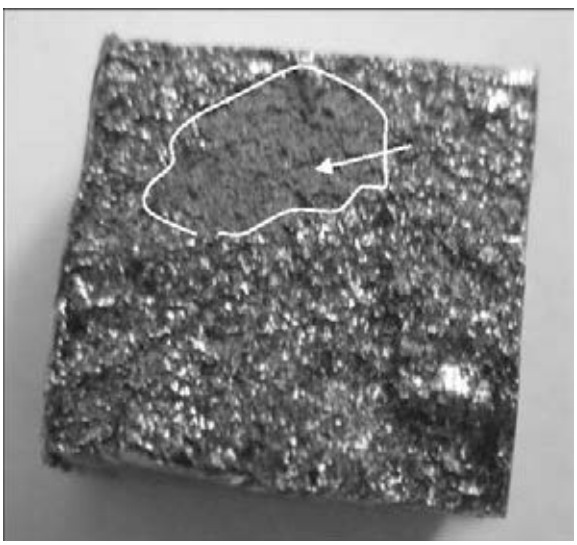

Figure 8. Dead spots in the fracture surface of rail welded joint

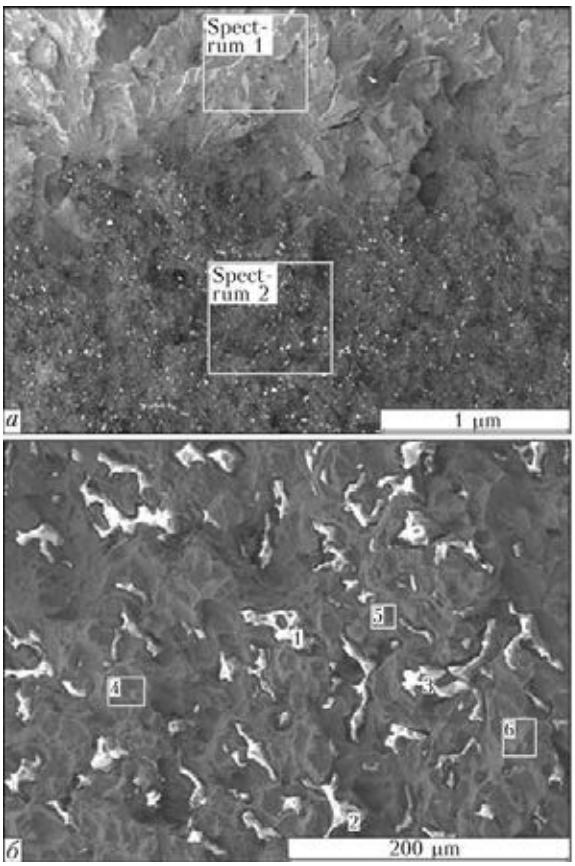

Number of spectrum	Element content, at.%						Note
	C	O	Al	Si	Mn	Fe	
1	8.34	2.74	0	0.25	0.13	88.55	Cleavage facet
2	7.01	16.52	0.45	4.08	5.86	66.08	Spot

Number of spectrum	Element content, at.%						Note
	C	O	Al	Si	Mn	Fe	
1	3.27	66.66	1.11	16.48	11.61	0.86	Inclusions
2	3.36	61.08	3.15	16.70	14.73	0.99	Same
3	2.41	68.91	1.32	16.39	6.90	0.90	»
4	4.43	1.57	0.11	0.00	0.80	93.09	Matrix
5	5.51	0.86	0	0.18	0.81	90.76	Same
6	4.70	1.50	0	0.15	1.11	92.54	»

Figure 9. Microstructure and results of analysis of chemical composition of fracture surface of rail joints on the area of a dead spot from area (*a*) and locally (*b*)

examined above, not only by the composition of their structure components but also by their thickness not exceeding 20 μm. Small thickness impedes their detection during ultrasonic testing, from the one hand, and on the other hand the presence of such defects in welds of rails does not have a considerable influence on the values at full-scale tests on static and impact bending. The limited number of DS in the joints of rails is admissible. Their total area is restricted to 15 mm^2 [2] by existing standards which is sufficiently grounded by experimental data.

In the last time, on the fractures of rails, fractured not only along the joint but also along the base metal, defective areas was found in the head area of the shape close to oval of dark color and non-developed relief (Figure 10).

It was established that fracture on the area of oval spot occurs according to the pit mechanism (Figure 11). Within the limits of area the groups of inclusions of 20 mm size were found representing the complex oxides composed of aluminium, silicon, magnesium, calcium (Figure 11, *a*). The inclusions, which are similar by their chemical composition, but finer in size, are pre-

Table 2. Results of X-ray spectral microanalysis of chemical composition of non-metallic inclusions in the rail steel, at.%

Steel grade	Fe	Mn	Si	S	V	Ti
M76	39.8–80.9	0.86–10.3	0.51–1.3	0.3–5.3	N/D	N/D
K76F	33.5–58.5	0.01–0.5	0.9–6.1	2.4–30.1	0.006	0.1–1.2
E76F	68.9–95.8	0.7–1.6	0.56–5.9	0.08–0.5	0.06–0.12	–

Table 2 (cont.)

Steel grade	P	Al	Ca	Cu	O	Mg
M76	0.02	N/D	0.03–5.3	0.01–0.11	6.3–55.2	N/D
K76F	0.02	0.001–5.3	0.1–5.3	0.01–0.15	11.9–30.5	0.2–0.5
E76F	0.01	0.29–0.31	0.55–5.2	0.15–0.18	1.86–21.8	0.4–0.7

sent in the pits (Figure 11, *b*). In the pits the inclusion of iron oxides can also be found, the size of which amounts to tenth fractions of micrometer (Figure 11, *c*).

The formation of oval spot is obviously occurs on the basis of DS as a result of interaction of aluminium silicates with ferrous oxide, for example, in the case of underoxidation of steel. Here more fusible oxide systems are formed, which are characterized by a high fluidity [8]. Under the thermodeformational conditions of rolling and welding these fusible oxides are penetrated along the structure boundaries and form the oval spots.

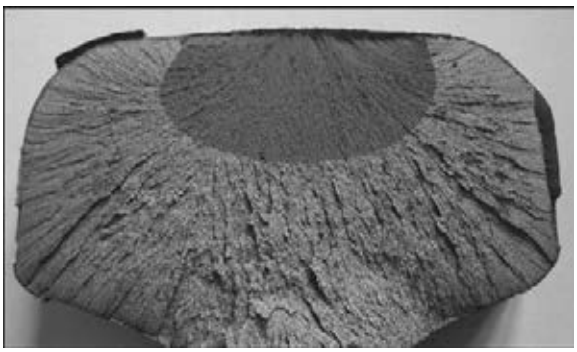

Figure 10. Oval spots on fracture of rails

The absence of metallic joint on the larger area results in considerable reduction in strength.

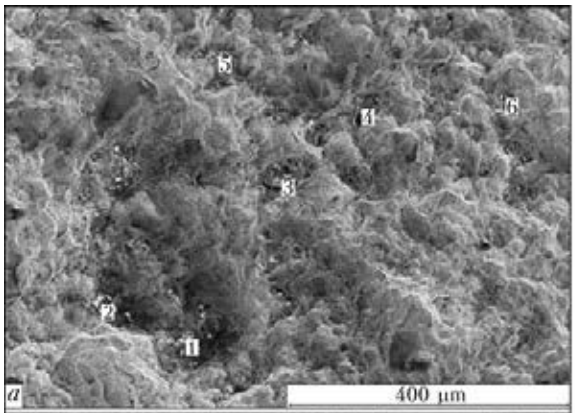

Number of spectrum	Element content, at.%							
	C	O	Mg	Al	Si	S	Ca	Fe
1	34.38	7.29	–	0.68	3.60	–	4.58	45.64
2	46.57	29.02	–	1.47	4.41	1.53	–	2.40
3	24.00	23.21	–	1.49	3.27	–	0.74	47.29
4	49.32	33.95	0.23	1.87	6.48	0.30	0.79	6.03
5	55,94	27.26	0.45	2.35	6.54	–	1.18	5.57
6	26.55	53.09	0.36	1.25	2.61	2.41	10.22	1.86

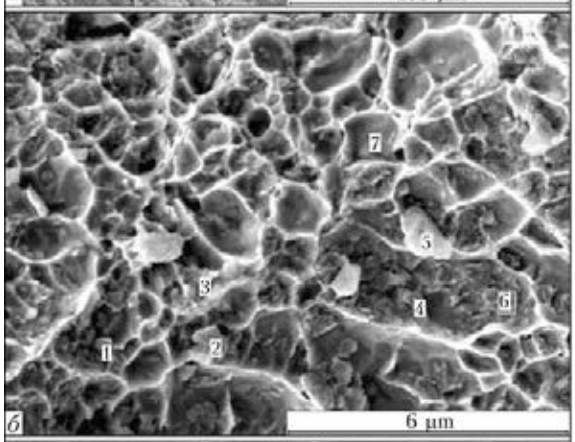

Number of spectrum	Element content, at.%							
	C	O	Al	Si	S	Ca	Cr	Fe
1	16.48	3.78	0	1.02	–	–	0.08	78.62
2	28.58	19.54	0	1.03	1.46	2.14	–	46.66
3	16.05	9.34	0.67	1.48	–	–	–	72.46
4	18.36	24.75	3.20	5.00	–	–	–	48.69
5	18.83	52.32	5.01	15.22	–	–	–	4.75
6	17.46	4.58	0.31	0.57	–	–	–	77.07
7	3.52	0.17	0	0.40	–	–	–	95.92

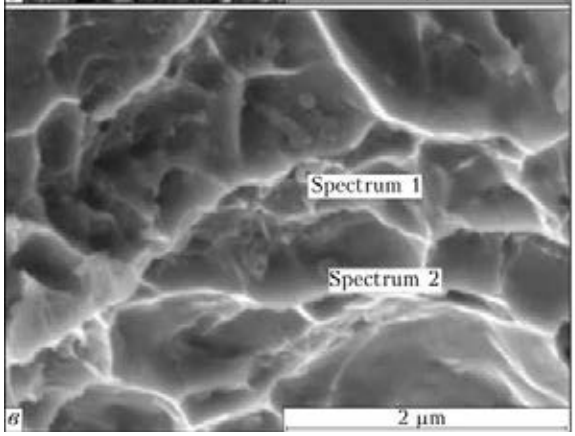

Number of spectrum	Element content, at.%			
	C	O	Si	Fe
1	13.61	22.79	0.81	62.79
2	16.87	10.99	0.52	71.63

Figure 11. Microstructure and results of analysis of chemical composition of non-metallic inclusions on the area of oval spot of fracture of rail welded joint: *a* — clusters of particles of aluminium, silicon, calcium, magnesium oxides; *b* — particles of oxides located in the pits; *c* — iron oxides

In welding of high-strength rails of modern production, as the results of large amount of test batches of welded rails show, the probability of DS formation increases as compared to the similar data obtained in welding of rails of open-hearth production. It is obviously connected with getting of aluminium into the steel as associated element, for example, during adding of vanadium, titanium, niobium or other technological operations. To eliminate the defects like these it is necessary to carry out works on improvement of processes of steel melting and pouring.

The increased tendency to DS formation in high-strength rails of current production presents difficulties during determination of optimal welding technologies. To obtain the values of plastic properties of joints required by the standards it is necessary to find the possibilities of producing additional reserve of metal ductility in HAZ to compensate the negative influence on this value of DS in case of their formation. The developers of technologies for welding of high-strength rails try to solve this problem by precision control of welding energy input and application of self-adjustable systems of flashing process control [9].

Basing on the carried out investigations the criteria for evaluation of joints of high-strength rails were determined which were laid into the basis of development of in-process and non-destructive testing of quality of welded rails produced by FBW using the modern systems for control of welding process and non-destructive testing.

Conclusions

As a result of carried out work on investigation of defects of welded joints of rails produced using FSW, it was established that most defects are located in the joint plane. According to their structure and influence on mechanical properties the defects can be divided into three groups.

The first group is represented by lacks of penetration. The second group of defects represents iron-manganese silicates not squeezed out during upsetting. The third group is the clusters of inclusions of manganese aluminium silicates, so-called dead spots.

The defects of the first and the second groups decrease considerably the values during mechanical tests. The defects of the third group at the total area of up to 15 mm^2 have no considerable influence on the values of mechanical properties of rails. The defects of the first, second and the third group of more than 15 mm^2 area are easily detected using modern of non-destructive ultrasonic testing.

1. Kuchuk-Yatsenko, S.I., Didkovsky, A.V., Shvets, V.I. (2008) Technology and equipment for flash-butt welding of high-strength rails. *The Paton Welding J.*, **11**, 111–120.
2. *TU U 27.1-31632138-1330–2010*: New welded rails for railways. Kharkiv regional scientific-production center of standardization, metrology and certification.
3. Gulyaev, A.I. (1985) *Technology and equipment for fluash-butt welding*. Moscow: Mashinostroenie.
4. Kuchuk-Yatsenko, S.I. (1992) *Flash-butt welding*. Ed. by V.K. Lebedev. Kiev: Naukova Dumka.
5. (2000) *Classification and catalogue of defects and damages of elements of pointworks and rails of Ukrainian railways*. Dnipropetrovsk: ArtPress.
6. Vinograd, M.I., Gromova, G.P. (1971) *Inclusions in alloy steels and doped alloys*. Moscow: Mashinostroenie.
7. Godik, L.A., Kozyrev, N.A., Polyakov, V.A. (2009) Optimization of oxygen content in rail steel. *Stal*, **3**, 29–32.
8. (1985) *Atlas of slags*: Refer. Book. Ed. by I.S. Kulikov. Moscow: Metallurgiya.
9. Kuchuk-Yatsenko, S.I., Didkovsky, O.V., Bogorsky, M.V. et al. *Method of flash-butt welding*. Pat. 46820 Ukraine. Int. Cl. B23K11/04, C2. Publ. 17.06.2002.

Received 26.06.2013

INFLUENCE OF CHEMICAL COMPOSITION OF MICROALLOYED STEEL AND COOLING RATE OF HAZ METAL OF PIPE WELDED JOINTS ON ITS STRUCTURE AND IMPACT TOUGHNESS

A.A. RYBAKOV, T.N. FILIPCHUK, V.A. KOSTIN and **V.V. ZHUKOV**
E.O. Paton Electric Welding Institute, NASU
11 Bozhenko Str., 03680, Kiev, Ukraine. E-mail: office@paton.kiev.ua

One of the most difficult tasks in manufacture of the gas-and-oil line pipes, from the point of view of technology of their welding, is fulfillment of the requirements of normative indices on impact toughness of HAZ metal of welded joint. The aim of present work is an investigation of effect of chemical composition of microalloyed steel and cooling rate of HAZ metal of pipe welded joints on its structure-and-phase state and toughness characteristics. Specimens of Kh70 grade steel of different chemical composition varying, mainly, in carbon content and different rate cooling conditions simulating HAZ metal of the pipe welded joints were studied using modern Gleeble-3800 complex. It is determined that a structure of bainite type, i.e. lamellar ferrite with strengthening second phase martensite-austenite-carbide — MAC or carbide phase), is mainly formed in the metal of studied chemical composition in sufficiently wide interval of the cooling rates. Density of distribution of the phase, its location (orientation), dimensions and morphology are determined, in preference, by chemical composition, and, to lesser degree, by metal cooling rate of the $V_{cool.8/5}$. In this connection, the possibilities of metallurgical factor influence should be use to greater extent in order to increase HAZ metal toughness. Strict limitation of weight fractions of the elements promoting formation of coarse ferrite packages with ordered carbide phase of lamellar morphology (for example carbon, niobium, molybdenum etc.) is also reasonable for formation of optimum structure and, respectively, improvement of HAZ metal toughness together with reduction of content of the detrimental impurities in steel (sulfur, phosphor and nitrogen) to minimum possible level. The results of investigations were used in production of pipes from low-alloyed steel of Kh70 grade for main gas-and-oil pipelines. 10 Ref., 3 Tables, 6 Figures.

Keywords: *microalloyed steel, welded joint, heat-affected zone, cooling rate, microstructure, impact toughness*

In recent time, a complex of requirements to pipes, including impact toughness of metal of the welded joints [1, 2], is continuously restricted due to necessity of providing of safe operation of the main pipeline systems used for transportation of liquid and gaseous carbohydrates. It is well known fact that large diameter welded pipes from high-strength microalloyed steels [3] are mainly used for such pipelines. Analysis of current normative documents, literature data and own investigations indicates that one of the most complex problems in the manufacture of gas-and-oil line pipes, from point of view of technology of their welding, is fulfillment of the normative indices on impact toughness of metal of welded joint heat-affected zone (HAZ).

Many researchers [4, 5] note a significant spread of impact toughness values in testing of HAZ metal of the welded joints from modern pipe steels that is caused by series of factors, i.e. structural heterogeneity of welded joints, notch location, metal structure state, in particular, adjacent to the notch, configuration of fusion line, portion and properties of the weld metal and different HAZ areas in fracturing section, reaction of steel on thermal-deformation welding cycle, etc.

Structural state of HAZ metal is one of the determining factors, affecting its impact toughness. Different structure areas of the welded joint, including coarse grain area of reduced toughness (local embrittlement zone — LEZ) adjacent to the fusion line, are incorporated in test section at any scheme of applying of the notch for evaluation HAZ metal toughness regulated by normative documents. Ductile characteristics of metal of HAZ near-weld area significantly [6–8] are reduced by considerable growth of austenite grain in LEZ, observed in welding, formation of large packages of lamellar ferrite, upper bainite and presence of martensite-austenite-carbide (MAC) phase. Dimensions, microstructure and properties of a welded joint area

with reduced toughness are determined by chemical composition of base metal and welding conditions (including metal cooling rate in temperature range of possible transformations, i.e. 800–500 °C). This area, in particular, has a decisive effect on integral index of impact toughness at HAZ metal testing.

LEZ area in the real welded joints has complex configuration and relatively small dimensions due to which the evaluation of impact toughness, particularly of this area, and its role in the integral toughness index is complicated. At the same time, the information about structure and metal properties in LEZ is very important for solving the task of providing of required welded joint ductile characteristics. From this point of view, the investigations applying the methods of physical modelling of metal structure transformations in welding, in particular, on modern complex Gleeble-3800 [9], which was used in the present work, are the most correct.

Aim of the work lied in the investigation of effect of chemical composition of microalloyed pipe steel and metal cooling rate on structure-phase characteristics of the metal in area of coarse grains in welded joint HAZ. The specimens, cut from steel of 25–33 mm thickness across the rolling direction (cylinder of 10 mm diameter or rectangular of 10 × 10 mm section), were heated around 40 °C/s rate. The maximum heating temperature of the specimens in simulation of the welding cycles made 1300 °C, time of holding at this temperature 1s. In these investigations the cooling rate of metal of tested specimens in 800–500 °C ($V_{cool.8/5}$) range was selected from the modes of submerged multiarc welding used in reality for manufacture of large diameter longitudinal welded pipes. Calculation of $V_{cool.8/5}$ for typical modes of five-arc welding of outside welds of the pipes with 22–36 mm wall thickness under condition of initial temperature of welded edges in the range from 20 up to 100 °C (increased initial temperature of the edges under conditions of continuous pipe production is possible due to insufficient time interval between the end of welding of inside weld and beginning of performance of outside weld) was carried out for determination of the limits of this parameter change. Well-known formula [10] was used in the calculation using which a time of metal staying in the indicated range $t_{8/5}$ was determined:

$$t_{8/5} = \frac{\eta^2}{4\pi\lambda\rho c}\left(\frac{UI}{V}\right)^2 \frac{1}{d^2}\left[\left(\frac{1}{500 - T_0}\right)^2 - \left(\frac{1}{800 - T_0}\right)^2\right],$$

where η is a welding heat efficiency, taken equal 1 for submerged arc welding; λ is a coefficient of thermal conductivity of steel, equal $3.8 \cdot 10^{-4}$ kJ/cm·s·deg; ρ is a steel density, g/cm^3; c is a specific thermal capacity of steel, J/g·deg; $\rho c = 0.005$ kJ/cm^3·deg; d is a sheet thickness, cm; T_0 is an initial metal temperature before welding; UI/V is a heat input of five-arc welding process.

Respectively, cooling rate $V_{cool.8/5}$ of the metal was determined as a value inverse to time of its staying in 800–500 °C temperature range.

According to the calculations the rate of metal cooling $V_{cool.8/5}$ makes 7.2–4.5 °C/s in submerged multiarc welding of pipes with 22–36 mm wall thickness at different initial temperature of welded edges (from 20 to 100 °C). Based on this data the time of metal staying in the indicated temperature range during welding thermal cycle simulation were set equal 45, 50 and 55 s that corresponds to cooling rate 6.7, 6.0 and 5.4 °C/s. Separate specimens of steel were cooled with lower (3 °C/s) or larger (12 and 30 °C/s) rate, at the $t_{8/5}$ made 100, 25 and 10 s, respectively.

Reaction of different origin K60 (Kh70) grade steel on thermal cycle of multiarc welding was investigated. This steel grade is used in production of the pipes for main gas-and-oil pipelines and conventionally marked by letter indices from A to D. Studied metal (Table 1) on chemical composition represents itself silicon-manganese steel with ultra-low content of detrimental impurities (in particular, weight fraction of sulfur made 0.001–0.002 %, phosphor was 0.008–0.012 % and content of nitrogen did not exceed 0.006 %), microalloyed by niobium (0.038–0.054 %) and vanadium (0.032–0.040 %, except

Table 1. Chemical composition of studied steels, wt.%

Symbolic key of the specimen	C	Mn	Si	P	S	Ni	Ti	Mo	Nb	V
A	0.032	1.79	0.27	0.011	0.001	0.21	0.019	< 0.03	0.050	0.032
B	0.045	1.79	0.23	0.012	0.002	0.21	0.013	< 0.03	0.054	0.038
C	0.080	1.62	0.11	0.014	0.002	0.23	0.012	< 0.03	0.038	< 0.02
D	0.076	1.53	0.26	0.008	0.002	0.20	0.013	0.11	0.043	0.040

for C grade steel specimens, in which weight fraction of vanadium is lower than 0.02 %). Quantity of manganese in the studied metal was in relatively narrow limits (from 1.53 to 1.79 %). The most significant differences in chemical composition of the examined metal lied in carbon content which changed in the ranges from 0.032 to 0.080 %. Examined specimens of steel can be divided into two groups on content of this element, i.e. with low content of carbon (0.032–0.045 % C, symbolic keys A and B) and with increased content of carbon (0.076–0.080 %, keys C and D). It should be noted that steel D, containing 0.076 % of carbon, was additionally microalloyed, except for niobium and vanadium, by small quantity of molybdenum, weight fraction of which made 0.11 %. The weight fraction of niobium (0.050–0.054 %) is somewhat larger in low-carbon steel A and B.

Kinetics of structural transformation of the metal of examined steel specimens (temperature of beginning T_b and ending T_e) at different rate of their cooling in 800–500 °C range were determined by analysis of heating and cooling dilatograms (Table 2).

As it was expected, increase of time of metal staying in 800–500 °C temperature range (reduction of cooling rate) rises the temperature of beginning and ending of transformation for all examined specimens, however these changes are not so significant. In this connection, sufficiently high structural stability of the examined steels, in particular steel D, additionally microalloyed by small quantity of molybdenum, should be noted. Thus, metal with carbon low content (specimens A and B) lies in 656–696 °C limits in $t_{8/5}$ range from 10 to 45 s ($V_{cool.8/5}$ from 30 up to 6.7 °C/s) and steels with increased carbon content (specimens C and D) belong to 640–657 °C. At that T_b of steel D, containing 0.11 % of molybdenum, does not virtually change in the indicated range of cooling rate and makes 656–657 °C. The same dependence on cooling rate was also determined for temperature of ending of metal structural transformations (Table 2) during investigations.

The following can be noted when analyzing the results of determination of T_b and T_e of different chemical composition steel under conditions of change of cooling rate. T_b and T_e of the examined steel specimens, virtually, do not change and to larger extent depend on chemical composition of steel (Figure 1) in the range of cooling rate $V_{cool.8/5}$ = 6.7–5.5 °C/s, corresponding to technical feasibility of its regulation under conditions of traditionally used submerged multiarc double-sided welding of pipe, including from heavy-wall metal. Thus, T_b of steel with reduced carbon content (specimens A and B) lies in the range 700 °C (695–702 °C) and T_e is around 500 °C (499–512 °C) at the indicated range of cooling rate. Respectively, T_b of steel with high content of carbon (specimens C and D) makes 645–600 °C and T_e is 432–492 °C. Minimum temperature of beginning and ending of transformation during the whole studied range of cooling rate is typical for steel with 0.076 % carbon, microalloyed by niobium, vanadium and small quantity of molybdenum (specimen D).

Table 2. Temperature of beginning and ending of austenite transformation in metal of the examined steel specimens at different cooling rate

Symbolic key of the specimen	$t_{8/5}$, s ($V_{cool.8/5}$, °C/s)	T_b, °C	T_e, °C
A (0.032 % C)	10 (30.0)	664	439
	25 (12.0)	671	456
	45 (6.7)	696	499
B (0.045 % C)	10 (30.0)	656	453
	25 (12.0)	682	485
	45 (6.7)	695	509
	50 (6.0)	700	510
	55 (5.5)	702	512
C (0.080 % C)	45 (6.7)	650	480
	50 (6.0)	659	491
	55 (5.5)	660	492
	100 (3.0)	707	500
D (0.076 % C)	25 (12.0)	656	432
	45 (6.7)	657	435
	50 (6.0)	659	440
	55 (5.5)	660	445
	100 (3.0)	670	450

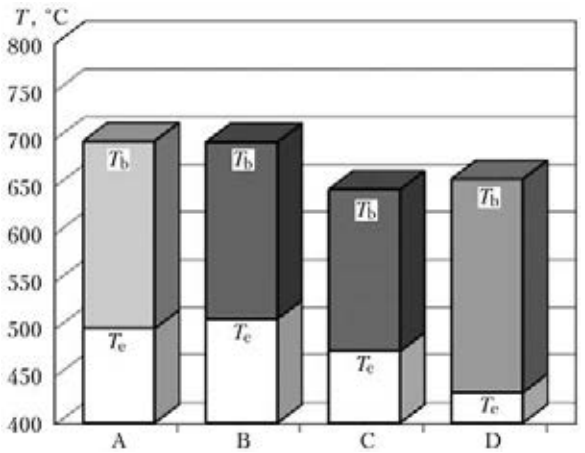

Figure 1. Temperature of beginning T_b and ending T_e of $\gamma \rightarrow \alpha$-transformation of metal of examined specimens at cooling rate $V_{cool.8/5}$ = 6.7 °C/s

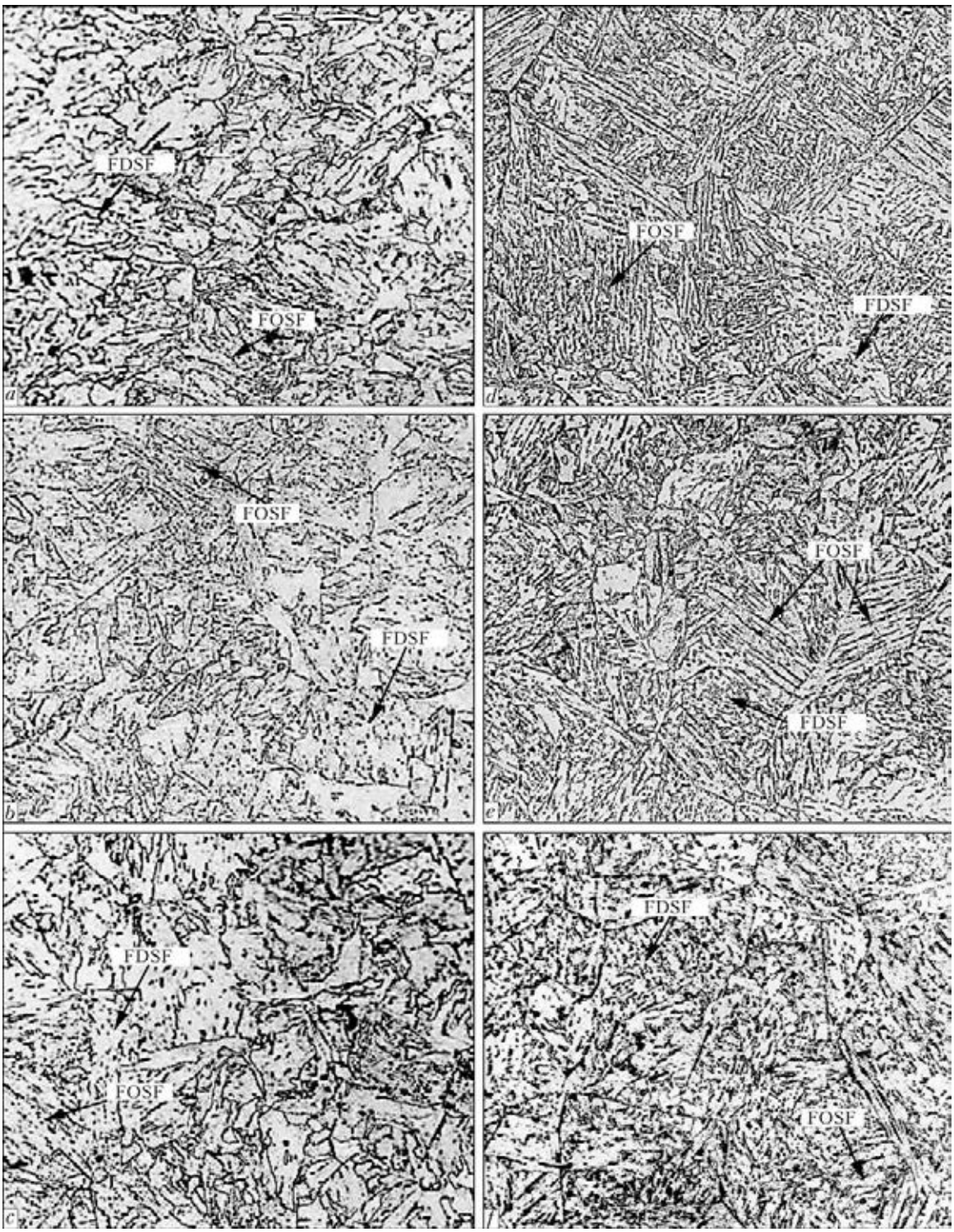

Figure 2. Microstructure (×400) of metal of HAZ simulated specimens (optical microscopy). Specimen A: $V_{cool.8/5}$ = = 6.7 °C/s (*a*); 12 (*b*); 30 (*c*). Specimen C: $V_{cool.8/5}$ = 6.7 °C/s (*d*); 12 (*e*); 30 (*f*). Ferrite with disordered second phase — FDSF, ferrite with ordered second phase — FOSF

Methods of optical and scanning metallography were used for investigation of peculiarities of structural characteristics of the metal of different chemical composition steel after thermal welding cycle simulation with different cooling rate. Microsections of cylinder and rectangular steel specimens were studied after etching in 4 % alcoholic solution of nitric acid (nital).

Coarse grain (number 4 on GOST 5639) structure of lamellar ferrite with sufficiently coarse carbon second phase (MAC-phase or carbide), mainly similarly oriented and normalized (Figure 2, *d* and 3, *a*), is formed in the metal with carbon weight fraction 0.08 % (steel B specimens) at cooling rate typical for HAZ metal of the welded joints of pipes with 25–36 mm wall

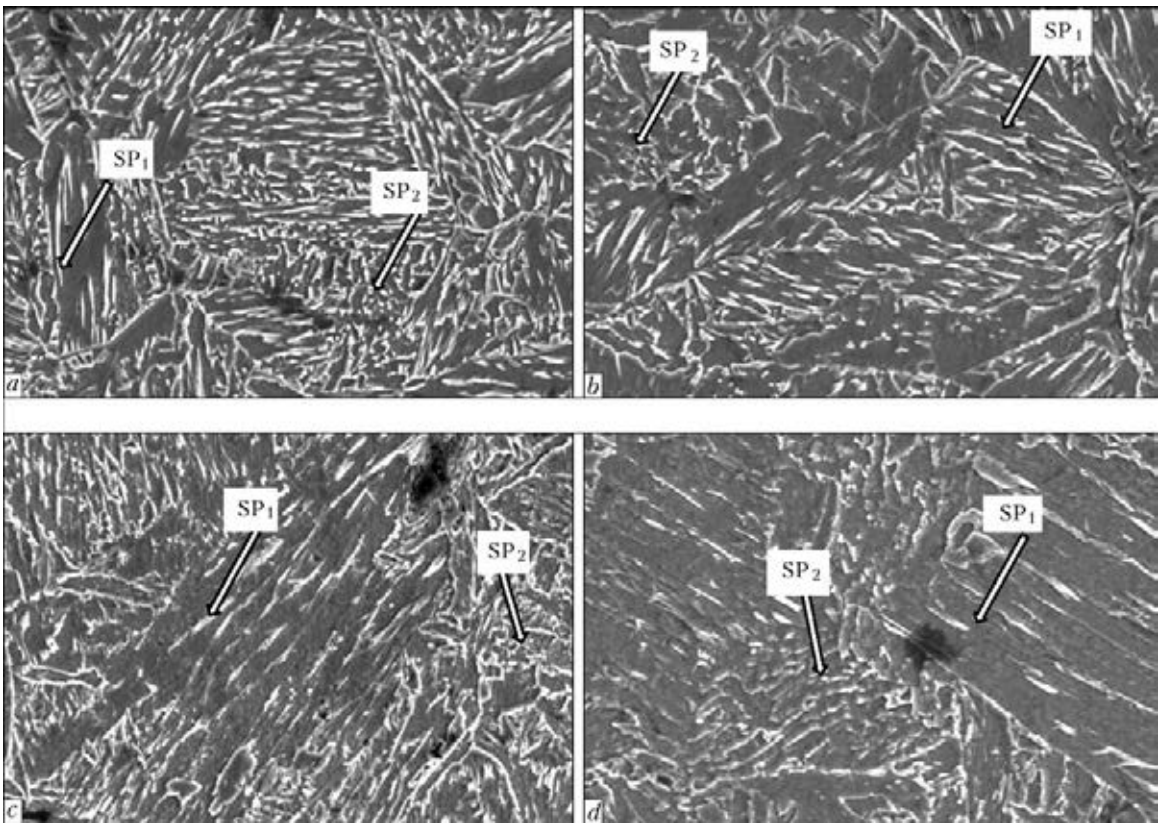

Figure 3. Microstructure of studied specimens of steel after welding thermal cycle simulation (scanning microscopy): *a*, *b* — $V_{cool.8/5}$ = 6.7 °C/s (*a* — specimen C; *b* — specimen D); *c*, *d* — specimen B (respectively $V_{cool.8/5}$ = 6.7 and 12 °C/s); SP_1, SP_2 are second phase of lamellar and grain morphology, respectively

thickness ($V_{cool.8/5}$ = 5.5–6.7 °C/s). It should be noted that majority of coarse grains was fragmented on separate subgrains that clearly determined by dimension and orientation of the second phase precipitations. Second phase, mainly of elongated (lamellar) morphology, is sufficiently tightly distributed in the ferrite matrix (Figure 2, *d* and 3, *a*). Increase of $V_{cool.8/5}$ of the metal above indicated limit (up to 12 °C/s) promotes some increase of dispersion and reduction of volume fraction (distribution density) of the second phase (Figure 2, *e*). The grains, sizes of which correspond to number 4-5 on GOST 5639, are also fragmented. Individual formations of grain morphology, including chaotically located (disordered) ones, are observed together with second phase of elongated form. More dispersed microstructure, representing itself ferrite with tightly located ordered (around 50 %) and disordered second phase mainly of grain morphology (Figure 2, *f*), is formed at cooling rate 30 °C/s. A fringe of hypoeutectoid polygonal ferrite (Figure 4, *a*) is observed along the boundaries of former austenite grain, except for coarse packages of ferrite with ordered second phase of lamellar morphology, at reduction of metal cooling rate $V_{cool.8/5}$ up to 3 °C/s (that is possible, for example, under condition, if initial temperature of the welded edges before performance of pipe outside weld equals approximately 150 °C) in the steel with carbon content 0.080 % (specimens C).

Similar dependence of the structural parameters at change of cooling rate $V_{cool.8/5}$ is also observed in the specimens with smaller content of carbon (specimens A and B, Figure 2, *a*–*c*; 3, *c*–*d*; 4, *b*) as well as in steel with 0.076 % carbon weight fraction and additionally microalloyed by small quantity of molybdenum (specimens D). At that, quantity of carbon structural constituent (MAC-phase) is significantly lower in the structure of simulated HAZ of low-alloy steel (specimens A and B), regardless higher content of niobium which can promote formation of the coarse bainite packages. Formation of MAC-phase in HAZ metal of this steel is more dispersed and, mainly, has grain morphology and their similar orientation is weakly expressed.

It should be noted that microstructure of metal specimens simulating welding thermal cycle with cooling rate around $V_{cool.8/5}$ = 6.7 °C/s, is very close to metal structure in area of coarse grain HAZ of the pipe welded joints, manufactured from steel of corresponding chemical composition (Figure 5).

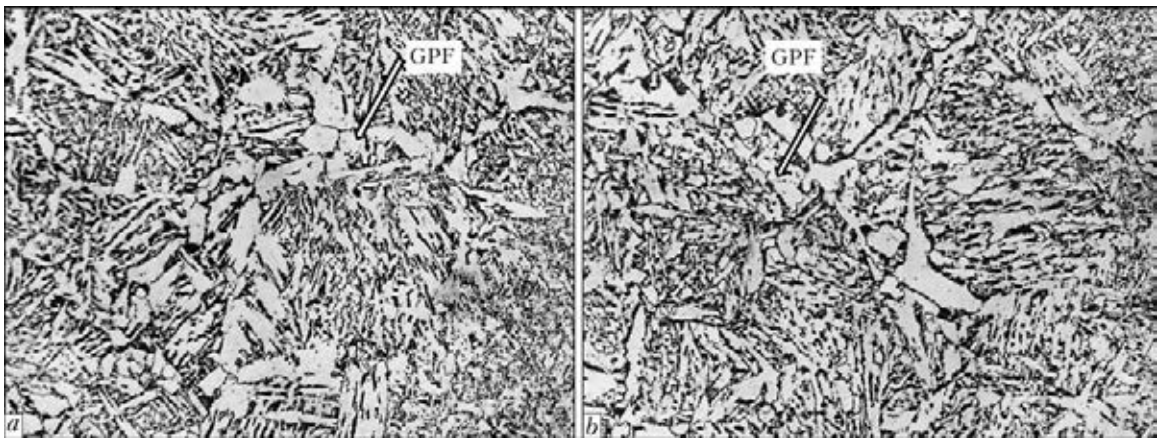

Figure 4. Microstructure (×400) of metal of simulated HAZ specimens with delayed cooling rate ($t_{8/5}$ = 100 s, $V_{cool.8/5}$ = = 3 °C/s): *b* — B (GPF — grain-boundary polygonal ferrite)

Effect of chemical composition on structural state of the metal of simulated HAZ is more significant than changing of the cooling rate in the investigated limits. Dependence of volume fraction (distribution density) of MAC-phase and its morphology on the content of carbon in steel was uniquely determined. Lower quantity of MAC-phase and preferential formation of ferrite grains with MAC-phase of grain type and its chaotic (disordered) distribution were determined in the metal with reduced carbon quantity. Thus, for example, the metal structure of A and B specimens (weight fraction of carbon 0.032 and 0.045 %, respectively) at all investigated $V_{cool.8/5}$ represents itself, mainly, ferrite with dispersed chaotically located carbon phase (MAC-phase, carbides) in preference of grain morphology (Figure 2, *a–c* and 3, *c–d*) and similar grain orientation of dispersed second phase is observed only in separate grains. Volume fraction (distribution density) of second phase in the metal of indicated specimens is significantly lower than in steel with higher carbon content (for comparison, see Figure 3, *a*, *c*).

Increase of weight fraction of carbon up to 0.080 % in steel rises volume fraction (distribution density) of MAC-phase particles in metal structure. At that, MAC-phase has mainly similar orientation (oriented) and, as a rule, lamellar morphology (Figure 2, *d–f* and 3, *a*).

Additional alloying of steel with 0.076 % carbon by molybdenum in 0.11 % quantity promoted some refining of MAC-phase, however, did not result in significant improvement of structural characteristics of the metal in HAZ.

Thus, metallographic investigations showed that structure of bainite type, i.e. lamellar ferrite with strengthening second phase (MAC- or carbide phase) are mainly formed in the metal of studied specimens in sufficiently wide range of cooling rate changing at 800–500 °C temperature. The phase distribution density, location (orientation), sizes and morphology are determined in preference by chemical composition, and to smaller extent, by cooling rate $V_{cool.8/5}$ (in the investigated range). The structure representing itself large packages of lamellar ferrite with similarly oriented second phase, mainly, of elongated shape, is formed in steel with 0.08 % weight fraction of carbon at the cooling rate close to the rate of metal cooling in welding of load bearing pipe welds (approximately 6.7 °C/s). Reduction of carbon content up to 0.032–0.045 % promotes significant reduction of distribution density and

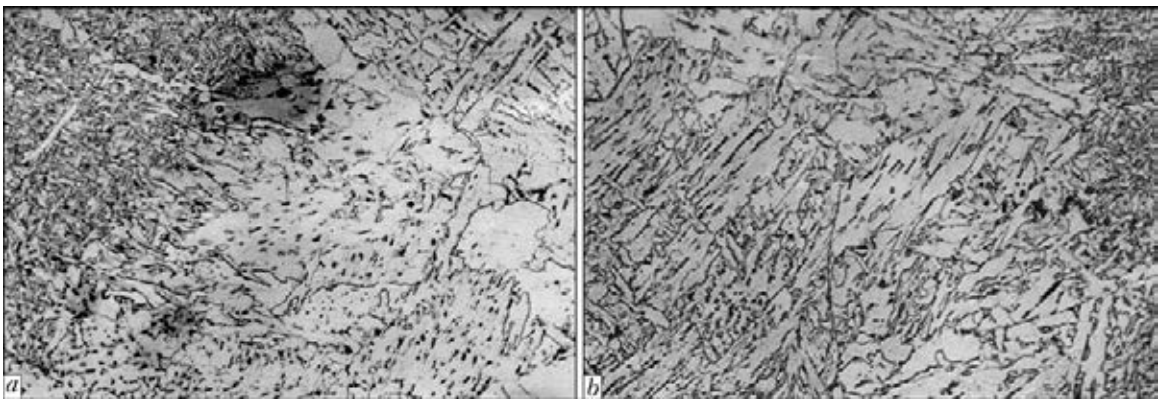

Figure 5. Microstructure (×400) of metal in area of coarse grain HAZ of pipe welded joints from Kh70 steel of different chemical composition: *a* — steel; *b* — B

Table 3. Impact toughness of metal of simulated HAZ specimens of welded joints

Symbolic key of the specimen (carbon content)	$V_{cool.8/5}$, °C/s	KCV, J/cm^2, at T, °C		
		−30	−20	−10
A (0.032 % C)	6.7	38.9; 46.7; 48.2 / 44.6	29.2; 45.8; 54.2 / 43.1	119.5; 125.8; 132.4 / 125.9
	12	41.5; 60.4; 61.2 / 54.4	39.5; 62.8; 77.3 / 59.9	120.4; 134.5; 178.7 / 144.5
	30	41.7; 59.9; 60.1 / 53.9	49.0; 62.9; 79.5 / 63.8	122.4; 135.2; 187.6 / 148.4
C (0.080 % C)	6.7	22.4; 25.8; 29.4 / 25.9	22.2; 31.6; 35.2 / 29.7	51.5; 55.8; 60.4 / 55.9
	12	30.8; 30.9; 35.2 / 32.3	30.7; 33.9; 50.1 / 38.2	51.0; 61.3; 70.1 / 60.8
	30	25.4; 22.8; 31.6 / 26.6	40.1; 41.5; 50.0 / 43.9	57.4; 57.7; 64.3 / 59.8
D (0.076 % C)	6.7	31.4; 34.5; 35.8 / 33.9	33.7; 35.3; 38.5 / 35.8	58.5; 68.3; 70.6 / 65.8
	12	40.2; 41.4; 42.9 / 41.5	42.4; 49.8; 52.9 / 48.4	85.1; 87.4; 95.7 / 89.4

Note. Unit values are indicated in a numerator, and average ones in a denominator.

increase of carbon phase dispersion. At that, the dispersed MAC-phase, mainly of grain morphology, is chaotically located. Such structure characteristics of metal from point of view of its impact strength are more preferable. Significant increase of dispersion and change of distribution density and morphology of MAC-phase in structure of the examined specimens with 0.08 % carbon content was observed only at increase of cooling rate $V_{cool.8/5}$ up to 30 °C/s. However, indicated cooling rate is out of the technical capabilities in submerged multiarc double-pass welding of gas-and-oil line pipes, in particular, with increased wall thickness.

Results of impact bending tests of 10 × 10 mm size specimens with sharp notch, simulating coarse grain area of HAZ of the pipe welded joints, shown in Table 3, well agree with the determined peculiarities of structural characteristics of metal. Thus, changing of cooling rate $V_{cool.8/5}$ in the studied range did not have significant influence on KCV value. For example, the average values of impact toughness KCV of steel C with 0.08 % C changed from 55.9 to 59.8 J/cm^2 at testing temperature minus 10 °C, from 29.7 to 43.9 J/cm^2, at minus 20 °C and 25.9 up to 26.6 J/cm^2 at minus 30 °C, i.e. not more than per 14 J/cm^2 with increase of $V_{cool.8/5}$ from 6.7 to 30 °C/s. Such an insignificant difference of the toughness indices was also observed at change of cooling rate of steel specimens with lower carbon content (Table 3, steel A).

Chemical composition of steel, and, first of all, carbon content had more influence on impact toughness of the metal of simulated HAZ as well as on its structure-phase state. The average KCV value at minus 10 °C made only 55.9 J/cm^2 for specimens of steel C (0.08 % C) which were cooled with 6.7 °C/s rate (typical for submerged multiarc pipe welding). Under the same conditions KCV_{-10} equaled 125.9 J/cm^2 on steel A (0.032 % C) specimens. Reduction of testing temperature up to minus 20 °C and minus 30 °C promoted decrease of level of KCV values of simulated HAZ metal. However, stated dependence on carbon content was preserved.

As fractography investigation showed, all tested impact specimens (from steel of different chemical composition and cooled with various speed) were fractured on quasi-brittle mechanism at temperature minus 30 °C, except for small region under the notch with ductile pit character of rupture (Figure 6, *a*, *c*).

Dimension of facets of quasi-cleavage made in preference 20–70 μm, that approximately corresponds to dimensions of the substructure formations of number 4 fragmented grains, observed in the metal during metallographic investigations (Figure 6, *e*, *h*).

Rupture surface of the specimens was etched in nital (for determination of configuration of MAC-phase particles) with the purpose of evaluation of MAC-phase effect (its sizes and morphology) on fracture character during impact bend testing. As was showed by investigations

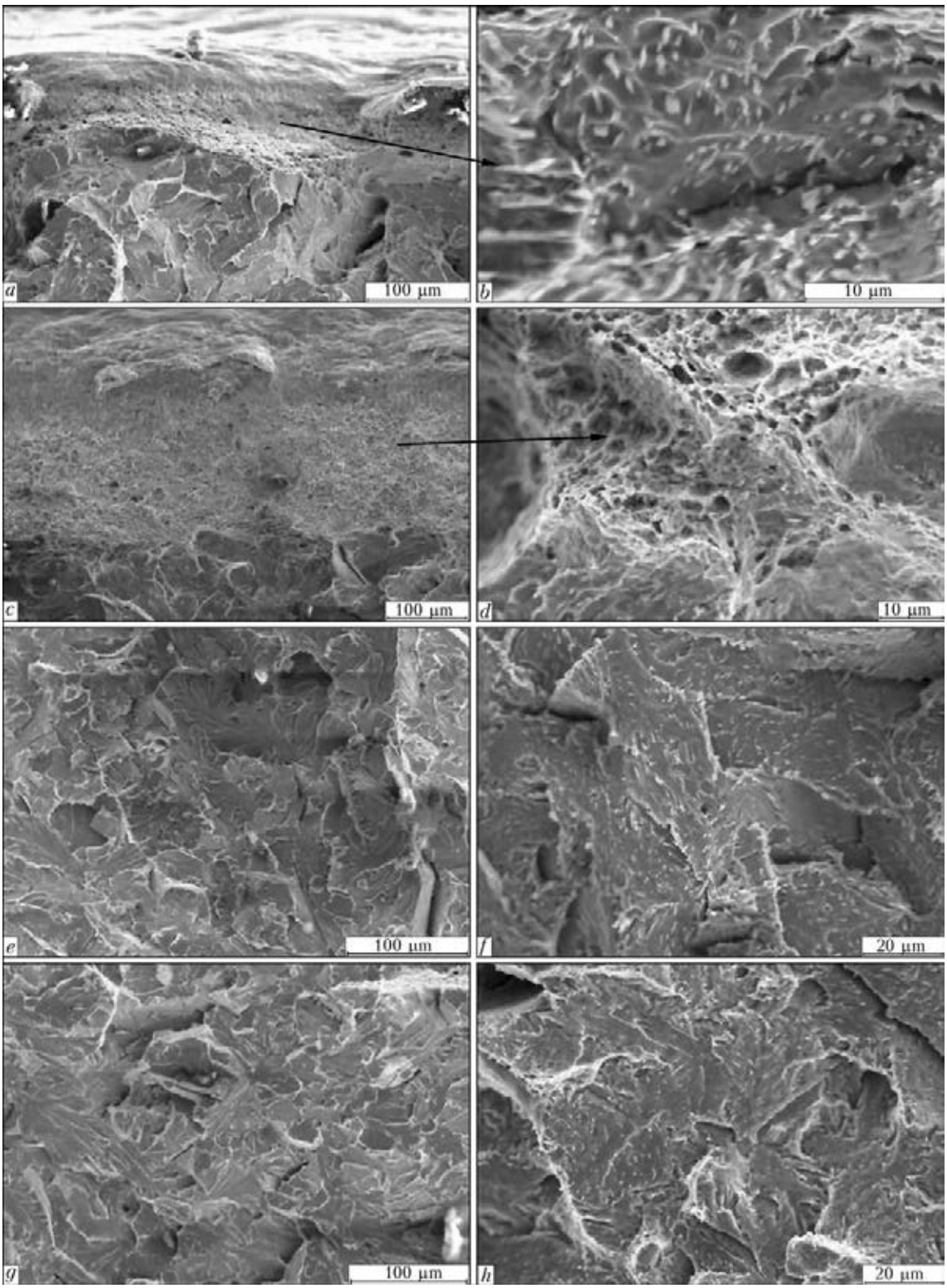

Figure 6. Typical fractogramms of fracture: specimen C — ductile part under notch (*a* — unetched; *b* — after etching); quasi-cleavage area (*e* — unetched; *f* — after etching); specimen A — ductile part under notch (*c* — unetched; *d* — after etching); quasi-cleavage area (*g* — unetched; *h* — after etching)

of these specimens, significant quantity of small fragmented particles of MAC-phase is observed inside the pits in ductile part of the rupture of steel specimens with increased carbon content (specimens C, Figure 6, *b*). Sizes and quantity of such particles is significantly lower (Figure 6, *d*) in steel with 0.032 % C (specimens A). Only small amount of sufficiently dispersed MAC-phase particles are found on the surface of quasi-cleavage facets. Their density distribution and morphology had not significant difference (Figure 6, *f*, *h*) in steel specimens with various carb-

on content. Meanwhile, metallographic investigations determined a sufficiently precise dependence between the quantity and morphology of MAC-phase precipitations and the carbon content in steel (see, for example, Figure 3, *a*, *c*).

Similar indices of metal impact toughness and fracture character of the specimens, simulating HAZ, were registered also at minus 20 °C temperature. Specimens A with low carbon content fractured, mainly, on ductile mechanism at minus 10 °C temperature, when, as it was noted, difference in the impact toughness values of metal of simulated HAZ for steel of different chemical composition is the largest. Portion of ductile fracture in the specimens with high carbon content (steel C, 0.080 % C) did not exceed 40 %.

Results of impact bending tests and fractographic investigations of fractured specimen rupture surface allow assuming that the peculiarities of MAC-phase particle precipitations (density of their distribution, sizes and morphology) affect the energy of ductile fracture to larger extent promoting formation of microvoids and their further coalescence during deformation. Influence of MAC-phase particles is less expressed at brittle fracture.

Conclusions

1. Specimens of steel with different chemical composition, simulating HAZ of the pipe welded joints and differing, in preference, by carbon content, were studied under conditions of metal cooling with different rate. It was stated that structure of bainite type, i.e. lamellar ferrite with strengthening second phase (MAC- or carbide phase) is, mainly, formed in the metal of investigated chemical composition in sufficiently wide range of cooling rates. Density distribution, location (orientation), sizes and morphology of the phase are determined, in preference, by chemical composition, and, to a lesser degree, by metal cooling rate $V_{cool.8/5}$ in the investigated range.

2. Technological capabilities of changing of welded joint cooling rate in multiarc double-pass welding of pipe, in particular, with increased wall thickness are limited. Therefore, increase of HAZ metal toughness requires application of capabilities of metallurgical factor to larger extent by limitation of content of elements reducing austenite transformation temperature as well as carbide-forming elements, in particular, carbon, molybdenum, niobium etc.

1. *OTT-23.040,-KTN-314–09*: Line pipes of large diameter. General specifications.
2. (2000) *Offshore standard DNV-OS-F101*. Submarine pipeline systems. Det Norske Veritas.
3. Morozov, Yu.D., Efron, L.I. (2006) Steels for pipes of main pipelines: state-of-the-art and tendencies of development. *Metallurg*, **5**, 56–58.
4. Graf, M., Niederhoff, K. (1990) Toughness behavior of the heat-affected zone (HAZ) in double submerged-arc welded large-diameter pipe. In: *Conf. on Pipeline Technology* (15–18 Oct. 1990, Oostende, Belgium).
5. Kiryan, V.I., Semyonov, S.E. (1995) Assessment of fitness for purpose of microalloy steel welded joints of main pipelines. *Avtomatich. Svarka*, **3**, 4–9.
6. Grabin, V.F., Denisenko, A.V. (1978) *Metals science of welding of low- and medium-alloy steels*. Kiev: Naukova Dumka.
7. Hrivnak, I., Matsuda, F. (1994) Metallographic examination of martensite-austenite component (MAC) of HAZ metal of high-strength low-alloy steels. *Avtomatich. Svarka*, **3**, 22–30.
8. Terada, Y., Shinokara, Y., Hara, T. et al. (2004) High-strength line-pipes with excellent HAZ toughness. *Nippon Steel Technical Report*, **90**, 89–93.
9. Grigorenko, G.M., Kvasnitsky, V.V., Grigorenko, S.G. et al. (2009) Actual problems of investigation of physical-mechanical properties of materials for welded and brazed structures. In: *Coll. of NUK*. Mykolaiv: NUK.
10. Uwer, D., Degenkolbe, I. (1977) Kennzeichnung von Schweisstemperaturzyklen hinsichtlich ihrer Auswirkung auf die mechanischen Eigenschaften von Schweissverbindungen. *Stahl und Eisen*, **24**, 1201–1208.

Received 26.06.2013

ELECTRODYNAMIC STRAIGHTENING OF ELEMENTS OF SHEET WELDED STRUCTURES

L.M. LOBANOV, N.A. PASHCHIN and **O.L. MIKHODUJ**
E.O. Paton Electric Welding Institute, NASU
11 Bozhenko Str., 03680, Kiev, Ukraine. E-mail: office@paton.kiev.ua

The need for regulation of residual distortion caused by welding in sheet metal structures is one of the urgent problems of modern welding fabrication. A promising approach featuring a low power consumption and not requiring metal-intensive equipment, is development of the method to lower welded joint distortion, based on application of electrodynamic treatment of welded joints by pulsed current. The objective of this work is investigation of effectiveness of electrodynamic straightening of elements of sheet welded structures. Influence of pulsed current electrodynamic treatment on lowering of residual form change in elements of sheet welded plates from AMg6 aluminium alloy and 30KhGSA and St3 structural steels was studied. Capacitive storage was used to generate pulsed current at electrodynamic treatment, and treatment was performed at contact interaction of working electrode, mounted in a flat inductor, with weld surface. A special fixture was used for electrodynamic treatment, allowing treatment of plates to be performed both in unrestrained state and with their pre-bending. Influence of successive application of current pulses at electrodynamic treatment and direction of plate treatment were studied. Results of the performed research showed that welded joint straightening by electrodynamic treatment allows an essential lowering of values of longitudinal and transverse deflection of welded plates from structural steels and aluminium alloy. It is established that the sequence of electrodynamic treatment performance in the direction «from middle to edges» is the most effective for reducing plate distortion, induced by welding. Application of «reverse» bending of plates initiating stresses on weld surface on the level of material yield point, in combination with electrodynamic treatment, allows practically eliminating residual distortion of longitudinal welded joints of AMg6 alloy and significantly lowering it in joints of structural steels. 12 Ref., 2 Tables, 3 Figures.

Keywords: *aluminium alloys, structural steels, longitudinal deflection, transverse deflection, electrodynamic treatment, preliminary outward bending, weld, automatic welding, coated electrode welding*

The need for regulation of residual distortion caused by welding in sheet metal structures is one of the urgent problems of modern welding production. At fabrication of new types of structures, materials and welding processes are used, for which the traditional methods of ensuring the specified fabrication accuracy are not always applicable. At the same time, under the conditions of rising prices for energy resources, the demand for straightening methods based on minimum power consumption [1], is quite high.

A promising approach differing by low power consumption and not requiring metal-intensive equipment, is development of straightening methods based on application of pulsed electromagnetic impacts on the welded joint.

Fundamental and applied investigations revealed the phenomenon of an abrupt increase of ductility and lowering of metal resistance to deformation under the impact of high-density current [2]. The phenomenon was called electroplasticity [3], and its practical application opened up new possibilities for technological treatment of structural elements from various metals and alloys, including refractory alloys.

Electrodynamic treatment (EDT) is one of the methods of current impact on metals and alloys. It is based on initiation of electrodynamic forces in the material, arising at transient processes accompanying current discharge running through the material [4]. At the impact of electrodynamic forces on the structure being treated, it may develop plastic deformations, lowering the level of its residual distortion. Here, the impact of current pulses on the welded joint leads to relaxation of its stress-strain state, determining the parameters of its residual form change [5–8].

The objective of this work was investigation of effectiveness of electrodynamic straightening of elements of sheet welded structures.

Treatment of welded joint samples by current pulses was performed in a unit, the main element of which was capacitive storage, and the work tool was a flat inductor connected to a disc from a nonferromagnetic material and cylindrical electrode, the spherical end face of which was the energy release zone at contact with welded joint treated surface at the moment of the discharge. The disc was designed for realization of the dynamic component of electrodynamic impact on

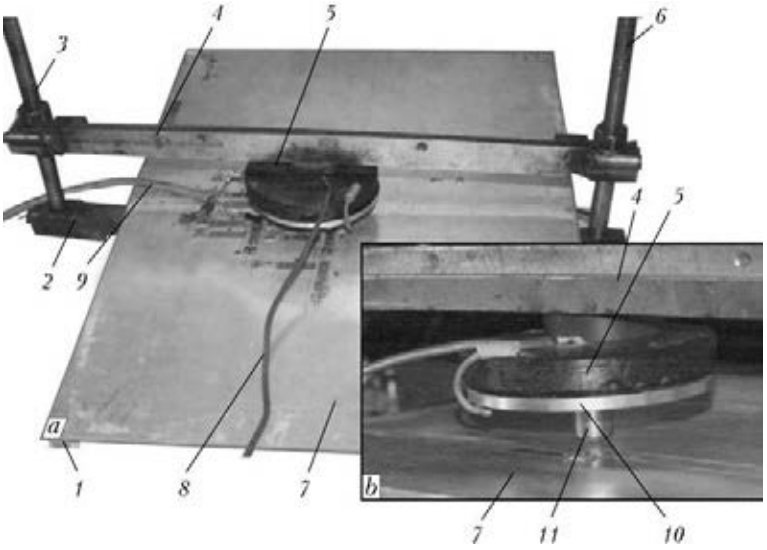

Figure 1. Appearance of fixture for EDT of AMg6 alloy welded joint (*a*) and inductor positioning on the weld (*b*) (for *1–11* see the text)

the metal. Principles of the unit operation [4] are based on transient electrodynamic processes running in the sample metal at storage discharge.

Considering the data of [4], where it is shown that the effectiveness of electrodynamic impact directly depends on current discharge stored energy, E, treatment mode, corresponding to E = = 800 J, was used to assess EDT influence on residual form change of welded plates.

Investigations of EDT influence on residual form change of welded structure elements was conducted on flat welded samples of 400 × 300 × × 3 mm size from 30KhGSA, St3 steels, as well as from aluminium alloy AMg6 (400 × 400 × × 4 mm). Butt welded joints of steels were made by coated electrode welding, and those of AMg6 alloy — by automatic welding in argon.

Treatment of welded joints was performed with application of a special fixture (Figure 1) designed for inductor positioning relative to the sample section to be treated, as well as fixed contact of electrode end face with metal surface. The fixture allows treatment of welded joints to be performed both in unrestrained state and after pre-bending.

Fixture (Figure 1, *a*) consists of supporting *2* and press-down *4* beams, designed for fastening welded joint sample *7* and flat inductor *5*, as well as for their switching into discharge circuit of capacitive storage using power cable *8*. Positioning of press-down beam *4* relative to sample *7* was performed with guide pins *6*, and vertical press-down force was created by loading nuts *3*. Strain-gauge ribbon cable *9* was used to monitor stresses at pre-bending, to achieve which toes *1* were mounted on plate corners. Relative position of inductor *5* with a disc from non-ferromagnetic material *10* and electrode *11* is shown in Figure 1, *b*.

The objective of the first stage of the work was investigation of influence of optimum sequence of electrodynamic impact application. For this purpose, assessment of influence of treatment zone location on the weld, as well as of the sequence of discharge running on residual distortion of plates was performed. Initial form imperfections caused by welding were preserved in the plates, and conditions of their assembly in the fixture ensured a guaranteed electric contact of the electrode with the surface of treated metal.

Sample assembly was performed at guaranteed contact of electrode end face with the weld surface, as shown in Figure 1, *b*. Selection of the weld as treatment zone is substantiated by the data of [9, 10], which show that effectiveness of electrodynamic impact is maximum at EDT of metal with elastic stress level close to $\sigma_{0.2}$. This is characteristic for weld central part, and, therefore, weld surface treatment should be performed for straightening of welded plates by EDT.

After plate assembly in the fixture, storage discharge was applied with subsequent assessment of the change of plate geometrical characteristics as a result of treatment. Initial values (after welding) of plate longitudinal deflection along unrestrained edges f_1 and f_3 and along the weld f_2, as well as values of transverse deflection at weld start Δ_s and finish Δ_f, were recorded as plate form change characteristics, as shown in Figure 2, *a*.

After EDT performance values of form change parameters f_{e1}–f_{e3}, $\Delta_{s.e}$ and $\Delta_{f.e}$ were also recorded. These parameters are shown in Table 1 together with the initial values.

Three treatment variants were studied, determining the sequence of current discharge application and their position. In the first variant EDT

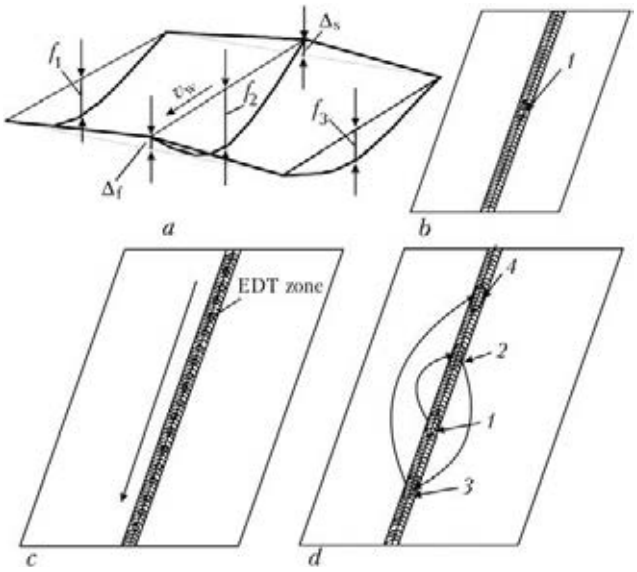

Figure 2. Geometrical characteristics of form change (*a*) and schematics of welded plate treatment: LOC (*b*), PASS (*c*), MTE (*d*) (*1–4* — sequence of EDT cycles)

cycle, consisting of five to six successive electrodynamic impacts, was performed in the weld localized zone (LOC schematic) (Figure 2, *b*; Table 1, Nos. 1, 4, 7), in the second variant — EDT cycle was run on the weld face in the pass direction (PASS schematic) (Figure 2, *c*; Table 1, Nos. 2, 5, 8). Third variant was realized by means of application of four EDT cycles along the weld line in the direction «from the middle to edges» (FME schematic) (Figure 2, *d*; Table 1, Nos. 3, 6, 9).

At realization of LOC schematic the weld central part was treated (Figure 2, *b*), allowing concentration of electrodynamic impact on a limited weld area, applying it in the zone, corresponding to maximum value of longitudinal deflection — f_2 (Figure 2, *a*). This schematic is characterized by minimum labour consumption, because of absence of the need for electrode displacement, but EDT effectiveness becomes lower with each subsequent current impact, applied to a fixed area of weld surface. This, according to the data of [4], is related to the fact that effectiveness of electrodynamic impact directly depends on the level of initial stresses σ_0 in the treated metal. Thus, each subsequent current discharge in EDT cycle makes its impact on the metal, σ_0 value of which decreased as a result of the previous discharge, and, therefore, electrodynamic impact on the stress-strain state of the plate becomes smaller.

Analysis of residual form changes in welded plates from AMg6 alloy treated by LOC schematic showed that before treatment the samples had the characteristic parabolic shape of longitudinal deflection of up to 2.5 mm, and that of transverse ones — from 2.5 up to 3.5 mm. After treatment, residual values of longitudinal and transverse deflection decreased by 60 % on average (Table 1, No.1).

Before treatment by LOC schematic samples from 30KhGSA steel had values of longitudinal deflection of 4.3–6.5 mm on the edges and 6.7 mm on the weld. After EDT residual values of deflection along longitudinal edges and weld decreased by 40 and 60 %, and along the transverse ones — by 50 %, respectively (Table 1, No.4).

Values of residual longitudinal deflection of welded plates from steel St3 reached 6.9–9.4 mm, and those of transverse one — 12–16 mm. After treatment by LOC schematic, residual values of longitudinal and transverse deflection decreased by 45 and 50 %, respectively (Table 1, No.7).

At comparison of values f_2 and f_{2e} one can see that maximum effect of treatment determining residual deflection of plates after EDT, is achieved in welded joint zone — in the area, where deflection values are maximum, as is the level of residual welding stresses, that is confirmed by the data given in [9].

At EDT by the PASS schematic (Figure 2, *c*) changes of plate deflection values were studied at progressive motion of the electrode in «the pass» direction from the joint start to its finish (shown by arrow). Longitudinal displacement of electrode end face was performed along the weld line with 15 mm step so that one electrodynamic impact was applied to each section of the treated surface. This

Table 1. Longitudinal *f* and transverse Δ deflection of welded plates before and after EDT

Plate number	Welded plate material	*f*, mm			Δ, mm		EDT schematic	f_e, mm			Δ_e, mm	
		f_1	f_2	f_3	Δ_s	Δ_f		f_{1e}	f_{2e}	f_{3e}	$\Delta_{s.e}$	$\Delta_{f.e}$
1	AMg6	2.5	2.5	2.5	2.5	3.5	LOC	1.1	1.0	1.2	1.1	1.2
2	AMg6	2.5	2.6	2.4	2.4	3.2	PASS	2.2	2.0	2.2	2.2	3.9
3	AMg6	2.4	2.6	2.6	2.6	3.4	FME	−0.5	0	−1.1	−2.3	−0.6
4	30KhGSA	4.3	6.7	6.5	9.3	12.6	LOC	3.3	2.8	3.2	4.1	6.4
5	30KhGSA	4.4	6.9	6.6	9.8	12.1	PASS	2.4	3.9	3.2	7.5	12.4
6	30KhGSA	6.3	6.8	4.9	9.4	12.9	FME	1.5	1.3	1.9	1.9	2.8
7	St3	7.3	9.4	6.9	16.0	12.1	LOC	4.6	4.0	4.2	8.1	6.0
8	St3	7.2	9.2	5.7	16.7	11.7	PASS	4.5	5.2	3.6	10.2	14.8
9	St3	7.0	9.1	6.8	15	11.3	FME	1.6	1.5	1.7	1.5	0.9

EDT schematic is the most labour consuming from all the enumerated ones, as it requires multiple positioning of electrode along weld line.

Analysis of values of residual displacements of welded plates from AMg6 alloy at EDT by PASS schematic showed that after treatment samples demonstrated a slight lowering of longitudinal deflection to 2.0 mm at increase of transverse deflection to 3.9 mm (Table 1, No.2).

It should be noted that at lowering of longitudinal deflection at treatment by PASS schematic of plates from steels of 30KhGSA and St3 grades transverse deflection increases up to 12.4–14.8 mm (Table 1, Nos. 5, 8). A similar effect was observed also on plates from AMg6 alloy (Table 1, No.2). Comparison of initial values of form change Δ_s and Δ_f with similar parameters $\Delta_{s.e}$ and $\Delta_{f.e}$ after EDT showed that during treatment a certain increase of transverse deflection is found at electrode motion along the butt in «the pass» direction.

Application of FME schematic (Figure 2, *d*) combines the advantages of earlier described LOC and PASS schematics. So, LOC schematic has the advantage of its low labour consumption (no need for electrode displacement along the butt), and the advantage of PASS schematic is the capability of weld surface treatment along its length.

FME schematic was realized by treatment of four sections of weld surface on welded plates in the sequence «from middle to edges». EDT cycle (five current discharges) was performed in each section.

Analysis of values of residual form changes in welded plates of AMg6 alloy at EDT by FME schematic showed that after sample treatment their longitudinal deflection in the weld decreased to zero values, and transverse deflection changed up to reaching form change of an opposite sign (Table 1, No.3).

Values of residual longitudinal deflection in the weld of welded plates from 30KhGSA and St3 steels after EDT by FME schematic decreased by 80 and 85 %, and those of transverse deflection — by 80 and 90 %, respectively (Table 1, Nos. 6, 9).

Conducted experiments lead to the conclusion that selected EDT schematics, such as the impact of series of current pulses on the zone «in weld center» (LOC schematic) and EDT along «the pass» (PASS schematic) do not provide complete elimination of residual distortion of welded plates from steels of St3 and 30KhGSA grades. Application of FME schematic at EDT of AMg6 alloy provides a slight reverse curvature of the studied plates at concurrent residual deflection of transverse edges.

Analyzing the data from Table 1, one can see that FME sequence is the most effective schematic of electrodynamic straightening.

Earlier performed research [11] showed that pre-loading of the HAZ of sheets to be welded by elastic bending, which is created by forces applied normal to the sheet plane, allows regulation of residual form changes of sheet structures from AMg6 alloy.

Data from [11] lead to the conclusion that pre-bending of welded plates before EDT allows improving the treatment capabilities, in order to reduce distortion of sheet structures. This is related to the fact that at realization of reverse bending an external load is applied to the welded structure, stimulating transformation of the elastic component of welded plate deformation into the plastic component at realization of electrodynamic impact. Here the force loop assigns the parameters of the restrained plate bending with the specified accuracy.

To assess the influence of parameters of metal stressed state at pre-bending on the effectiveness of straightening by EDT method treatment of stretched flat samples from aluminium alloy AMg6 and St3 steel with gauge area of 30×4 mm was first conducted. Sample tension was performed in TsDM-10 testing machine in the «stringent» loading mode at deformation rate of 0.1 mm/s up to specified σ_0 values. Testing temperature was equal to 293 K. Influence of electrodynamic impact on treatment effectiveness determined as the ratio of values of material deformation resistance $\Delta\sigma$ to initial stress σ_0 was assessed. $\Delta\sigma$ value was determined as the difference of σ_0 value and current value of stress recorded after electrodynamic impact. σ_0 values were assigned both in the elastic and elastoplastic load ranges that allowed determination of the stressed state parameters corresponding to optimal magnitude of outward bending.

Comparative assessment was performed of the influence of electrodynamic impact at various σ_0 levels on EDT relative effectiveness $(\Delta\sigma/\sigma_0)\cdot 100$ % for AMg6 alloy and St3 steel, which was determined after single current discharge. Values of EDT energy were assigned in the range of 130–800 J, and σ_0 value for AMg6 alloy — from 55 up to 294 MPa, for St3 steel it was from 180 up to 310 MPa. Selection of values $\sigma_0 > 1.5\sigma_{0.2}$ for samples from AMg6 alloy is dictated by the need for assessment of the influence of material strain hardening on EDT effectiveness in the elastoplastic loading range. Performance of similar research on samples from St3 steel is difficult, because of impossibility of ensuring stable σ_0 values after initial load values exceeding $1.2\sigma_{0.2}$ as a result of local yield of metal.

It should be noted that as $\sigma_{0.2}$ values are significantly different for steel and aluminium alloy, plotting $(\Delta\sigma/\sigma_0)\cdot 100\ \% = f(\sigma_0)$ dependence will make it difficult to compare the characteristics

of EDT effectiveness from the level of initial stresses for the studied materials in the set range of charge energies. For a more correct comparison of obtained values, relative load $\sigma_0/\sigma_{0.2}$ was used, showing the ratio of initial stress to yield limit of St3 steel and AMg6 alloy.

Dependencies of $\Delta\sigma/\sigma_0$ on $\sigma_0/\sigma_{0.2}$ at different values of stored charge energy for AMg6 alloy and St3 steel are given in Figure 3. It is seen from the Figure that maximum EDT effectiveness corresponds to the level of initial stresses, which are close to $\sigma_{0.2}$ for AMg6 alloy (curves *3*, *5*). In this case lowering of $\Delta\sigma/\sigma_0$ values at $\sigma_0/\sigma_{0.2}$ increase is attributable to the influence of strain hardening earlier noted in [4]. For St3 steel at E increase the effectiveness increased monotonically with load increase (curves *1*, *4*) that is probably related to high ductility. It should be noted that at E = 130 J the effectiveness of EDT of St3 steel is close to zero.

Analysis of the data (Figure 3) leads to the conclusion that for AMg6 alloy plates bending parameters should correspond to σ_0 values in the elastic loading region close to $\sigma_{0.2}$. Considering the monotonic nature of increase of $\Delta\sigma/\sigma_0 = f(\sigma_0/\sigma_{0.2})$ dependence for St3 steel (Figure 3, curves *1*, *4*) it is rational to study the parameters of pre-bending of plates, corresponding both to elastic and to elastoplastic σ_0 ranges.

Considering the data (Figure 3 and [11]), effectiveness of straightening welded plates by EDT method was studied with preliminary assigning of the values of longitudinal deflection f_l^* in the direction opposite to that of deflection caused by welding. Plate pre-bending was performed in welded joint center, using a fixture (Figure 1, *a*) and deflection value was assigned by regulation of the height of supports mounted along plate edges. Here f_l^* was determined as deflection of plates after vertical load application.

Bending was applied by clamping electrode end face to plate surface in the joint central part.

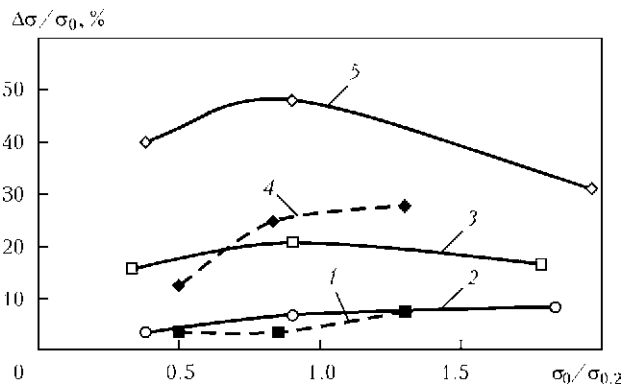

Figure 3. Influence of magnitude of relative load $\sigma_0/\sigma_{0.2}$ for samples from steel St3 (*1*, *4*) and AMg6 alloy (*2*, *3*, *5*) on EDT effectiveness at different stored charge energy: *1* — E = 300 J; *2* — 130; *3* — 300; *4* — 800; *5* — 800

After specified f_l^* values have been reached, longitudinal component of compressive stresses σ_{xx} along the fusion line was controlled, these stresses arising on plate surface as a result of bending. Here $\sigma_{xx} = 0$ value corresponded to deflection f_2 of the plate in the weld zone as a result of welding. It should be noted that evaluation of the influence of initial load on EDT effectiveness was performed by assigning σ_0 values for flat samples in the tensile region (Figure 3), and compressive stresses σ_{xx} were found on plate surface after bending. Data of [12] lead to the conclusion that dependencies $\Delta\sigma/\sigma_0 = f(\sigma_0/\sigma_{0.2})$, derived at tension of aluminium alloy and low-carbon steel, are valid also in the region of compressive stresses, but with an opposite sign.

Recording of σ_{xx} values was conducted using a wire strain gauge, pasted on the plate surface in EDT zone, and stub of IDTs-10 strain gauge unit. f_l^* and σ_{xx} values are given in Table 2. EDT cycle, similar to previous experiments, consisted of five current discharges applied to the plate by LOC schematic, with subsequent recording of its form change as a result of treatment. Values of initial longitudinal deflection of plates f_1–f_3 and after treatment f_{1e}–f_{3e} (f_2, f_{2e} is deflection in weld zone) are given in Table 2. Initial values of transverse bending of plates in the zone of weld start and finish Δ_s and Δ_f, and after EDT — $\Delta_{s.e}$ and $\Delta_{f.e}$ are also shown in Table 2.

It should be noted that assigned f_l^* values at $\sigma_{xx} = -0.3\sigma_{0.2}$ do not lead to any noticeable lowering of parameters of residual distortion of the plates for all the studied materials.

Proceeding from the data (Tables 2, No.1), we can see that at achievement of value $\sigma_{xx} = -0.6\sigma_{0.2}$ on a sample of AMg6 alloy and respective deflection $f_l^* = -2.5$ mm the longitudinal and transverse components of form change decrease by 70 and 60 %, respectively. Maximum values of residual deflection components were obtained at EDT at $\sigma_{xx} = -\sigma_{0.2}$ (Table 2, No.2) that corresponds to $f_l^* = -5.5$ mm, where form change reduction ensured practical straightening of the plates. This is confirmed by the data in Figure 3, which shows that maximum effectiveness of electrodynamic impact for AMg6 alloy is achieved at initial stress values close to $-\sigma_{0.2}$.

After bending 30KhGSA steel plate up to value $\sigma_{xx} = -0.45\sigma_{0.2}$ (Table 2, No.3) and subsequent EDT, values of longitudinal and transverse components of deflection decreased by 70 and 65 %, respectively. EDT influence was maximum at $\sigma_{xx} = -0.5\sigma_{0.2}$ and $f_l^* = -20$ mm (Table 2, No.4) where reduction of longitudinal and transverse components of plate form change reached 80 %. Further increase of values σ_{xx} and f_l^* did not lead to any essential change of plate deflection characteristics.

Table 2. Influence of preliminary longitudinal bending f_1^* on residual form change of welded plates at EDT

Plate number	Welded plate material	f, mm			Δ, mm		f_s^*, mm	σ_{xx}, MPa	f_e, mm			Δ_e, mm	
		f_1	f_2	f_3	Δ_s	Δ_f			f_{1e}	f_{2e}	f_{3e}	$\Delta_{s.e}$	$\Delta_{f.e}$
1	AMg6	2.5	2.6	2.5	2.4	3.8	−2.5	−90	0.7	0.8	0.7	1.0	1.4
2	AMg6	2.4	2.7	2.6	2.6	3.4	−5.5	−145	0.1	0	0.2	0.2	0.2
3	30KhGSA	4.4	7.2	5.9	9.0	11.8	−1.0	−430	2.2	2.2	2.4	3.5	4.2
4	30KhGSA	4.8	7.1	6.6	9.2	12.0	−2.0	−475	1.4	1.3	1.6	1.5	1.6
5	St3	7.4	9.8	6.1	15.9	12.1	5	−250	2.1	3.8	1.5	3.1	3.6
6	St3	7.3	9.4	6.9	16.3	12.1	3	−330	1.0	2.5	0.9	1.7	1.3

For St3 steel when $f_1^* = 4.0$ mm was reached (Table 2, No.5), σ_{xx} increased to $\sigma_{0.2}$ values. In this case EDT led to lowering of deflection component values to 85 %, respectively.

The rationality of studying EDT influence on form change of welded plates from St3 steel under the conditions of plastic outward bending is substantiated by data of Figure 3, which shows the comparative assessment of the influence of initial load on EDT effectiveness for St3 steel and AMg6 alloy. These data (Figure 3) lead to the conclusion that while for AMg6 alloy EDT effectiveness decreases at transition of initial load into elastoplastic stress region, for St3 steel it rises monotonically. With this purpose residual deflection $f_1^* = 3.0$ mm was created in the plate, at which σ_{xx} value on the plate outer surface reached 330 MPa that is equal to $1.4\sigma_{0.2}$ for St3 steel. Lowering of transverse deflection is maximum — up to 90 % (Table 2, No.6).

These data (Table 2) lead to the conclusion that EDT with pre-bending of welded plates inducing on plate surface stresses on the level of material yield point, allows practical elimination of residual distortion of longitudinal welded joints from AMg6 alloy and lowering it by an order of magnitude in structural steel joints.

Comparison of the data in Table 1 (Nos. 3, 6, 9) and Table 2 (Nos. 2, 4, 6) leads to the conclusion that EDT under the conditions of pre-bending at σ_{xx} values close to $-\sigma_{0.2}$ is comparable in its effectiveness for the studied metals to treatment by FME schematic, but more readily adaptable to fabrication, due to absence of the need of inductor positioning along the weld line.

EDT labur consumption is lower at application of outward bending than of FME schematic, as this does not require repeated repositioning of the electrode along the weld line.

Conclusions

1. It is established that different variants of the sequence of weld EDT performance lower the level of residual distortion of welded sheets from AMg6 alloy and from structural steels of 30KhGSA and St3 grades.

2. It is shown that both EDT of a localized weld section and EDT of weld in «the pass» direction are comparable in their effectiveness and lower the values of longitudinal and transverse deflection of welded plates several times. Maximum EDT effectiveness is found at weld surface treatment in the direction «from middle to edges».

3. Application of «reverse» bending of plates inducing on weld surface stresses on the level of material yield point, in combination with EDT, allows practically eliminating residual distortions of longitudinal welded joints from AMg6 alloy and essentially lowering it in structural steel joints.

1. Lobanov, L.M., Makhnenko, V.I., Trufyakov, V.I. (1993) *Welded building structures*. Vol. 1. Kiev: Naukova Dumka.
2. Baranov, Yu.V., Troitsky, O.A., Avraamov, Yu.S. et al. (2001) *Physical principles of electric pulse and electroplastic treatments and new materials*. Moscow: MGIU.
3. Bataronov, I.D. (1999) Mechanisms of electroplasticity. *Sorosovsky Obrazovat. Zhurnal*, **10**, 93–99.
4. Lobanov, L.M., Pashchin, N.A., Cherkashin, A.V. et al. (2012) Efficiency of electrodynamic treatment of aluminium alloy AMg6 and its welded joints. *The Paton Welding J.*, **1**, 2–6.
5. Stepanov, G.V., Babutsky, A.I., Mameev, I.A. et al. (2011) Redistribution of residual welding stresses as a result of pulse electromagnetic field treatment. *Problemy Prochnosti*, **3**, 123–131.
6. Tang, F., Lu, A.L., Mei J.F. et al. (1998) Research on residual stress reduction by a low frequency alternating magnetic field. *J. of Mater. Proc. Technology*, **74**, 255–258.
7. Stepanov, G.V., Babutsky, A.I., Mameev, I.A. et al. (2011) Nonstationary stress-strain state in long rod caused by pulses of high density electric current. *Problemy Prochnosti*, **3**, 123–131.
8. Lobanov, L.M., Pashchin, N.A., Loginov, V.P. et al. (2010) Effect of electric pulse treatment on residual form change in shape of thin-sheet welded structures (Review). *The Paton Welding J.*, **3**, 10–13.
9. Lobanov, L.M., Pashchin, N.A., Loginov, V.P. et al. (2007) Change of the stress-strain state of welded joints of aluminium alloy AMg6 after electrodynamic treatment. *Ibid.*, **6**, 7–14.
10. Strizhalo, V.A., Novogrudsky, L.S., Vorobiov, E.V. (2008) *Strength of materials at cryogenic temperatures taking into account the action of electromagnetic fields*. Kiev: IPS.
11. Kasatkin, B.S., Lobanov, L.M., Pavlovsky, V.I. (1979) Influence of initial bending of sheets to be welded on residual distortions. *Avtomatich. Svarka*, **9**, 38–41.
12. Bell, J.F. (1984) *Experimental principles of mechanics of deformed solids*. Pt 2: Final deformations. Moscow: Nauka.

Received 04.06.2013

MODELLING OF PROCESSES OF NUCLEATION AND DEVELOPMENT OF DUCTILE FRACTURE PORES IN WELDED STRUCTURES

E.A. VELIKOIVANENKO, G.F. ROZYNKA, A.S. MILENIN and **N.I. PIVTORAK**
E.O. Paton Electric Welding Institute, NASU
11 Bozhenko Str., 03680, Kiev, Ukraine. E-mail: office@paton.kiev.ua

Evaluation of serviceability and residual life of the critical welded structures with found defect, including pipelines and pressure vessels, assumes a complex analysis of interrelated multidimensional processes, influencing their bearing capacity. At that, grounded reduction of conservatism of such an evaluation is rational that requires description of structure limiting state considering main fracture mechanisms. In particular, ductile fracture is a main mechanism of development of material damage in the main pipelines with typical surface defects of local corrosion wall thinning without accompanying sharp concentrators. Complex methodology for numerical analysis of processes of nucleation and development of ductile fracture pores of metal welded structures as well as criteria for determination of their limiting state was developed in the scope of present work. Thus, a procedure for calculation of stress-strain state in-service structure considering change of load-carrying net-section of structure areas at microporosity growth was build on the basis of Gurson–Tvergaard model. The criteria of pore nucleation as well as mathematical description of different mechanisms of their development depending on character of external force action were proposed for non-isothermal metal state, in particular, in the process of welding heating. Application of the developed approaches was shown on the example of analysis of limiting state of main pipeline element with local wall thinning defect in area of circumferential site weld. It is shown that limiting internal pressure in the pipeline with such service damage is determined by character of interaction of local stresses in zone of the weld and geometrical anomaly, i.e. the lower is the distance between them, the less is the loading necessary for formation of common zone of microdamage in which the macrodefects are formed as a consequence. Similarly, significant effect of pores on the bearing capacity in pipeline site weld is shown. Generality of the developed approaches of numerical analysis of ductile fracture processes allows applying them for evaluation of limiting state and residual life of the welded pressure vessels from high-strength steels. 18 Ref., 1 Table, 3 Figures.

Keywords: *ductile fracture, pore formation, stress-strain state, limit load, welded joint, main pipeline*

Analysis of limiting state of the modern welded structures is an important stage in diagnostics of their real condition and prediction of safe operation residual life. At that, a description of processes resulting in breaking of integrity of the structure material in micro- and macroscale, nucleation and development of the typical defects requires joint application of procedures for modelling of stress-strain state kinetics depending on value and nature of external force effect, basics of fracture mechanics and current interpretations about behavior of crystalline structures under limiting force action. Besides, presence of the welded joints assumes the necessity of additional consideration of structure state in welding area (heat treatment) from point of view of residual stress-strain and structural states of the metal as well as development of scattered damage based on modelling of processes of continuous medium thermoplasticity. As it is shown by experience, the fracture of welded pressure vessels and pipelines from high-strength steels is determined in series of cases by the ductile fracture processes in area of welds and geometric anomalies [1, 2]. At that, most of the existing ductile fracture models consider structurally-homogeneous materials in isothermal case [3–5], whereas in real structures the welds are weak zones and analysis of their limiting state is an important aspect of technical diagnostics of the critical structures. In particular, approaches of Gurson, Tvergaard and Needleman [6–8], which make a basis of the most current models of limiting state of the structures tend to ductile fracture, have found a wide application in description of the development of stress-strain state of the materials with pores. In addition, series of works is dedicated to expansion of these models applicable to the welded structures, but mathematical description of a welding process itself and its influence on peculiarities of the ductile fracture has rather phenomenological character and requires large number

of experimental investigations. Numerical procedure for analysis of the ductile fracture was developed and examples of the typical cases of main pipeline damage were considered in the scope of present work in order to study the peculiarities of limiting state of welded pipeline elements under internal pressure.

Studied fracture mechanism in the general case can be divided on several successive stages:

- nucleation of ductile fracture pores in production of structures, including in a zone of local welding heating and at developed plastic flow in area of physical and/or geometry concentrators;
- increase of pore sizes at plastic strain;
- interaction and coalescence of ductile fracture pores;
- nucleation of macrodefect and related with it reduction of bearing capacity of defective area as well as structure in the whole;
- development of macrodefect.

Each of these steps has different physical-mechanical nature, therefore, their description requires construction of the corresponding interrelated models.

It is accepted that the pore nucleation in zone of the structural defects and inhomogeneities (primary pores) is related with significant development of the plastic strains that can be described by Odkvist parameter [9]:

$$\kappa = \int d\varepsilon_i^p, \qquad (1)$$

where $d\varepsilon_i^p = \frac{\sqrt{2}}{3}\sqrt{d\varepsilon_{ij}^p d\varepsilon_{ij}^p}$, $d\varepsilon_{ij}^p$ are the components of tensor of plastic strain increment ($i, j = x, y, z$).

Respectively, if current value of Odkvist parameter exceeds critical value κ_c, it serves as a condition for pore nucleation in the isothermal case.

Appearance of metal structure inhomogeneities, in particular, in area of its solid-liquid state interface (between the liquidus and solidus temperatures) takes place in the process of welding as a result of local welding heating, first order phase transformations and concurrent liquation processes. At that, general sized dependence of Odkvist parameter critical value κ_c on metal state at different temperatures T can be used for description of micropores nucleation:

$$\kappa_c(T) = \kappa_{c0} \exp\left\{\left[\frac{F_0 - F(T)}{B}\right]^{\beta}\right\}, \qquad (2)$$

where $F(T)$ is a function of material resistance to plastic strain; κ_{c0}, B, F_0, β are the constants.

If the expressed temperature embrittlement interval and significant strengthening are not typical for the studied metal, then the yield strength temperature dependence $\sigma_y(T)$ can be taken as $F(T)$ function. Thus, it follows from (2) that κ_{c0} and F_0 are the critical values of Odkvist parameter of the studied metal at room temperature and its normative yield strength σ_y, respectively, and temperature dependence of the Odkvist parameter critical value can be represented in the following way:

$$\kappa_c(T) = \kappa_{c0} \exp\left\{\left[\frac{\sigma_y - \sigma_y(T)}{B}\right]^{\beta}\right\}. \qquad (3)$$

B value for structural steels $\beta \approx 3$ [10] is characterized by material susceptibility to pore formation and lies in $(1.0–1.5)\sigma_y$ ranges.

Criterion of pore nucleation in the metal at variable temperature field with developed kinetics of plastic strain accumulation can be described by following relationship:

$$\chi_\kappa = \int \frac{d\kappa}{\kappa_c(T)} \geq 1. \qquad (4)$$

If condition (4) is fulfilled, it can be assumed that an inhomogeneity in a form of spherical micropores with volume concentration f_{pl} is nucleated in studied area of the structure.

It should be noted that the second typical mechanism of pore nucleation in welding is a formation of impurity bubbles in a welding pool, which do not have enough time to evolve in a gas phase before metal solidification [11]. Modelling of such a process is sufficiently complex and is not included in the scope of present work. Effect of indicated process can be taken into account as a priori either by setting of the spherical macrodefects in the weld area or considering the total volume concentration of nucleated pores f_0 in the specific studied volume:

$$f_0 = f_{pl} + f_{ev}, \qquad (5)$$

where f_{ev} is a volume concentration of pores, nucleated as a result of evaporation processes.

Further growth of ductile fracture pores depends on a rigidity of stressed state and intensity of plastic strain of the metal and is described by Rice–Tracy law [9]:

$$dR = R_0 K_1 \exp\left(K_2 \frac{\sigma_m}{\sigma_i}\right) d\varepsilon_i^p, \qquad (6)$$

where R, R_0 are the current and initial radiuses of pores, respectively; $\sigma_m = (\sigma_{xx} + \sigma_{yy} + \sigma_{zz})/3$ is a membrane stress; $\sigma_i = (\sigma_{ij}\sigma_{ij}/2)^{1/2}$ is a stress intensity; σ_m/σ_i is a parameter of stressed state rigidity; $K_1 = 0/28$, $K_2 = 1.5$ are the constants.

If the parameter of stressed state rigidity in studied area of the structure is not enough for intensive growth of pores according to (6), then significant influence of the plastic strains can result in appearance of the secondary discontinuities. Speed of nucleation of the secondary spherical pores depends on concentration of inclusions in the structure metal and development of plastic strains on the following law [9]:

$$f = f_0 + f_i \exp\left(-\frac{\kappa^*}{\kappa - \kappa_c}\right), \quad (7)$$

where f_i is a volume concentration of the inclusions; κ^* is a metal constant characterizing maximum possible increment of Odkvist parameter.

It should be noted that f_i value in the studied case depends on a structure state of metal in weld area and heat-affected zone (HAZ), in particular, on quantity of cementite (Fe_3C) as well as initial and acquired non-metallic inclusions in the process of welding [12]. Analysis of stress-strain state of the welded structure from point of view of ductile fracture was carried out in the present work from point of view of numerical solution of boundary problem of non-stationary thermoplasticity by means of tracing of elasto-plastic strains from the moment of welding beginning up to complete cooling of the structure and at further loading up to limiting pressure in the scope of finite-element model. Relation of stresses and strains is determined by Hooke's law and associate law of plastic flow, originating from the following relationships:

$$\Delta\varepsilon_{ij} = \Psi(\sigma_{ij} - \delta_{ij}\sigma_m) + \delta_{ij}(K\sigma_m + \Delta\varepsilon_m + \Delta f/3) - \\ - \frac{1}{2G}(\sigma_{ij} - \delta_{ij}\sigma_m)^* + (K\sigma_m)^*, \quad (8)$$

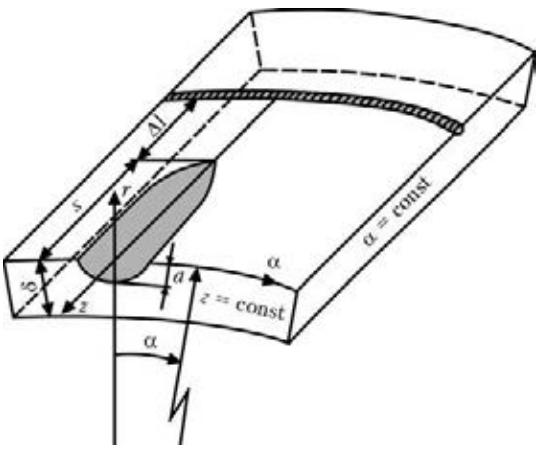

Figure 1. Scheme of pipeline section with local wall thinning and circumferential weld (in cylindrical coordinate system, r, α, z)

where $K = \frac{1-2\nu}{E}$; E is an Young modulus; ν is a Poisson ratio; $G = \frac{E}{2(1+\nu)}$; Ψ is a function of material state. Ψ function is determined by condition of the plastic flow according to Mises criterion with additional consideration of reduction of bearing net-section of the finite element as a result of formation of the discontinuity in scope of Gurson–Tvergaard model, namely:

$$\Psi = \frac{1}{2G}, \text{ if } \sigma_i < \sigma_s, \quad \Psi > \frac{1}{2G}, \text{ if } \sigma_i = \sigma_s, \\ \sigma_s = \sigma_y \sqrt{1 + (q_3 f^*)^2 - 2q_1 \cosh\left(q_2 \frac{3\sigma_m}{2\sigma_y}\right)}, \quad (9)$$

where $q_1 = 1.5$, $q_2 = 1$; $q_3 = 1.5$ are the constants; f^* is an equivalent volume concentration of pores considering their interaction in the finite element.

Value of equivalent pore concentration, appearing in (9), is determined from a relation, proposed by Gurson and Needleman [7]:

$$f^* = \begin{cases} f, & \text{if } f \le f_c; \\ f_c + \frac{f_u^* - f_c}{f_F - f_c}(f - f_c), & \text{if } f > f_c, \end{cases} \quad (10)$$

where f_c is a critical concentration of the discontinuities up to which separate pores do not interact (taken as $f_c = 0.15$); f_F is a pore concentration at which fracture of the finite element takes place; $f_u^* = 1/q_1$.

Limiting state of each finite element is determined from two possible fracture mechanisms [15], i.e. plastic instability in $\Psi \to \infty$ case according to McClintock condition and microcleavage.

Limiting state of the pipeline element (diameter 1420 mm, wall thickness 20 mm, material — steel 17G1S, properties of which is given, in particular, in [16]) with circumferential weld and external surface wall thinning of metal loss type (Figure 1) of $2s = 50$, $a = 5$ mm size which is allowable according to [17], was considered as an example of application of the developed complex model for analysis of the welded structures. The following values of parameters and necessary constants were taken as input data of the present numerical investigation, i.e. $f_0 = 0.01$; $f_i = 0.01$; $\kappa^* = 0.1$; $\kappa_{c0} = 0.05$; $B = \sigma_y$; $R_0 = 0.0167$ mm. It should be noted that influence of possible errors in determination of the values of given constants on the results of investigations reduces significantly at approximation of loads to limiting ones (i.e. in the case, if at least one of the finite elements had lost the bearing capacity and macrode-

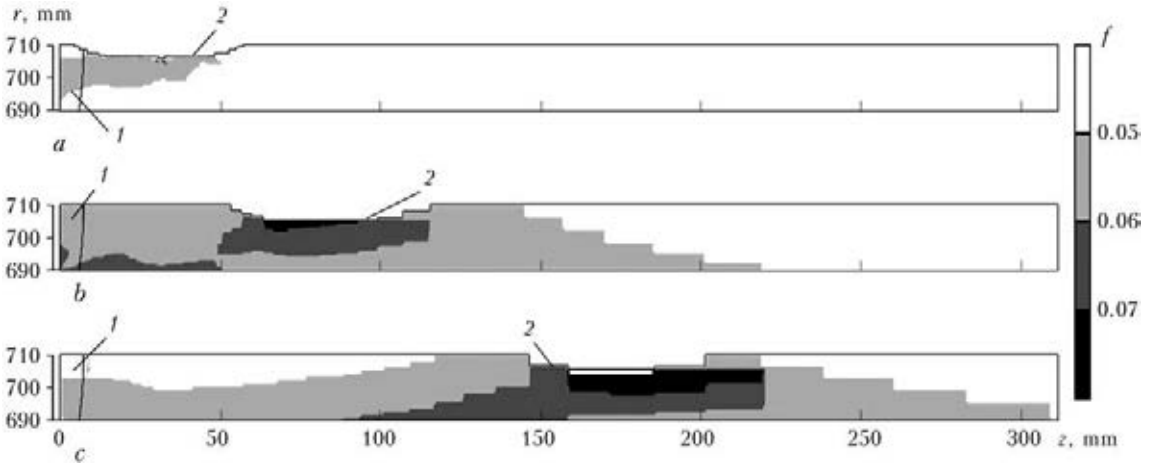

Figure 2. Distribution of volume concentration of micropores f in studied pipeline section at limiting pressure P_{max} depending on Δl distance between weld and wall thinning defect: *a* — Δl = 5 mm, P_{max} = 18.8 MPa; *b* — Δl = 50 mm, P_{max} = 19.8 MPa; *c* — Δl = 150 mm, P_{max} = 20.2 MPa; *1* — half of symmetrical weld; *2* — defect

fect appeared), since at that state of the structure is characterized by plastic strain.

Different mutual location of the weld taking into account residual stress-strain state as well as scattered damage, accumulated in the process of welding, and concentrator in area of geometry anomaly assume different fracture mechanisms [15] as well as different limiting pressure in the pipeline. The results of numerical experiments showed that the appearance of small pore concentration (around 0.05) along the fusion line was promoted by local thermal cycles and corresponding to them kinetics of stress-strain state of the structure metal in area of weld metal and HAZ. Such a damage has insignificant effect on the structure bearing capacity, since rigidity parameter of stress-strain state σ_m/σ_i of the pipeline element does not achieve significant values under internal pressure effect due to absence of sharp concentrators. Therefore, plastic strain in the studied case does not promote significant pore development in welding according to (6) and prevailing mechanism of damage development is the appearance of new pores in area of concentrator and secondary pores from plastic strain on (4) and (7), respectively.

At that, the damage develops independently in area of maximum defect depth and in HAZ of the weld at the initial stages of structure loading by internal pressure. Typical peculiarity of the limiting state is an obvious interaction between two types of studied inhomogeneities from point of view of microporosity formation (Figure 2). At that, the larger is the distance between weld and surface thinning Δl, the more is the force action necessary for formation of volume of metal damage between them, where microfracture (Figure 3) is nucleated at further increase of load. As can be seen from the presented data, close location of allowable thinning defect and site weld can reduce bearing capacity of the pipeline up to 10 %.

As was mentioned above, the possible nucleation of pores in the weld as a result of evaporation of interstitial impurities in a case, when gas bubbles do not have enough time to appear on the surface before complete metal solidification, is one more factor affecting pipeline bearing capacity. This situation was investigated by means of setting of hollows (linear size 1 mm) near the fusion line, i.e. being macrodefects and taking total volume fraction of weld metal around 0.07. Calculation of microporosity development, according to the created procedure, results of which are given in the Table, showed a tangible influence of macropores on the pipeline bearing capacity, namely, reduction of internal limiting pressure from 20.4 up to 17.6 MPa. This result correlates with known experimental investiga-

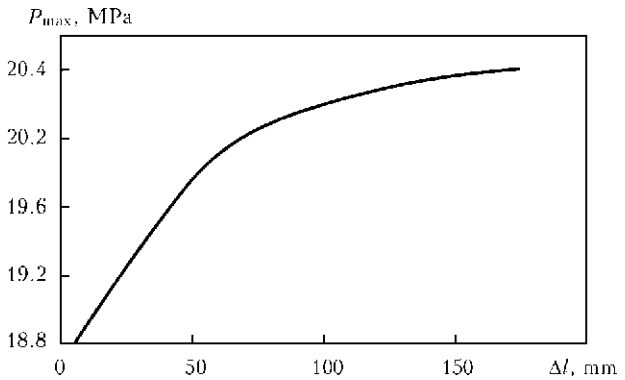

Figure 3. Dependence of limiting pressure in the pipeline from distance between thinning defect and circumferential weld

Concentration of micropores in weld area of pipeline element taking into account presence of macropores at limiting pressure 17.6 MPa

r, mm / *z*, mm	1	2	3	4	5	6	7	8	9	10	11
1	0	0	0	0	0	0	0	0	0	0	0
2	0	0	0	0	0	0	0	0	0	0	0
3	0	0	0	0	0	0	0	0	0	0	0
4	0	0	0	0	0	0	0	0	0	0	0
5	0.064	0.052	0	0	1.0	0	0	0	0	0	0
6	0.104	0.063	1.0	1.0	0.05	1.0	0.057	0.051	0	0	0
7	0.102	0.085	0.05	0.05	0.05	0.05	0.058	0.051	0	0	0
8	0.096	0.101	1.0	1.0	1.0	1.0	0.153	0.118	0.089	1.0	1.0
9	0.101	0.123	0	0	0	0	0.13	0.135	0.143	0.05	0.05
10	0.117	0.163	0	0	0	0	0.088	0.115	0.097	1.0	1.0
11	0.079	0	0	0	0	0	0.058	0.063	0.063	0	0
12	0	0	0	0	0	0	0	0	0.086	0.051	0
13	0	0	0	0	0	0	0	0.061	0.056	0	0
14	0	0	0	0	0	0	0	0	0	0	0
15	0	0	0	0	0	0	0	0	0	0	0
16	0	0	0	0	0	0	0	0	0	0	0

Cont.

r, mm / *z*, mm	12	13	14	15	16	17	18	19	20	21
1	0	0	0	0	0	0	0	0	0	0
2	0	0	0	0	0	0	0	0	0	0.05
3	0	0	0	0	0	0	0	0	0	0
4	0	0	0	0	0	0	0	0	0	0
5	0	0	0	0	0	0	0	0	0.06	0.057
6	0	0	0	0	0	0	0	0.057	0	0
7	0	0	0	0	0	0	0.063	0	0	0
8	1.0	1.0	1.0	1.0	1.0	1.0	0.086	0.062	0	0
9	0.05	0.05	0.05	0.05	0.05	0.05	0.082	0.062	0.05	0
10	1.0	1.0	1.0	1.0	0.05	0.05	0.067	0.062	0.06	0.059
11	0	0	0	0	1.0	1.0	0.09	0.081	0.07	0.073
12	0	0	0	0	0	0	0.07	0.074	0.08	0.075
13	0	0	0	0	0	0	0.056	0.066	0.07	0.071
14	0	0	0	0	0	0	0	0.059	0.06	0.064
15	0	0	0	0	0	0	0	0.054	0.06	0.059
16	0	0	0	0	0	0	0	0	0.05	0.055

Note. Weld area is marked by grey color.

tions [18] and existing requirements to quality of site welds of the main pipelines.

Conclusions

1. Complex procedure for numerical evaluation of limiting state of the welded structures inclined to ductile fracture under effect of external stresses was developed. A model of nucleation, development and interaction of ductile fracture micropores as well as the criteria of microdefect formation and coming of structural element limiting state were proposed for this based on the finite-element solution of nonstationary thermoplasticity boundary problem.

2. Regularities of the development of damage in metal structure under effect of the internal pressure were considered on the example of main pipeline section with the external defect of local metal loss near the site circumferential weld. It is shown that the limiting state of defective structure is characterized by formation of the general damage area between weld and geometry anomaly. At that, the less is the distance between defect and weld, the lower is the service loading, necessary for showing the mutual effect between them and further appearance of macrodefects. This, in turn, can reduce the pipeline bearing capacity to 10 % in comparison with defect-free structure.

3. Considered are the peculiarities of effect of macropore type weld defects, formed from gas bubbles solidified in the weld metal. Possible significant effect of indicated defects on the structure bearing capacity is shown, i.e. reduction of the pipeline limiting pressure to 17.6 MPa for volume concentration of arbitrary distributed pores 0.07 in the weld metal.

1. Rybin, V.V. (1986) *High plastic strains and fracture of metals*. Moscow: Metallurgiya.
2. Tvergaard, V. (1990) Material failure by void growth to coalescence. *Adv. Appl. Mech.*, **27**, 83–151.
3. Hancock, I., Mackenzie, A.C. (1976) On the mechanism of ductile failure of a high strength steel subjected in multi-axial stress state. *J. Mech. and Phys. Solids*, 24(**213**), 147–149.
4. Xue, L. (2008) Constitutive modeling of void shearing effect in ductile fracture of porous materials. *Eng. Fract. Mech.*, **75**, 3343–3366.
5. Nahshon, K., Hutchinson, J.W. (2008) Modification of the Gurson model for shear failure. *Eur. J. Mech. Solids A*, **27**, 1–17.
6. Gurson, A.I. (1977) Continuum theory of ductile rupture by void nucleation and growth. Pt 1: Yield criteria and flow rules for porous ductile media. *J. Eng. Mater. and Technol.*, **1**, 2–15.
7. Tvergaard, V., Needleman, A. (1984) Analysis of the cup-cone fracture in a round tensile bar. *Acta Metallurgica*, **32**, 157–169.
8. Needleman, A. (1972) Void growth in an elastic-plastic medium. *J. Appl. Mech.*, **39**, 964–970.
9. Karzov, G.P., Margolin, B.Z., Shvetsova, V.A. (1993) *Physical-mechanical modeling of fracture processes*. St.-Petersburg: Politekhnika.
10. Reznikov, A.N., Shaterin, M.A., Kunin, V.S. et al. (1986) *Cutting of metals with plasma heating*. Moscow: Mashinostroenie.
11. (1970) *Theoretical principles of welding*. Ed. by V.V. Frolov. Moscow: Vysshaya Shkola.
12. Sedmak, A., Younise B., Rakinetal, M. et al. Ductile fracture resistance of the weld metal and heat affected zone in a HSLA steel welded joint. *http://www.structuralintegrity.eu/pdf/esis/TC/1/ESIS-TC1-Freiburg-Sedmak%20et%20al.pdf*
13. Makhnenko, V.I. (1976) *Calculation methods of examination of welding stress and strain kinetics*. Kiev: Naukova Dumka.
14. Makhnenko, V.I. (2006) *Resource of safety service of welded joints and assemblies of current structures*. Kiev: Naukova Dumka.
15. Makhnenko, V.I. (2013) Problems of examination of modern critical welded structures. *The Paton Welding J.*, **5**, 21–28.
16. (1967) *Physical properties of steels and alloys applied in power engineering*: Refer. Book. Ed. by B.E. Nejmark. Moscow; Leningrad: Energiya.
17. (2008) *DSTU-N B V2.3-21:2008*: Guideline. Determination of residual strength of main pipelines with defects. Kyiv: Minregionbud Ukrainy.
18. Izbenko, V.F., Avramenko, V.I., Krivosheya, V.S. (1974) Experimental investigation of design strength of 14KhGN2MD and VMSt.3 steel joints by hydrostatic buckling method. *Avtomatich. Svarka*, **3**, 26–29.

Received 20.06.2013

SOME TECHNIQUES FOR REDUCING FILLER POWDER LOSSES IN MICROPLASMA CLADDING

K.A. YUSHCHENKO, A.V. YAROVITSYN, D.B. YAKOVCHUK, A.A. FOMAKIN and **V.E. MAZURAK**
E.O. Paton Electric Welding Institute, NASU
11 Bozhenko Str., 03680, Kiev, Ukraine. E-mail: office@paton.kiev.ua

At reconditioning of the edges of gas turbine engine blades by microplasma powder cladding losses of cladding materials are inevitable. In order to increase the process effectiveness in this work the method of assessment of deposited bead mass at successive increase of weld pool dimensions on a wide and a narrow substrate was used to study the regularities of radial distribution of two-phase flows of microplasma-filler powder. It is established that experimental data of radial distribution of such flows on the anode surface are in satisfactory agreement with the normal distribution law. The method of calorimetry on a two-section water-cooled anode was used to evaluate the coefficient of concentration of specific heat flow of microplasma arc for cladding. It is shown that in the region of modes of microplasma cladding filler powder can be fed into the product plane with the concentration up to four times greater than the specific heat flow of the arc, and the ratio of effective diameters of powder feeding and heating spot is equal to 0.57–0.92. Influence of some design parameters of microplasmatron and process parameters of cladding on gas-powder flow concentration is described. Relationships between bead width, microplasmatron focusing nozzle diameter and characteristics of concentration of powder feeding into the weld pool required to limit filler powder losses within 1.44–2.56 % at deposition of metal of less than 3 mm thickness on blade edges are established. 11 Ref., 2 Tables, 7 Figures.

Keywords: *microplasma powder cladding, blade edges, microplasmatron, coefficient of powder utilization, concentration of two-phase flow, microplasma-filler wire*

Investigations performed at the E.O. Paton Electric Welding Institute and practical verification of the process of microplasma powder cladding (welding) showed a reliable achievement of technological strength in fusion welding and subsequent heat treatment, as well as high performance of welded joints of high-temperature nickel alloys with γ′-phase content of more than 45 % [1–4]. Microplasma powder cladding at repair of edges of gas turbine engine blades is characterized by: range of effective thermal power of the arc of 100–650 W and heat input of 250–3000 J/mm; capability of application of filler material identical in its chemical composition to blade material, for instance, ZhS32-VI, IN738LC, ZhS6U; reliable protection of repair zone and good formation of deposited metal. The process does not require item preheating and in most of the cases preliminary homogenizing of blade material before cladding.

At reconditioning of edges of gas turbine engine blades losses of cladding materials are inevitable, which, in their turn, are assessed as difference of masses of consumed filler material and deposited metal. Comparative analysis [5] showed that at microplasma powder cladding of the edges of blades by a bead 3.5 mm thick an increased level of filler material losses is observed compared to argon arc cladding. More than 3/4 of them are remains unsuitable for further application. An acceptable level of losses (≈ 10.5 %) in microplasma powder cladding on a narrow substrate (blade edge) with more than 3 mm deposit thickness was achieved due to re-use of powder remains at the coefficient of powder utilization (CPU) of 0.625 after collection of its remains, sieving and drying. During batch microplasma powder cladding of blade edges less than 3 mm wide [3, 4], it was established that the fraction of remains unsuitable for use can increase up to 30 % of the initial amount of filler material. Further utilization of such filler remains at cladding of high-temperature nickel alloys with γ′-phase content of 45 % is not rational in view of considerable deterioration of the quality of bead formation. Analysis of surface morphology of powder samples after using it three times at cladding showed that approximately 50 % of oxidized particles are present in the field of view of optical microscope (×50). Gradual accumulation of such particles in the dispersed filler material, probably, is the main cause for deterioration of welding-technological properties of filler material.

Thus, in the case of deposition of metal of not less than 3 mm thickness on blade edges, filler powder losses, despite it re-use, become much

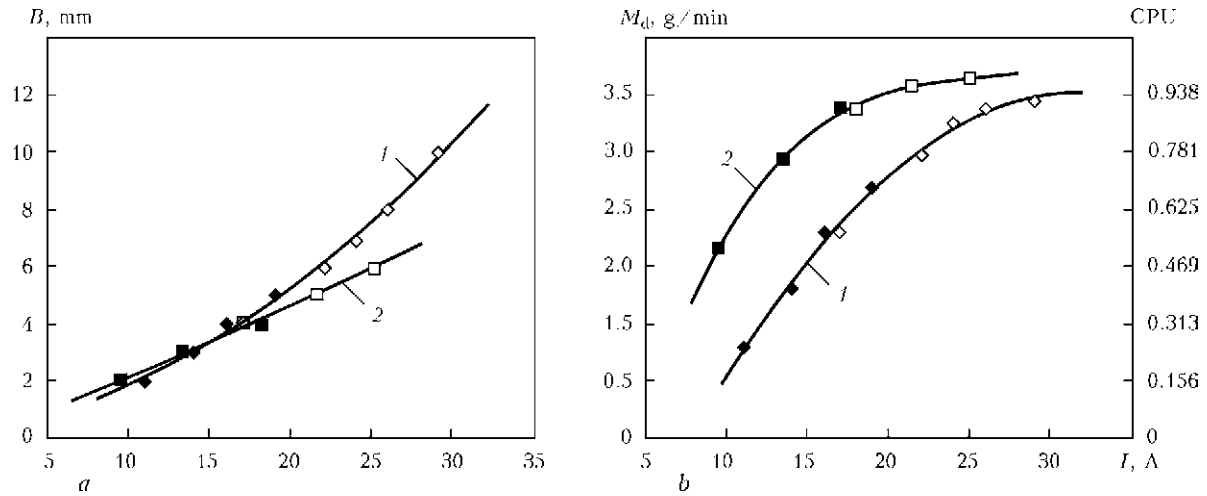

Figure 1. Dependence of bead width B (*a*), deposited metal specific mass M_d and CPU (*b*) on welding current I at v_d = = 2.75 m/h (flow rate of carrier gas (argon) 2.5; shielding gas (mixture of 90 % Ar + 10 % H_2) 7 l/min; base metal — austenitic stainless steel); *1* — microplasmatron with d_{pl} = 2.5 mm, d_f = 4.5 mm; 2 — d_{pl} = 1.8 mm; d_f = 2.5 mm; dark symbols — deposition on a narrow substrate; light ones — deposition on a wide substrate

greater. In view of the high cost of filler materials, such tasks require additional optimization of the process of microplasma powder cladding.

The main cause for filler losses is movement of its disperse particles on the periphery of plasma arc column, and furtheron — elastic recoil from the clad item surface beyond the weld pool zone [6]. In order to optimize the paths of filler material motion in the plasma arc, it is recommended to apply filler powders with particle diameter below 150–200 μm, adding them to the arc with the velocity of not less than 2 m/s at up to 40–45° angle to plasmatron axis. In view of considerable width of the weld pool (18–35 mm), filler powder losses in optimum modes of plasma-powder cladding do not exceed 5–8 % [6].

For deposition of less than 3 mm thick metal layer on blade edges, it is rational to lower powder losses by increasing microplasma arc concentration with fed disperse filler, i.e. increasing its relative quantity hitting the weld pool. The objective of this work is to consider the technological features of focusing of two-phase flows of microplasma-filler powder, which ensure concentrated delivery of filler material through the high-temperature region of the microplasma arc into the weld pool on a narrow substrate less than 3 mm wide.

Microplasmatron PPS-004 with side distributed feed of filler powder and focusing nozzle channel diameters of 2.5 and 4.5 mm was selected as the object of study. With these nozzles its stable operation is provided at up to 30–50 A welding current. It is known that plsmatrons with 4.0–4.5 mm diameter of focusing nozzle channel provide the most concentrated feeding of filler powder into the plasma arc at plasma-powder cladding [6, 7].

Concentration of filler powder feeding through the microplasma arc to the anode plane was assessed by determination of the mass of powder, hitting the weld pool at successive increase of its dimensions. Weld pool width was changed with increase of welding current at constant speed of microplasma arc displacement (Figure 1) within 2–5 mm for a narrow substrate (Table 1) and 4–10 mm for a wide substrate (2 mm thick plate). At cladding of a narrow substrate the bead was formed with more than 90° angle of contact to its surface, i.e. with side reinforcement from two sides. During a simple experiment at successive increase of weld pool width by 5 times, dependencies of variation of deposited bead specific weight M_d and CPU were derived, which characterize radial distribution of filler powder in the anode plane (see Figure 1). The above procedure allows elimination of the influence of elastic recoil of particles, inevitable at filler powder collection into multisection catchers.

Filler powder of austenitic stainless steel with 63–160 μm particle size was used in the experi-

Table 1. Deposited metal specific mass M_d and bead width B at deposition on a narrow substrate of width δ, depending on diameter d_f of plasmatron focusing nozzle channel

d_f, mm	δ, mm	I, A	B, mm	M_d, g/min
4.5	1.0	11.0	2.0	0.80
	1.6	14.0	3.0	1.30
	2.0	16.0	4.0	1.80
	2.5	19.0	5.0	2.18
2.5	1.0	9.5	2.0	1.66
	1.6	13.5	3.0	2.42
	2.5	18.0	4.0	2.88

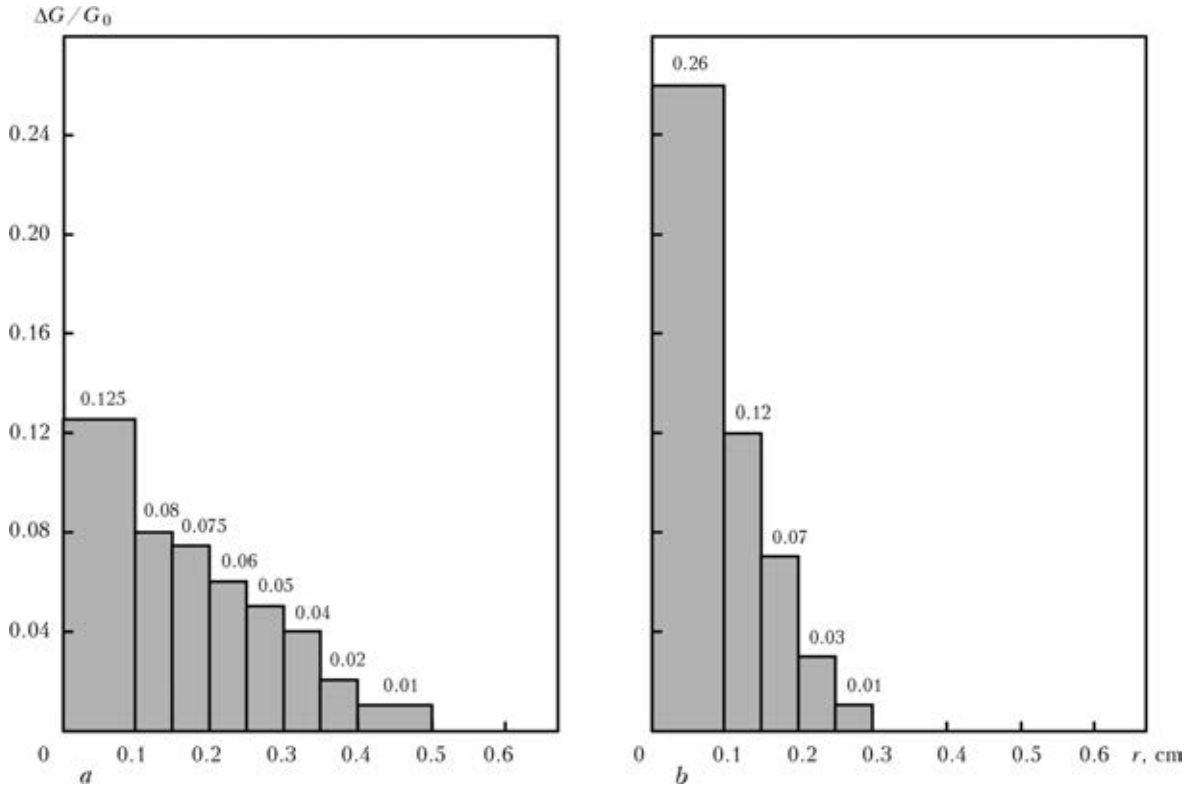

Figure 2. Histrogram of fed powder distribution in the direction normal to deposited bead axis, depending on parameters of PPS-004 microplasmatron: *a* — d_{pl} = 2.5 mm, d_f = 4.5 mm; *b* — d_{pl} = 1.8 mm; d_f = 2.5 mm

ments. Its tentative granulometric composition was as follows: –63 μm — 7 %; +63–80 μm — 10 %; +80–100 μm — 32 %; +100–125 μm — 39 %; +125–160 μm — 12 %. Efficiency of filler powder feed G_0 was equal to 3.20 g/min; powder was fed with 1 s interval. Such a specific amount of filler in all the experiments provided a stable formation of beads and was selected proceeding from practical application of blade edge building-up. M_d was experimentally determined by weighing the sample-plate with 0.02 g accuracy before and after cladding of 1 min duration. CPU was determined as the ratio of M_d to powder feed efficiency G_0.

Relative distribution of the amount of deposited metal $\Delta G/G_0$ in the direction normal to deposited bead axis (Figure 2), was calculated by experimental data in Figure 1 as:

$$(\Delta G/G_0)_i = (M_{B_{n+1}} - M_{B_n})/(2G_0), \qquad (1)$$

where $M_{B_{n+1}}$, M_{B_n} is the mass of deposited metal at successive increase of the weld pool width; n is the experiment number; i is the ordinal number of distribution. Obtained results, presented in Figure 2 in the form of histograms, characterize the distribution of filler powder in microplasma arc on the anode level during the process, and show the preference of application of microplasmatrons with $d_f < 4.5$ mm at deposition on a narrow substrate in terms of effectiveness of filler powder application.

In order to describe the specific heat flow of the arc a normally-circular heat source is widely used in the theory of welding processes, in which the intensity of its specific heat flow diminishes from the center to the edges of the heating spot by the so-called normal law (Gaussian distribution). The main parameters of such a representation were defined by N.N. Rykalin [8] and are interrelated by known relationships:

$$q_2(r) = q_{2m}e^{-kr^2}, \qquad (2)$$

$$q_{2m} = \frac{k}{\pi}q_{ef}, \qquad (3)$$

$$r_0 = \frac{1}{\sqrt{k}}, \qquad (4)$$

$$d_{ef} = 3.46/\sqrt{k}, \qquad (5)$$

where $q_2(r)$ is the radial distribution of power of welding arc heat flow in the item; q_{ef} is the effective thermal power of the arc; q_{2m} is the power of heat flow in heat source center or thermal energy density in the equivalent heating spot; r is the distance from the heat source center; k is the coefficient of specific heat flow concentration; r_0 is the equivalent radius of the heating spot, i.e. radius of a circle with uniform distribution of the heat flow from the source equivalent in its power to normal-circular distribution of

heat flow; d_{ef} is the effective diameter of the heating spot, i.e. diameter of the spot, through which 95 % of specific heat flow for the welding heat source passes into the item.

In our case establishing the relationships between the concentration of specific heat flow of microplasma arc and concentration of filler powder feeding into the weld pool is of interest.

Closeness of experimental histrograms (see Figure 2) to exponential dependence and of the weld pool shape in typical modes of microplasma powder cladding to a circle leads to an assumption of filler material distribution in the microplasma arc on the level of anode surface (weld pool) following the normal law. This was checked by the procedure of [9] based on superposition of the data of experimental histograms (Figure 2) onto an imaginary two-section powder catcher, successively moving with the histogram step along y axis (Figure 3). Distance from 0 to r_i (current step of histogram values) corresponded to $-y$ coordinate, and the sum of histogram ordinate values $\Delta G/G_0$ from r_i to ∞ characterized the relative intensity of powder flow in the right segment of powder feeding spot circumference.

Presentation of experimental data of histograms in the form of dependence $G(r) = G_{2m} \exp(-k_{p.c} r^2)$ is in good agreement with the normal law of distribution (Figure 3, *b*), where $k_{p.c}$ is the coefficient characterizing the concentration of filler powder feeding into the weld pool similar to the coefficient of concentration of arc specific thermal flow; G_{2m} is the relative density of application of filler powder on the level of anode surface. A number of parameters of filler powder feeding concentration calculated by experimental data, are given in Table 2.

It is established that decrease of channel diameter of focusing microplasmatron from 4.5 to 2.5 mm ensures a change of the area of effective spot of power feeding from 128.6 to 30.2 mm^2, i.e. actually by 4 times. Analysis of experimental (see Figure 2) and calculated (see Table 2) data shows that CPU values in the range from 0.84 to 0.88 correspond to equivalent radius of powder feeding spot.

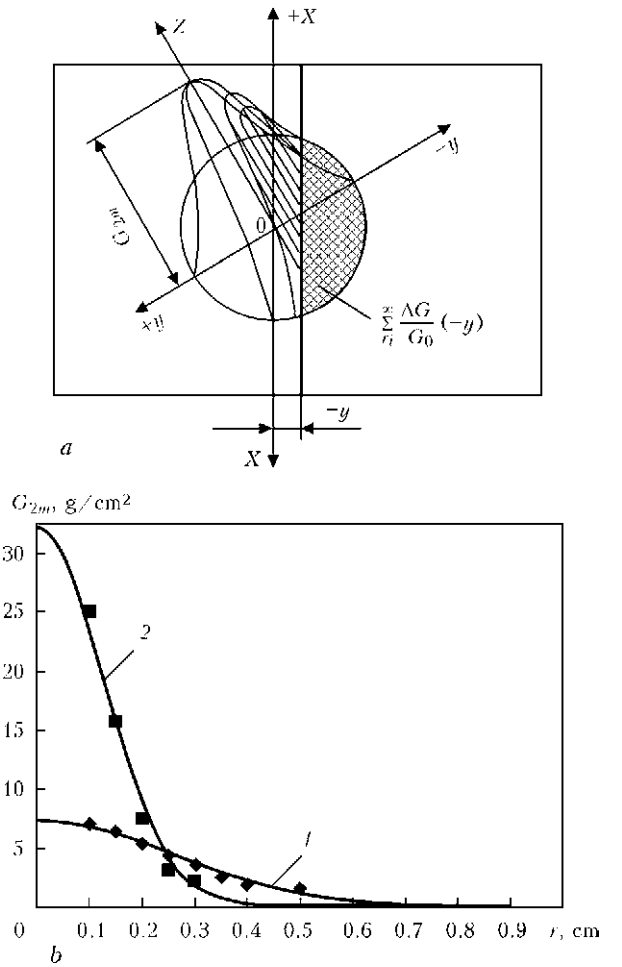

Figure 3. Schematic of two-phase microplasma-filler powder flow over two-section powder catcher (*a*) and calculated distribution of fed powder by a normal law in anode plane (*b*): *1* — d_{pl} = 2.5 mm, d_f = 4.5 mm; 2 — d_{pl} = 1.8 mm, d_f = 2.5 mm; symbols — experimental data, solid curve — simulation

Thus, in order to ensure a high effectiveness of filler powder utilization at certain design parameters of microplasmatron, determined mainly by value d_f, weld pool width should be larger than the equivalent diameter of powder feeding spot ($B \geq 2r_0$). In the general form for deposition on a narrow substrate the above dependence, allowing for (4), can be written as:

$$B = \delta + 2y_d \geq 2r_0 = \frac{2}{\sqrt{k_{f.c}}}, \qquad (6)$$

where y_d is the design side allowance at bead formation.

Table 2. Characteristics of radial distribution of two-phase microplasma–filler powder flow in anode plane (5 mm distance from focusing nozzle edge)

Designation	d_f, mm	d_{ef}, cm	$k_{p.c}$, cm^{-2}	r_0, cm	CPU at $B = 2r_0$	B, cm	P_{res} at $B = 2r_0$
Experimental	4.5	1.28	7.24	0.37	0.88	0.74	0.0144
Experimental	2.5	0.62	31.60	0.18	0.84	0.36	0.0256
Calculated	1.6	0.35	100.00	0.10	0.85	0.20	0.0225

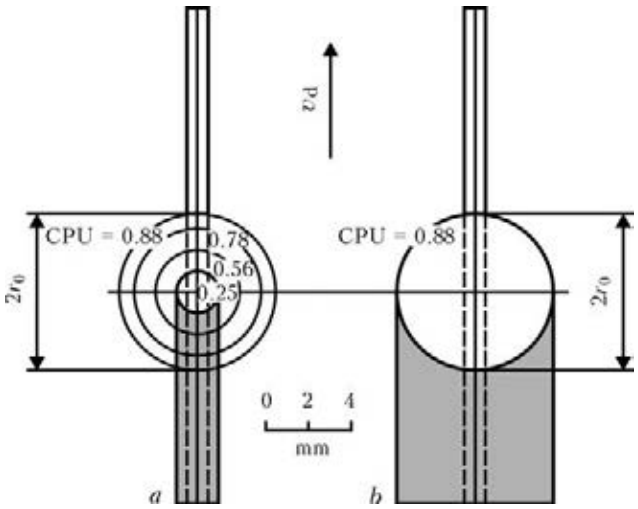

Figure 4. Features of cladding of a narrow substrate 1 mm wide at application of microplasmatron with d_f = 4.5 mm with insufficient concentration of two-phase microplasma-filler powder flow: *a*, *b* — see the text

At insufficient concentration of powder feeding into the weld pool during deposition on a narrow substrate of a bead 1–3 mm wide two limit cases can be distinguished, lowering the effectiveness of the process of microplasma powder cladding:

- increased powder losses at cladding at lower current (Figure 4, *a*);
- increased side allowances of the deposited bead at cladding at higher current (Figure 4, *b*).

In case $B \geq 2r_0$ anticipated powder losses P_{res} after two cycles of its utilization, calculated by the dependence given below

$$P_{res} = (1 - CPU) - (1 - CPU)CPU = \\ = CPU^2 - 2CPU + 1, \quad (7)$$

will be not more than 1.44–2.56 %.

Detected regularities further allowed prediction of parameters of concentration of powder feeding onto the anode plane (see Table 2), required for microplasma powder cladding with low powder losses at 2 mm width of the weld pool.

Coefficient of concentration of specific heat flow, *k*, of microplasma arc without powder feeding, corresponding to conditions of experiments in Figures 2, 3, was determined by the procedure of [9] by calorimetry in a two-section flow calorimeter.

For the given microplasma arc in the range of currents of 10–40 A, *k* experimental values are equal to 5.5–10.5 cm^{-2} (Figure 5). Appearance of microplasma arc for cladding with different kinds of shielding gas and degree of its constriction by plasmatron nozzles is given in Figure 6. For plasma arcs in plasma-powder cladding in the range of currents of 50 to 300 A, respective *k* values are equal to 1.8–2.0 — 4.8–6.5 cm^{-2} [6, 7]. For a microplasma arc for welding [10], running in argon, by the data of [11], coefficient of concentration of specific heat flow in the range of currents of 4–25 A is equal to 40–150 cm^{-2}.

Comparison of experimental data for radial distribution of filler powder in its feeding spot and of specific heat flow on anode surface (see Table 2 and Figure 5) shows that at microplasma powder cladding the ratio of the respective concentration coefficients is in the range of 0.96 to 4.00. In its turn, the ratio of effective diameters

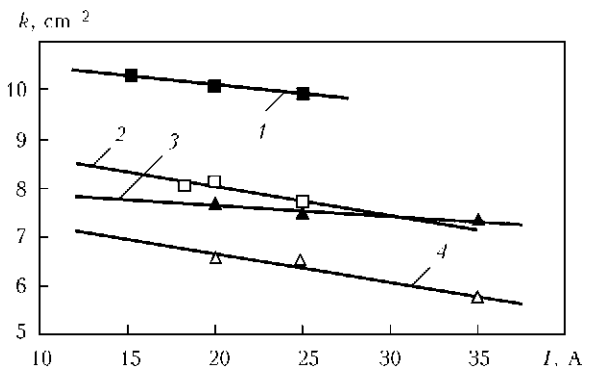

Figure 5. Dependence of coefficient of concentration of specific heat flow *k* into microplasma arc anode on welding current: *1* — d_{pl} = 1.8 mm; d_f = 2.5 mm, shielding gas — 90 % Ar + 10 % H_2; *2* — d_{pl} = 1.8 mm; d_f = 2.5 mm, shielding gas — Ar; *3* — d_{pl} = 2.5 mm; d_f = 4.5 mm, shielding gas — 90 % Ar + 10 % H_2; *4* — d_{pl} = 2.5 mm; d_f = 4.5 mm, shielding gas — Ar

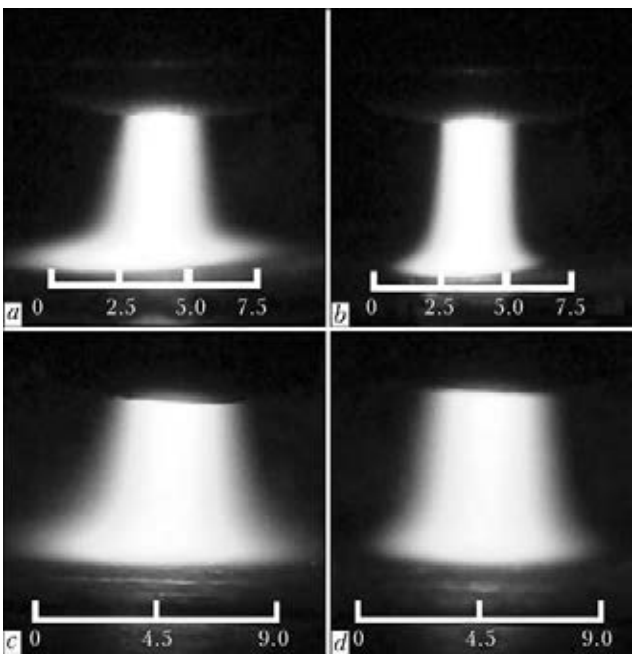

Figure 6. Appearance of a microplasma arc with effective thermal power of 341 W at different degrees of arc constriction by microplasmatron nozzles: *a* — d_{pl} = 1.8 mm, d_f = = 2.5 mm, shielding gas — Ar; *b* — d_{pl} = 1.8 mm; d_f = = 2.5 mm, shielding gas — 90 % Ar + 10 % H_2; *c* — d_{pl} = = 2.5 mm, d_f = 4.5 mm, shielding gas — Ar; *d* — d_{pl} = = 2.5 mm; d_f = 4.5 mm, shielding gas — 90 % Ar + 10 % H_2. Distance to anode is 5 mm

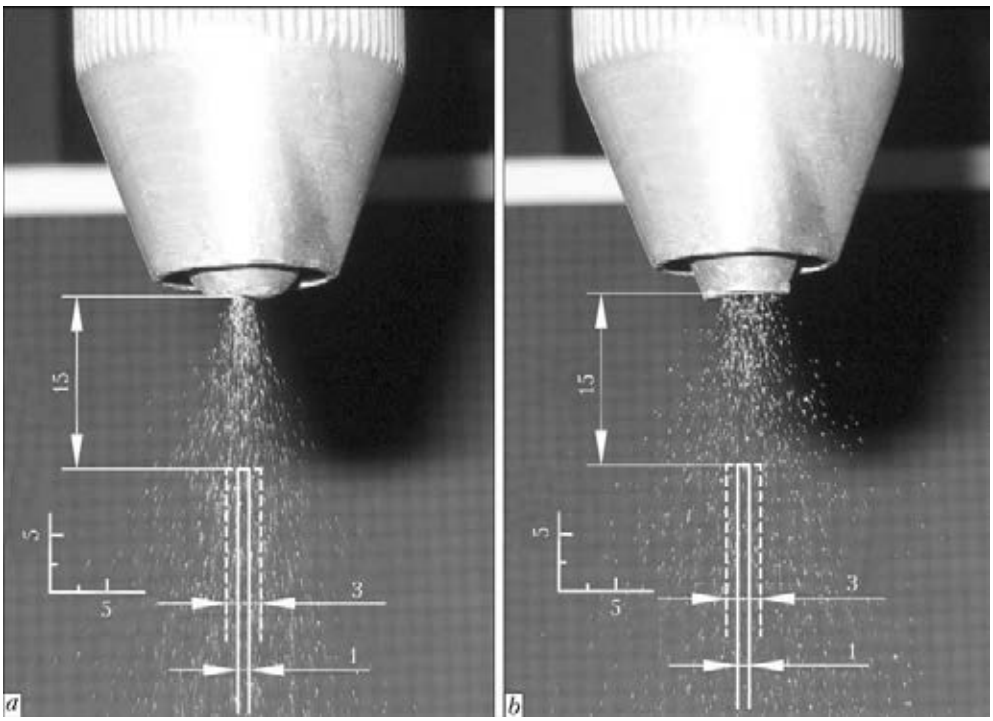

Figure 7. Appearance of powder flow at exit from microplasmatron focusing nozzle, depending on its channel diameter: *a* — d_f = 2.5 mm; *b* — d_f = 4.5 mm

of powder feeding and heating spot is equal to 0.57 to 0.92.

Analysis of experimental and published data shows that characteristics of specific heat flow of microplasma arc for cladding are close to respective characteristics of plasma arc for plasma-powder cladding. However, the task of optimization of concentration of powder feeding for deposition of metal less than 1.5 mm thick on blade edges (see Table 2), requires application of microplasmatrons with nozzle design parameters similar to those of plasmatrons for microplasma welding [10]. Derived dependencies of radial distribution of heat flow of microplasma arc and filler powder can be used for further optimization of design parameters of microplasmatrons with a high concentration of disperse filler feeding (ensuring the necessary stability of arcing and cladding, and reliability of weld pool shielding).

In microplasma powder cladding of blade edges with deposition of metal 1–3 mm thick, filler losses can be reduced not only by reducing d_f in microplasmatron, but also by optimizing the concentration of microplasma-powder flow through rational selection of the distance from focusing nozzle to item. A feature of microplasma powder cladding is the fact that at powder feeding at less than 5 g/min, its flowing either in the arc column, or in the mode of power feed checking, is poorly registered by the human eye.

Powder flow photographing against a contrast background was used for visual assessment of the concentration of powder flow in the mode of powder feed checking (Figure 7). Analysis of photographs showed that such a flow preserves its concentration assigned by the diameter of focusing nozzle channel, at 5 to 7 mm distance from its edge, and then becomes considerably wider. In this case dependence (6) for the above distance can be complemented by:

$$B = \delta + 2y_d \geq 2r_0 = \frac{2}{\sqrt{k_{p.c}}} \approx d_f. \qquad (8)$$

With flow expansion at more than 7 mm distance from the focusing nozzle edge, quantity of powder, which can hit the weld pool on a narrow substrate 1–3 mm wide, becomes essentially smaller.

Conclusion

The paper deals with technological features of focusing of two-phase flows of microplasma-filler powder, delivering filler material to the weld pool through high-temperature region of the arc for the case of microplasma cladding of blade edges less than 3 mm wide. Technological recommendations have been substantiated on selection of focusing nozzle channel diameter and distance from microplasmatron to the item, depending on the width of narrow substrate being clad.

A good agreement was established between the normal law of distribution for a radial distribution of a two-phase flow of microplasma-

filler powder in the spot of its feeding in the anode plane.

For the conditions of microplasma powder cladding, a relationship between the coefficients of concentration of specific heat flows of filler powder and arc heat (0.96–4.00) was established, as well as the ratio of effective diameters of powder feeding spot and heating spot (0.57–0.92).

Relationships of bead width, diameter of microplasmatron focusing nozzle and characteristics of concentration of powder feeding into the weld pool were established, which are required for limitation of filler powder losses within 1.44–2.56 % in cladding of blade edges. It is shown that for cladding on a narrow substrate less than 3 mm wide it is necessary to provide the coefficient of concentration of specific flow of powder in its feeding spot in the range of 31.6–100 cm^{-2}. Derived regularities can be used for further optimization of design parameters of microplasmatrons with a high concentration of disperse filler feed.

1. Savchenko, V.S., Yushchenko, K.A., Savolej, N.I. (1993) Peculiarities of welding of high-nickel dispersion-hardened heat-resistant alloys and repair of products manufactured from them. *Avtomatich. Svarka*, **10**, 31–33.
2. Yushchenko, K.A., Cherviakova, L.V., Nakonechny, A.A. (2002) High-strength repairs of IN738LC blades and vanes. *IIW Doc. XII-1724-02–2002*.
3. Yushchenko, K.A., Savchenko, V.S., Yarovitsyn, A.V. et al. (2010) Development of the technology for repair by microplasma powder cladding of flange platform faces of aircraft engine high-pressure turbine blades. *The Paton Welding J.*, **8**, 21–24.
4. Yushchenko, K.A., Yarovitsyn, A.V. (2012) Improvement of the technology for repair of upper shroud web of aircraft gas-turbine engine blades. In: *Problems of resource and safe service of structures of buildings and machines*. Kiev: PWI.
5. Yarovitsyn, A.V., Yushchenko, K.A., Nakonechny, A.A. et al. (2009) Peculiarities of low-amperage argon-arc and microplasma powder cladding on narrow substrate. *The Paton Welding J.*, **6**, 31–35.
6. Gladky, P.V., Pereplyotchikov, E.V., Ryabtsev, I.A. (2007) *Plasma cladding*. Kiev: Ekotekhnologiya.
7. Som, A.I. (1999) New plasmatrons for plasma powder cladding. *Avtomatich. Svarka*, **7**, 44–48.
8. Rykalin, N.N. (1951) *Calculations of thermal processes in welding*. Moscow: Mashgiz.
9. Demyantsevich, V.P., Mikhajlov, N.P. (1973) Investigation of distribution of microplasma arc heat in displacement of center of heating spot from joint axis. *Svarochn. Proizvodstvo*, **6**, 1–3.
10. Paton, B.E., Gvozdetsky, V.S., Dudko, D.A. et al. (1979) *Microplasma cladding*. Kiev: Naukova Dumka.
11. Demyantsevich, V.P., Mikhajlov, N.P. (1973) Interaction of microplasma arc with heated body. *Svarochn. Proizvodstvo*, **8**, 2–4.

Received 26.04.2013

MECHANICAL PROPERTIES OF JOINTS OF HEAT-RESISTANT 10Kh12M, 10Kh9MFBA GRADE STEELS, MADE BY ELECTRON BEAM WELDING

V.M. NESTERENKOV, L.A. KRAVCHUK and **Yu.A. ARKHANGELSKY**
E.O. Paton Electric Welding Institute, NASU
11 Bozhenko Str., 03680, Kiev, Ukraine. E-mail: office@paton.kiev.ua

In the course of development of works on the technology of electron beam welding of special steels the investigations of properties of the joints of heat-resistant 10Kh12M, 10Kh9MFBA grade steels of δ_m = = 30 mm thickness, made by single- and multipass electron beam welding using horizontal electron beam at the speed of v_w = 3 mm/s without preheating, were carried out. The results of mechanical tests on rupture and impact toughness and also nature of fracture after electron beam welding and after it with the next tempering are given. It was established that toughness and ductility of welded joints of both heat-resistant steels after the first main pass and after the second one in electron beam welding with the next tempering are preserved almost at the same level. The fracture of welded specimens of both alloys, oriented across the weld metal, occurs along the base metal far from the weld, beyond the heat affected zone. The fracture surface is dull. The formed relief has characteristic features of plastic fracture. As a result of tempering the strength of welded joints of both alloys decreases not considerably, and toughness with ductility increase. The third of the passes in electron beam welding results in formation of defects in a form of middle cracks and brittle low-ductile structures in weld structure and near-weld zone. 7 Ref., 2 Tables, 3 Figures.

Keywords: *electron beam welding, heat-resistant steels, welded joints, welding speed, preheating, tempering, strength, toughness, elongation, reduction in area, number of passes*

One of the decisive factors influencing the rate of increment of tensile stresses during weld crystallization and resistance of weld metal to formation of longitudinal hot cracks in the middle of a weld is energy input of welding. As is shown in work [1], the electron beam welding (EBW) of heat-resistant steels of martensite-ferrite class of grades 10Kh12M and 10Kh9MFBA of δ_m = = 30 mm thickness without preheating should be performed at the speed of $v_w \leq 3$ mm/s which corresponds to the energy input of 2.56 kJ/mm. At the increase of EBW speed along the weld axis on the line of abutting crystallites growing in the direction meeting each other from the opposite sides of cast zone boundaries, the longitudinal crystallization cracks («middle» cracks) of 2–15 mm height and 0.05–0.2 mm width appear. Besides, with increase of width of a weld and also at the presence of local extensions with increment of tensile stresses on it during crystallization of a weld, the probability of formation of middle cracks grows considerably [2–7]. To prevent the formation of cracks it is necessary to provide formation of narrower welds with a uniform width along the depth of penetration.

In this work the mechanical properties and nature of fracture of welded joints of heat-resistant 10Kh12M and 10Kh9MFBA steels, made by single- and multipass EBW without preheating were investigated.

The control of quality and strength properties of welded joints of heat-resistant steels 10Kh12M and 10Kh9MFBA after EBW at the speed of $v_w \leq$ ≤ 3 mm/s can be performed by mechanical tests in accordance with the GOST 6996–66. To determine static and dynamic characteristics of welded joints the given standard establishes the shapes and sizes of specimens and sequence of mechanical tests.

The specimens of welded joints of heat-resistant steels 10Kh12M and 10Kh9MFBA were tested in their initial state and after tempering. The result of tempering is influenced by temperature and heating rate, holding time and cooling rate. The heat temperature was selected coming from the conditions of recovery of ductility and toughness of near-weld zone of heat-resistant steels with martensite structure and weld reaching the values close to the base metal. With the growth of tempering temperature the hardness and tensile strength of steel are decreased whereas toughness and ductility are increased. The time of holding depends on thickness of specimen, initial structure and chemical composition of the steel. Thus, the optimal conditions of tem-

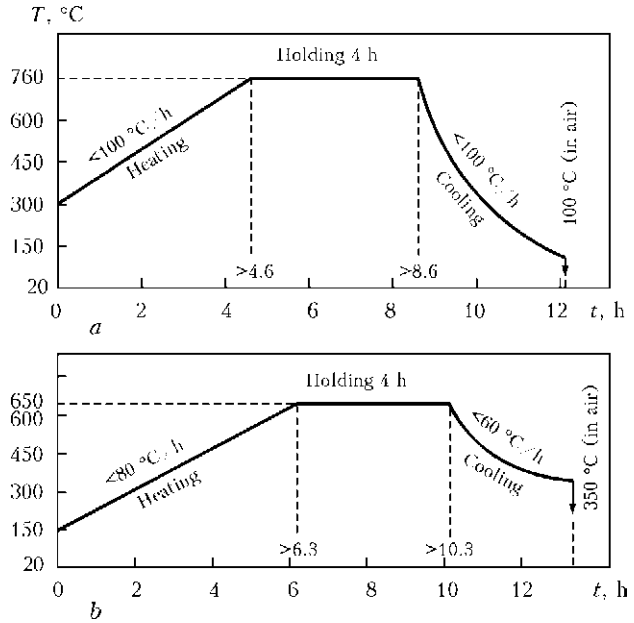

Figure 1. Diagram of tempering of welded specimens of heat-resistant steels 10Kh9MFBA (*a*) and 10Kh12M (*b*) (*t* — duration of tempering)

pering of heat-resistant steels 10Kh12M and 10Kh9MFBA for obtaining the required mechanical parameters of welded joints can not be the same. As is seen from Figure 1, the diagrams of tempering of test alloy welded specimens are differed by their temperature, heating and cooling rates.

The rupture tests of welded joints of heat-resistant steels 10Kh12M and 10Kh9MFBA were carried out on the cylindrical specimens of dumbbell type with the diameter of test part d_0 = = 6 mm after EBW and after EBW with the next tempering at the following conditions: U_{acc} = = 60 kV, I_b = 128 mA, v_w = 3 mm/s, $-\Delta I_f$ = = 15 mA, d_{circle} = 1.5 mm, $l_{w.d}$ = 200 mm. The specimens for tests were cut out at the half of the penetration depth of billets of δ_m = 30 mm thickness in welding using horizontal electron beam and movement of electron beam gun in the horizontal plane. As is seen from Figure 2 the specimens of both alloys after EBW and EBW with next tempering oriented across the weld metal are fractured along the base metal far from the weld beyond the heat affected zone (HAZ): for the specimens after EBW — at the distance of 9–10 mm from the weld axis, for the specimens after EBW with next tempering — at the distance of 6–6.5 mm from the weld axis. The formed relief in the place of fracture has a «pit» nature and has the typical features of plastic fracture: the surface of fracture is located in an inclined position (approximately at the angle of 45°) relatively to the direction of normal stresses, the fracture surface is dull, the edges of fractured area are considerably deformed. As a result of rupture tests, except of σ_t value other parameters of welded joint: $\sigma_{0.2}$, δ, ψ were also determined.

To control the dynamic characteristics of welded joints and make a correct selection of welding technology, the tests on impact bending of weld metal of some areas of a near-weld zone were carried out (on notched specimens). The tests were carried out using specimens of 10 × × 10 mm section with a semicircular notch profile for weld metal and V-shape notch profile for the

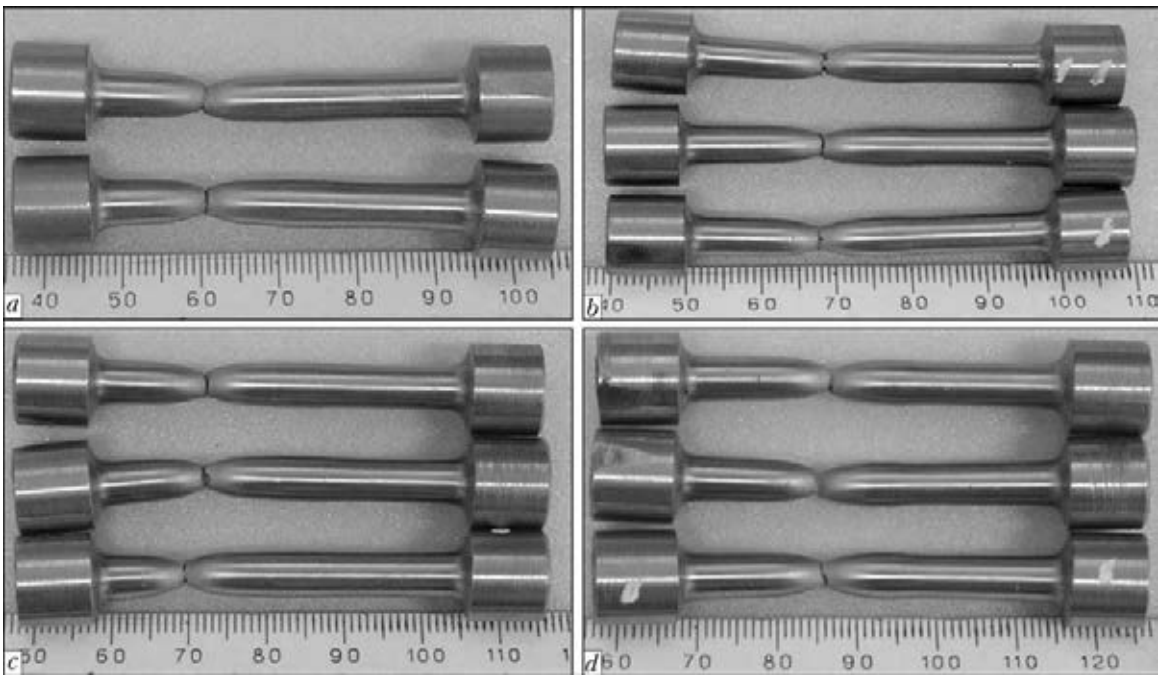

Figure 2. Specimens after mechanical rupture tests of welded joints of heat-resistant steels 10Kh12M (*a*, *b*) and 10Kh9MFBA (*c*, *d*) after EBW (*a*, *c*), EBW and next tempering (*b*, *d*)

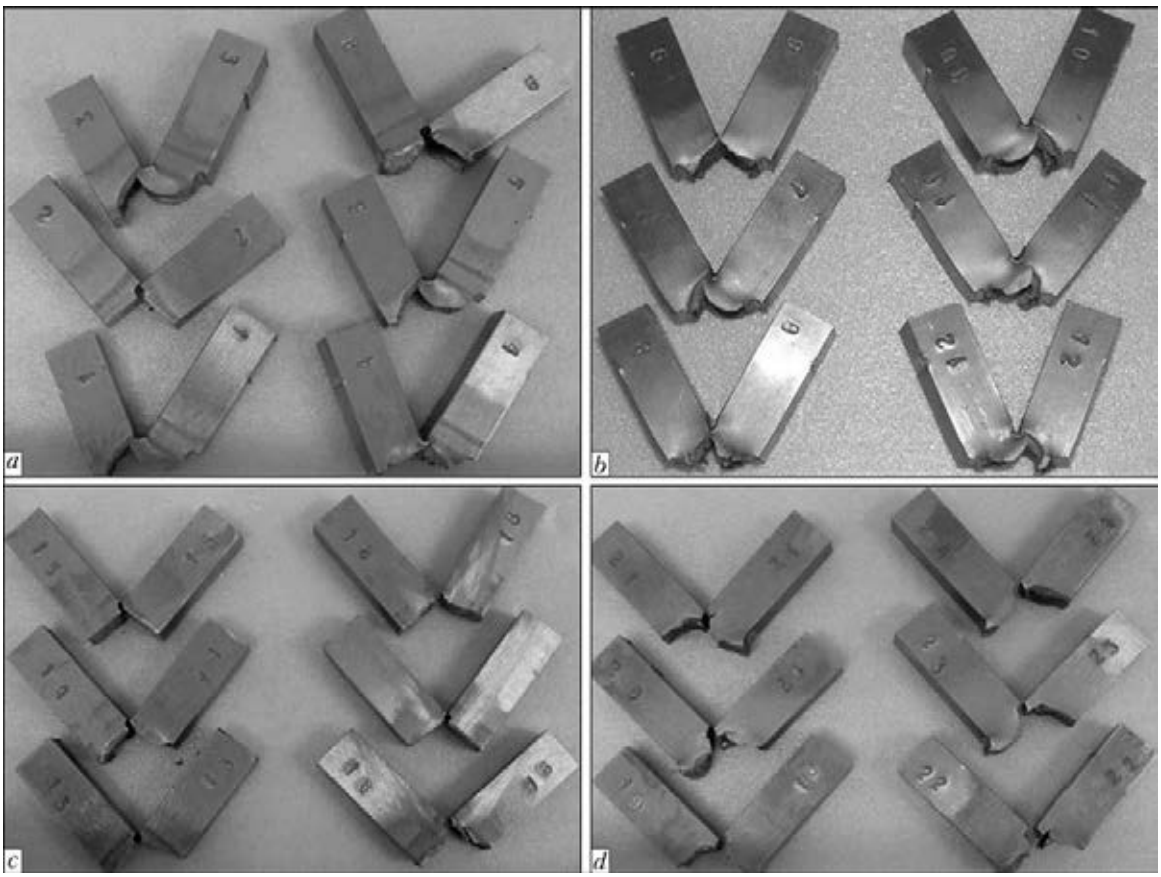

Figure 3. Specimens after mechanical tests on impact toughness of welded joints of heat-resistant steel 10Kh12M (*a*, *b*) and steel 10Kh9MFBA (*c*, *d*): *a* — after EBW (*1–3* — bending along the weld axis; *4–6* — bending along the fusion line); *b* — after EBW and next tempering (*7–9* — bending along the weld axis; *10–12* — bending along the fusion line); *c* — after EBW (*13–15* — bending along the weld axis; *16–18* — bending along the fusion line); *d* — after EBW and next tempering (*19–21* — bending along the weld axis; *22–24* — bending along the fusion line)

fusion line with the base metal. As is seen in Figure 3, *a*, *b*, all the specimens of heat-resistant steel 10Kh12M after EBW and after EBW with next tempering are bent in the process of impact toughness test mainly without the complete fracture; at incomplete fracture the formed relief has a «pit» nature and features of plastic fracture. The specimens after mechanical impact toughness tests of welded joints of heat-resistant steel 10Kh9MFBA (Figure 3, *c*, *d*) after EBW and after EBW with next tempering are bent with the complete fracture, the fracture surface is dull, the formed relief has features of plastic fracture.

The obtained data of mechanical properties of welded joints of heat-resistant steels 10Kh12M and 10Kh9MFBA after EBW and after EBW with next tempering are given in Table 1. As a result of tempering the strength of welded joints (σ_t, $\sigma_{0.2}$) is decreased, whereas toughness and ductility (*KCU*, *KCV*, ψ) are increased. The influence of tempering on mechanical properties of welded joints of heat-resistant steel 10Kh9MFBA has a stronger effect than that which can be predetermined by a larger amount of alloyed elements.

The ductility of test specimens, evaluated by the values of reduction in area, for heat-resistant steel 10Kh12M amounts to 68 % and for steel 10Kh9MFBA it is 73 %.

To optimize the repair technology of EBW of heat-resistant steels, removing the inner defects of welded joints and evaluate changes in shape and sizes of penetration zone and also strength characteristics, the investigations were carried

Table 1. Mechanical properties of welded joints of heat-resistant steels 10Kh12M (numerator) and 10Kh9MFBA (denominator)

State of metal	σ_t, MPa	$\sigma_{0.2}$, MPa	ψ, %	*KCU*, J/cm^2 (weld)	*KCV*, J/cm^2 (fusion line)
After welding	739/721.9	584.6/653	67/71	121.6/216.8	101.3/183.2
After welding and heat treatment (tempering at 650 °C, 4 h)	730/677.8	564/536.4	68/73	163.0/302.6	151.2/296.6

Table 2. Mechanical properties of welded joints of heat-resistant steels 10Kh12M (numerator) and 10Kh9MFBA (denominator) at the temperature of +20 °C depending on number of passes in EBW

Number of passes in EBW	σ_t, MPa	$\sigma_{0.2}$, MPa	ψ, %	KCV, J/cm^2 (fusion line)
Two passes + tempering	728.4/660.0	562.4/524.6	66/71.5	188.3/222.0
Three passes + tempering	718.0/664.0	552.0/522.4	70/70.6	10.2*/37.2**

*On the specimen of steel 10Kh12M with three passes the defect in a form of a middle crack is present.
**On the specimen of steel 10Kh9MFBA with three passes the brittle fracture is present.

out on influence of double and triple remeltings of the same weld. The preparation and tests of specimens with welded joints were carried out according to the procedure described above. To prevent influence of concurrent heating on the formation of face and reverse weld beads, the holding in time was performed before the second and the third passes for cooling down the specimen to room temperature. To provide the accurate movement of welding electron beam along the weld axis the position of specimen and welding program were preserved unchanged. It was found that such succession in producing of double and triple remeltings of the same weld does not influence the change in shape and sizes of penetration zone, and width of face and reverse beads remains almost unchanged. The fracture of specimens of dumbbell type of both steels after double and triple remeltings of the same weld with next tempering occurs on the base metal far from the weld, beyond the HAZ. The formed relief at the place of fracture has characteristic features of plastic fracture.

The obtained data of mechanical properties of welded joints on heat-resistant steels 10Kh12M and 10Kh9MFBA at the test temperature of +20 °C depending on the number of passes using welding electron beam with next tempering are given in Table 2. As is seen from the Table, toughness and ductility of welded joints (KCV, ψ) of both steels after the second pass and next tempering are preserved at the level of toughness and ductility of welded joints after the first pass (see Table 1). It should be noted that specimens after mechanical tests on impact toughness of welded joints after the second pass with next tempering of heat-resistant steel 10Kh12M are bent with the complete fracture along the fusion line, and heat resistant-steels 10Kh9MFBA are bent with the fracture along the fusion line, but specimens remain integral.

As is seen from Table 2 the mechanical properties of welded joints of heat-resistant steels 10Kh12M and 10Kh9MFBA are sharply deteriorated after the third pass with next tempering. The impact toughness of specimens of heat-resistant steel 10Kh12M is $KCV = 10.2$ J/cm^2, which is predetermined by the formation of defect in the form of a middle crack. The value of impact toughness of specimens of heat-resistant steel 10Kh9MFBA amounted to $KCV = 37.2$ J/cm^2 and was connected with the formation of brittle structures along the fusion line.

Thus, in EBW of heat-resistant steels 10Kh12M and 10Kh9MFBA only one pass after the first basic welding is admitted, as far as it does not lead to deterioration of mechanical properties of welded joints. The toughness and ductility of welded joints of both heat-resistant steels after the second pass in EBW and next tempering are preserved at the level of toughness and ductility of welded joints after the first basic pass.

1. Nesterenkov, V.M., Kravchuk, L.A., Arkhangelsky, Yu.A. et al. (2013) Welds formation in EBW of heat-resistant steels of the grades 10Kh12M and 10Kh9MFBA. *The Paton Welding J.*, **6**, 38–42.
2. Shida, T., Kita, H., Okamura, H. et al. Effect of welding parameters and prevention of defects in deep penetration EBW of heavy section steel. *IIW Doc. IV-239–78*.
3. Koshelev, Yu.V., Kovbasenko, S.N. (1985) Weld width as a criterion of hot cracking in electron beam welding . In: *Proc. of Int. Conf. on Electron Beam Technologies* (Varna, 26 May–2 June). Sofia, 1985.
4. Kasatkin, B.S., Kovbasenko, S.N., Nesterenko, V.I. (1989) One-pass electron beam welding of large thickness structural steels. *Avtomatich. Svarka*, **4**, 18–27.
5. Paton, B.E., Leskov, G.I., Zhivaga, L.I. (1976) Specifics of weld formation in electron beam welding. *Ibid.*, **3**, 1–5.
6. Morochko, V.P., Sorokin, L.I., Zorin, N.Ya. (1975) Influence of electron beam welding conditions on weld shape and properties of 10–15 mm thick welded joints of heat-resistant alloys. *Svarochn. Proizvodstvo*, **6**, 32–36.
7. Sorokin, L.I. (1998) Electron beam welding of heat-resistant alloys. *Ibid.*, **5**, 9–15.

Received 13.06.2013

STRUCTURE OF MULTILAYER SAMPLES SIMULATING SURFACED TOOLS FOR HOT DEFORMING OF METALS

I.A. RYABTSEV, A.A. BABINETS, G.N. GORDAN, I.I. RYABTSEV, T.V. KAJDA and **L.T. EREMEEVA**
E.O. Paton Electric Welding Institute, NASU
11 Bozhenko Str., 03680, Kiev, Ukraine. E-mail: office@paton.kiev.ua

Structure of multilayer deposited samples, which simulate the surfaced tools for hot deforming of metals and alloys by composition of deposited metal and sizes of deposited layers, was investigated. The surfacing was performed on samples of low-alloy medium-carbon steel 40Kh. To perform surfacing of working layer, the flux-cored wire PP-Np-25Kh5FMS was used, producing deposited metal of type of tool semiheat-resistant steel. To deposit a sublayer, two wires were applied: solid wire Sv-08A or flux-cored wire PP-Np-12KhMF. The investigations showed that the deposited metal 25Kh5FMS has a structure, consisting of bainite-martensite mixture and residual austenite, structure of sublayer 12KhMF is sorbite-like pearlite, and that of sublayer, deposited by wire Sv-08A, is ferrite. It was found that depending on chemical composition and structure of deposited sublayer the residual stressed state of deposited wear-resistant layer is greatly changed. In particular, the surfacing of sublayer by flux-cored wire PP-Np-12KhMF approximately 3 times decreases the residual stresses in working wear-resistant layer. 9 Ref., 2 Tables, 7 Figures.

Keywords: *arc surfacing, multilayer surfacing, structure of deposited metal, sublayer, thermal fatigue*

In metallurgy and machine building the tools and fixture for hot deforming of metals, which are applied under conditions of wear and simultaneous action of cyclic thermal and mechanical loads, are rather widely used. They include mill rolls, dies of hot stamping, rollers of machines for continuous casting of billets, knives of hot cutting, etc. As a rule, the defects in the form of thermal fatigue cracks are appeared on the surface of above-mentioned parts after several thousands of thermal cycles. At the same time the fatigue damages are appeared as a result of service cyclic mechanical loads after several millions of cycles.

To deposit a working layer on these parts, in particular on steel mill rolls, the materials of type of tool heat-resistant or semiheat-resistant steels are used. Taking into account that carbon or high carbon non-alloyed or low-alloyed structural steels are used as a base metal for mill rolls, the surfacing of steel mill rolls is performed with a ductile sublayer to improve the weldability. For the sublayer surfacing the wires Sv-08A, Sv-08G2S and other similar types are used [1–3].

Thermal fatigue cracks are propagated, as a rule, for a small depth from the roll surface. Therefore, after their appearance the damaged working deposited layer is periodically removed and resurfacing of part is made. Theoretically and in practice, the resurfacing can be made before the appearance of fatigue cracks in the roll from cyclic mechanical loads, which can lead to its fracture.

Residual (technological) and service thermomechanical loads, imposed on them, significantly influence the fatigue life of surfaced tools for hot deforming of metals. The experimental evaluation of effect of these characteristics on thermal and mechanical fatigue life of surfaced parts is complicated enough and requires great expenses.

To solve this problem, the authors of work [4] suggested the mathematical models and method of calculation of stress-strain state of deposited part directly after surfacing and during service. In particular, it was shown that surfacing of a ductile layer leads to the reduction and redistribution of residual stresses in the deposited working wear-resistant layer, thus leading to the increase in its thermal resistance. An important role in calculations is given to the processes of changing the structural state of base metal, deposited sublayer and working layer in the process of surfacing and next service. During calculations the thermokinetic diagrams of overcooled austenite decay [5] in the materials investigated and approaches, developed in works of V.I. Makhnenko, were used [6, 7].

The aim of this work was the experimental investigation of structure of multilayer deposited samples and comparison of their results with calculated data. In both cases the low-alloy medium-carbon steel 40Kh was selected as a base metal. For surfacing the working layer the flux-cored

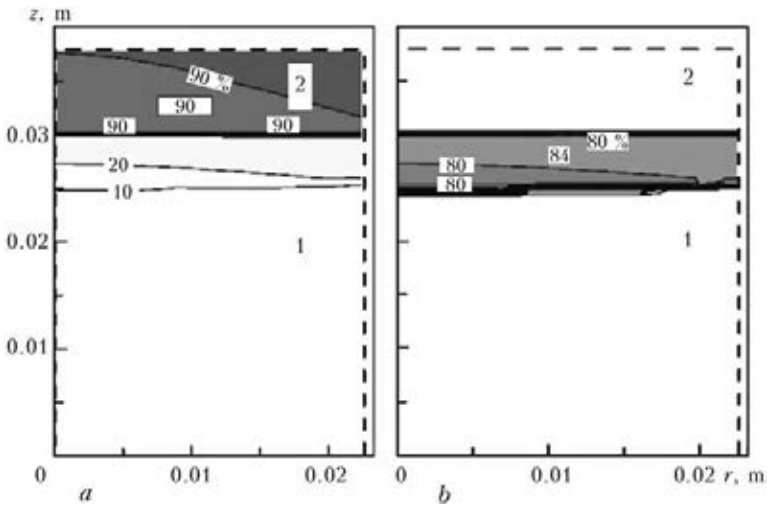

Figure 1. Calculation structure of sample deposited without sublayer: *a* — martensite; *b* — bainite; 1 — base metal, steel 40Kh; 2 — deposited wear-resistant layer of 25Kh5FMS

wire PP-Np-25Kh5FMS, was used providing the deposited metal of type of tool semiheat-resistant steel of appropriate composition. For surfacing the sublayer two wires: solid wire Sv-08A or flux-cored wire PP-Np-12KhMF were used. The flux-cored wire PP-Np-12KhMF had to provide the higher mechanical properties in the deposited steel sublayer.

As an example, Figures 1 and 2 give data about the microstructure of two deposited samples, determined by the calculation method. Two types of samples were studied: first one is the surfacing by flux-cored wire PP-Np-25Kh5FMS on steel 40Kh without sublayer (Figure 1); second one is the surfacing of sublayer by solid wire Sv-08A on steel 40Kh and then surfacing of base layer by flux-cored wire PP-Np-25Kh5FMS (Figure 2).

In the first sample the calculated concentration of a martensitic phase in external wear-resistant layer of 25Kh5FMS reaches 90 %, the rest ones are bainite and carbides (Figure 1, *a*). In the transition zone on the side of 40Kh steel the basic structure constituent is bainite (about 80 %), there is also a small amount (up to 10 %) of martensite (Figure 1, *b*).

In the sample, deposited with a sublayer, the structure of deposited working layer, corresponding to tool steel 25Kh5FMS, consists also of martensite (about 88 %), bainite (about 10 %) and carbides (Figure 2, *a*). Sublayer, corresponding to steel, containing 0.08 % of carbon, has a ferritic structure. In the transition zone from sublayer to base metal (steel 40Kh) a bainite-pearlite structure is observed (Figure 2, *c*).

In carrying out of experimental investigations of microstructure three types of semi-products were surfaced by above-mentioned wires using submerged arc method: No.1 — surfacing by flux-cored wire PP-Np-25Kh5FMS on steel 40Kh without a sublayer; No.2 — surfacing by flux-cored wire PP-Np-25Kh5FMS on steel 40Kh with a sublayer, deposited by flux-cored wire PP-Np-12KhMF; No.3 — surfacing by flux-cored wire

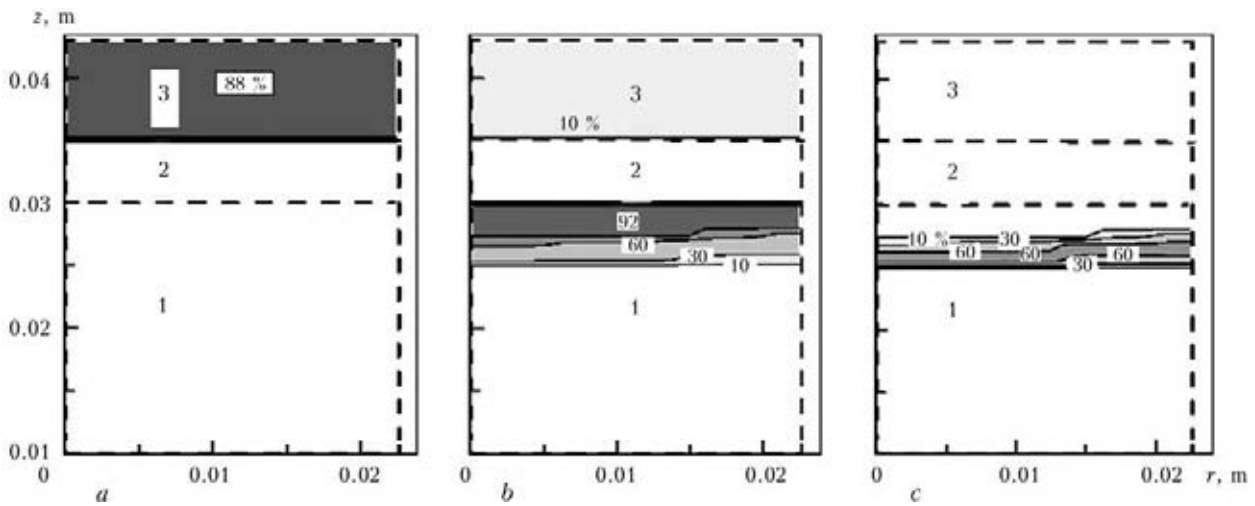

Figure 2. Calculation structure of sample, deposited with sublayer: *a* — martensite; *b* — bainite; 1 — base metal, steel 40Kh; 2 — deposited ductile layer of Sv-08A; 3 — deposited wear-resistant layer of 25Kh5FMS

PP-Np-25Kh5FMS on steel 40Kh with a sublayer deposited by solid wire Sv-08A.

Chemical composition of metal, deposited by these wires, is given in Table 1.

Samples were cut out of deposited semi-products for examination of microstructure and hardness of deposited metal and transition zone, as well as for their X-ray spectral and X-ray diffraction microanalyses.

Microstructure of deposited metal 25Kh5FMS and transition zone with base metal, steel 40Kh, (sample No.1) is presented in Figure 3. The deposited wear-resistant layer, steel 25Kh5FMS, has a martensitic-bainitic structure of hardness $HV0.5$ — 3410–4120 MPa (Figure 3, *a*). Small amount of light regions in structure can be classified as a residual austenite. It should be noted that deposited metal 25Kh5FMS has the same structure and hardness in two other experimental samples. Microstructure of transition zone, steel 40Kh + 25Kh5FMS, on the side of base metal is bainite and small amount of martensite (Figure 3, *b*).

Microstructure of sample No.2 is presented in Figure 4. In the transition zone (Figure 4, *a*) on the side of wear-resistant deposited metal 25Kh5FMS the transition from martensite-bainite structure (steel 25Kh5FMS) to structure of sorbite-like pearlite (steel 12KhMF) is observed. Microhardness on the side of steel 25Kh5FMS is $HV0.5$ — 2860 MPa, while on the side of sublayer 12KhMF it is $HV0.5$ — 2320–2340 MPa. Hardness of sublayer 12KhMF on the side of base metal 40Kh is within the ranges $HV0.5$ — 2570–2600 MPa. Such increase in hardness on the side of base metal can be explained by diffusion of carbon from steel 40Kh into sublayer 12KhMF. Microstructure of deposited sublayer 12KhMF is sorbite-like pearlite (Figure 4, *b*) with hardness $HV0.5$ — 2570–2600 MPa.

Table 1. Chemical composition of investigated types of deposited metal

Wire grade	C	Mn	Si	Cr	Mo	V
PP-Np-25Kh5FMS	0.33	0.60	0.54	6.05	1.30	0.68
PP-Np-12KhMF	0.12	0.64	0.35	1.16	0.41	0.32
Sv-08A	0.07	0.47	0.05	<0.3	–	–

Figure 5 presents a microstructure of sample No.3 (PP-Np-25Kh5FMS + Sv-08A). In the transition zone from sublayer to wear-resistant deposited layer 25Kh5FMS a coarse-grain ferrite structure is formed ($HV0.5$ — 1750 MPa) with fine-dispersed precipitations of pearlite along the grain boundaries (Figure 5, *a*). The sublayer has a pure ferritic structure with a rather smaller size of grain (Figure 5, *b*). Hardness in this zone is $HV0.5$ — 1550 MPa.

Rockwell hardness of deposited metal and transition zone was measured (Figure 6). In the sample, deposited without sublayer and with sublayer 12KhMF, a smooth transition from base

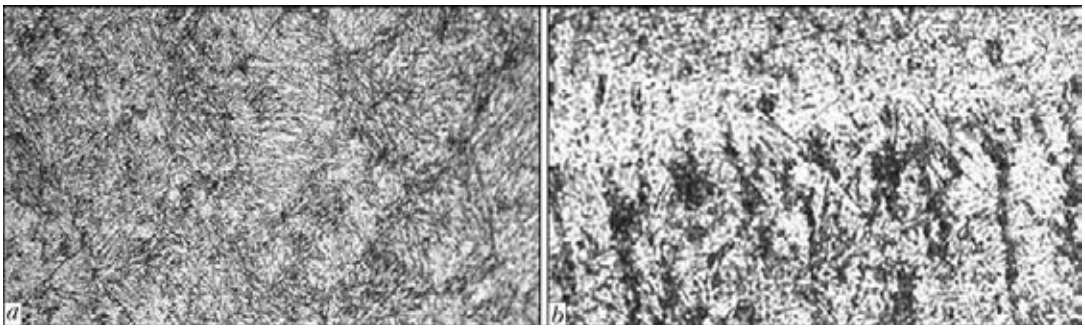

Figure 3. Microstructure (×320) of deposited metal of 25Kh5FMS (*a*) and transition zone of 25Kh5FMS + 40Kh (*b*)

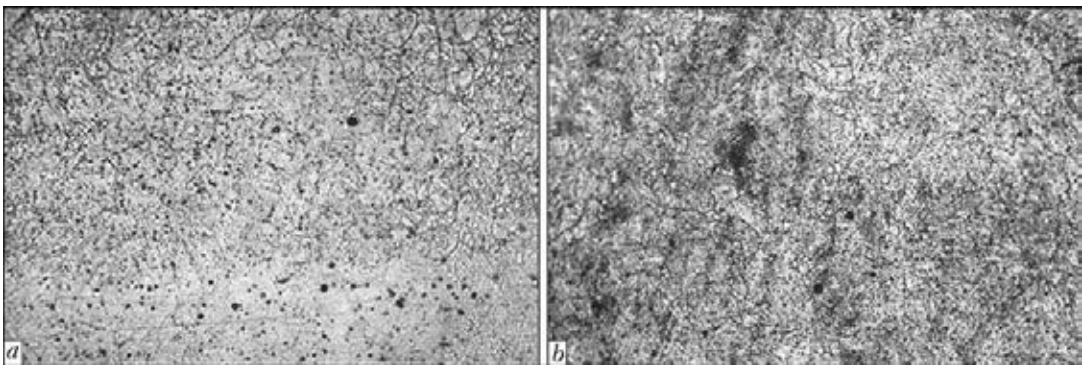

Figure 4. Microstructure (×320) of transition zone of 25Kh5FMS + 12 KhMF (*a*) and deposited sublayer of 12KhMF (*b*)

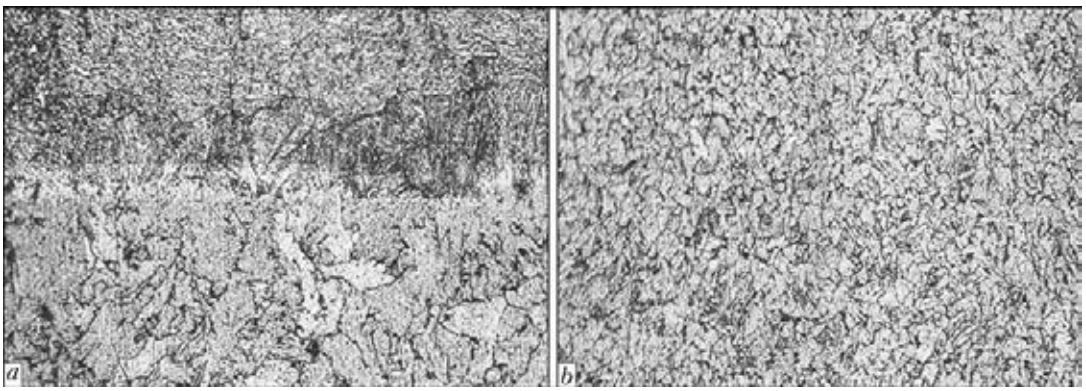

Figure 5. Microstructure (×320) of transition zone of 25Kh5FMS + Sv-08A (*a*) and deposited sublayer of Sv-08A (*b*)

metal to deposited wear-resistant layer 25Kh5FMS is observed. As was expected, in surfacing with sublayer Sv-08A an abrupt reduction in hardness directly in the sublayer was observed.

Using the X-ray spectral microanalyzer Camebax SX50 the distribution of basic alloying elements in all three samples was examined. The total length of scanning was 150 μm, pitch — 2 μm. Figure 7, *a* shows the distribution of chromium and molybdenum in surfacing by flux-cored wire PP-Np-25Kh5FMS directly on steel 40Kh (sample No.1). Distribution of the same elements in the fusion zone of wear-resistant layer and sublayer in samples Nos. 2 and 3 is given in Figure 7, *b* and *c*, respectively.

Analysis of data, given in Figure 7, shows that the narrowest transition zone (29.2 μm) is observed in surfacing by flux-cored wire PP-Np-25Kh5FMS directly on steel 40Kh. The transition zone between the sublayer and wear-resistant layer is wider. It is about 51 μm with sublayer, deposited by wire Sv-08A and about 58 μm with sublayer, deposited by flux-cored wire PP-Np-12KhMF (Table 2).

X-ray diffraction microanalyses of all the deposited samples were carried out that allowed determining their phase composition in a quantitative ratio and comparing it with calculated data (see Figures 1 and 2). Table 2 gives generalized data about microstructural state of deposited samples and data about stressed state of wear-resistant layer, determined from the results of X-ray diffraction analysis.

If to compare the calculated data (Figures 1 and 2) with data of X-ray diffraction microanalysis (Table 2), then, first of all, the presence of

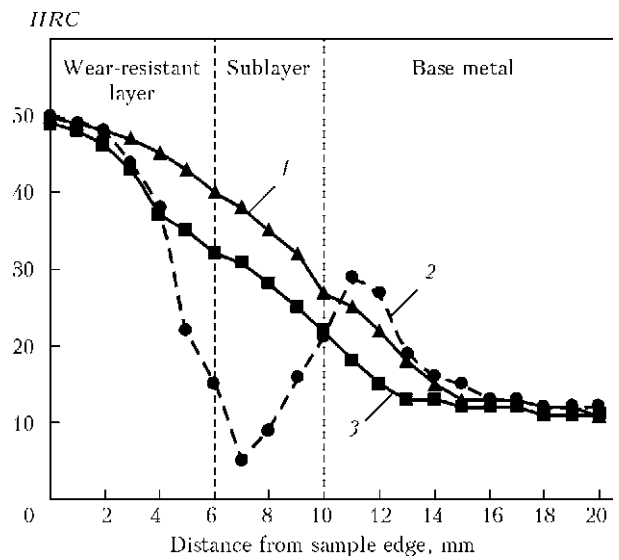

Figure 6. Hardness of deposited metal and transition zone in investigated samples: *1* — sample without sublayer; *2* — with sublayer of Sv-08A; *3* — with sublayer of 12KhMF

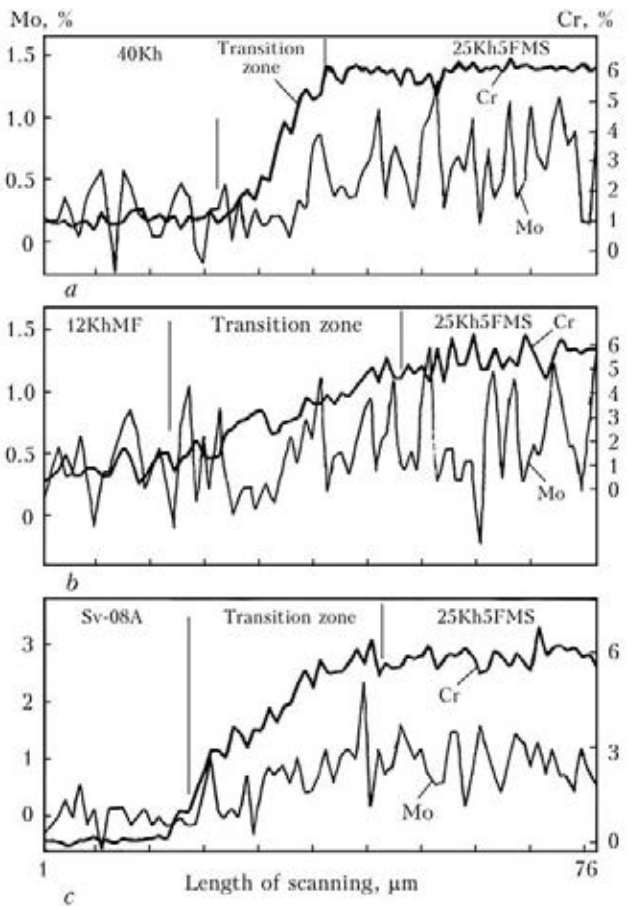

Figure 7. Distribution of chromium and molybdenum in fusion zone of sample Nos. 1 (*a*), 2 (*b*), 3 (*c*)

Table 2. Microstructural state of deposited samples

Sample number	Microstructure	Length of transition zone on side of deposited metal 25Kh5FMS, μm	Phase composition of steel 40Kh, %	Phase composition of deposited metal 25Kh5FMS, %	Stresses in wear-resistant layer of 25Kh5FMS, GPa
1	Wear-resistant layer is bainite-martensite mixture and residual austenite; base metal is pearlite-ferrite mixture	≈29.2	85 — pearlite; 15 — ferrite	92.3 — α; 7.7 — γ	−0.2
2	Wear-resistant layer is bainite-martensite mixture and residual austenite; sublayer is sorbite-like pearlite; base metal is pearlite-ferrite mixture	≈58.0	87.2 — pearlite; 12.8 — ferrite	90.57 — α; 9.43 — γ	−0.062
3	Wear-resistant layer is bainite-martensite mixture and residual austenite; sublayer is ferrite; base metal is pearlite-ferrite mixture	≈51.0	83 — pearlite; 17 — ferrite	90.32 — α; 9.68 — γ	−0.15

austenite in the amount up to 10 % in the deposited layer 25Kh5FMS should be noted. This fact should be taken into account in precise calculations of stress-strain state of samples and appropriate deposited parts. The base metal, steel 40Kh, has a ferritic-pearlitic structure, the sublayer, deposited by wire Sv-08A, has a ferritic structure, and structure of sublayer, deposited by wire PP-Np-12KhMF, is sorbite-like pearlite. Identification of structure and, in particular, the determination of quantitative ratio of its separate constituents in transition zones encounters significant difficulties, moreover, all they in this case refer, in principle, to α-Fe.

The determination of stresses in wear-resistant deposited layer of samples was performed on the basis of results of X-ray diffraction analysis by the procedure, described in work [8]. The highest stresses are observed in wear-resistant deposited layer in sample, deposited without a sublayer. They are somewhat lower in the sample, deposited with a sublayer Sv-08A. Minimum stresses were in sample No.2, in which the sublayer was deposited by flux-cored wire PP-Np-12KhMF. Qualitatively, these data coincide with calculated data given in work [9].

Conclusions

1. It was found that depending on chemical composition and structure of deposited layer the residual stressed state of deposited wear-resistant layer is changed to a great extent. In particular, the surfacing of sublayer by flux-cored wire PP-Np-12KhMF approximately 3 times decreases the residual stresses in working wear-resistant layer as compared with surfacing without sublayer and approximately 2 times — as compared with surfacing with sublayer Sv-08A.

2. It is shown that unlike the calculated data, the structure of deposited metal 25Kh5FMS of experimental samples contains up to 10 % of residual austenite. This fact should be taken into account in calculations of stress-strain state and possible service life of multilayer deposited parts.

1. (1961) *Automatic electric arc surfacing*. Kharkov: Metallurgizdat.
2. Ryabtsev, I.A., Kondratiev, I.A. (1999) *Mechanized electric arc surfacing of metallurgical equipment parts*. Kiev: Ekotekhnologiya.
3. Ryabtsev, I.A. (2004) *Surfacing of parts of machines and mechanisms*. Kiev: Ekotekhnologiya.
4. Senchenkov, I.K., Ryabtsev, I.A., Chervinko, O.P. et al. (2011) Calculation method for evaluation of deposited metal resistance under simultaneous action of cyclic mechanical and thermal loads. *Tekhnologicheskie Sistemy*, **4**, 89–96.
5. Popov, A.A., Popova, L.E. (1961) *Handbook of heat-treater. Isothermal and thermokinetic diagrams of supercooled austenite decomposition*. Moscow-Sverdlovsk: GNTI Mashinostr. Lit-ra.
6. Makhnenko, V.I. (1976) *Calculation methods of study of welding stress and strain kinetics*. Kiev: Naukova Dumka.
7. Makhnenko, V.I. (2006) *Safety service resource of welded joints and assemblies of current structures*. Kiev: Naukova Dumka.
8. Umansky, Ya.S., Skakov, Yu.A., Ivanov, A.N. et al. (1982) *Crystallography, radiography and electron microscopy*. Moscow: Metallurgiya.
9. Senchenkov, I.K., Ryabtsev, I.A., Chervinko, O.P. (2010) Calculation of residual stresses in multilayer surfacing of worn dies and assessment of their effect on fatigue strength. *Problemy Tertya ta Znoshuvannya*, Issue 54, 67–72.

Received 19.06.2013

EFFECT OF RESIDUAL STRESSES ON JOURNAL FIXING IN GRINDING MILL BODY DURING SURFACING

V.A. KOROTKOV
Nizhni Tagil Technological Institute (branch), Ural Federal University (UrFU)
59, Krasnogvardejskaya Str., Nizhni Tagil. E-mail: vk@udgz.ru

External surfaces of journals of the raw processing mills are subjected to intensive wear due to friction in bearing parts. The wear reduces journal thickness. This can result in formation of longitudinal cracks in combination with residual tensile stresses from external repair surfacing. Recovery of journal strength by their surfacing on internal surface is proposed. Therefore effect of journal fixing is achieved, at that, lying in that the negative residual stresses reduce the operating stresses and allow the hollow cylinders to bear higher loads. Design analysis and experimental check of stressed state, forming in surfacing of the mill journal on internal surface, showed that the residual compression stresses are formed on the journal external surface. They are significant on value and develop autofixing effect increasing crack resistance of the journals from operating loads. 8 Ref., 3 Figures.

Keywords: *surfacing, residual stresses, mill journals*

End walls of mills (MSTs 3.6×4.5 etc.) represent themselves a disk with pressed-in it journal. The disk is worn out at operation in regions of abutment to mill body, as a result of pulp penetration under the seal, and journals on external surface due to friction in the bearings. Their repair surfacing was mastered by «Komposit» Ltd. at the end of 90^{th}. The disk was firstly deposited by «soft» steel in order not to have difficulties during mechanical processing and by hard alloy for wear resistance increase after grooving with removal of 3 mm layer «to size». The journals were deposited by semi-automatic welding machine (Figure 1) and grooved up to dimension on a drawing. More than 50 pcs of end walls were repaired for Kachkanarsky and Vysokogorsky ore mining and processing enterprises, Sredneuralsky and Krasnouralsky copper smelting plants at economy around 1 mln. of rubles on each item.

Repair significantly, by almost 2 times, prolonged the service life of the end walls during which increase of wear of internal surface of the journals contacting with charging spouts takes place. It achieved 20 mm on some journals. The wear reduces the journal thickness and, as a result, increases the operating stresses, which in combination with the residual tensile stresses in external surfacing promote formation of longitudinal cracks. Around 10 pcs. of journals, having cracks on the external surface, some of which transformed in through-the-thickness cracks, were discovered in a course of two last years. Thus, it is necessary to increase the strength of the repaired mill journals.

Surfacing of journals on the internal surface is an obvious measure for strength recovery. At that, surfacing proportional to wear (20 mm) is seemed to be impossible due to probable journal shrinkage and loss of strength of its fixing (press fit) in the end wall. Surfacing of thinner layer (around 5 mm), in order to avoid shrinkage, at first glance, does not seem to be justified since complete repair of journal cross-section and, respectively, complete strength recovery are not provided. But attitude to it can change, if possibility of concurrent autofixing of the journals by welding stresses is considered. The autofixing effect lies in that the opposite sign residual stresses, i.e. reducing operating stresses, allow the hollow cylinders to bear higher loads, applied to them [2, 3]. In conformity with the present case, resistance to longitudinal crack formation can be increased by residual circumferential compression stresses on the external surface of journals. Possibility of their inducing from surfacing on the internal surface was studied in the present work.

Analysis of residual stresses forming in surfacing of mill journals on the internal surface. Residual stresses in welding (surfacing) are formed as a result of heat shrinkage of heated metal, representing itself deposited metal and part of heat-affected zone (HAZ) in base metal, received plastic compression deformation in heating [4–6]. Scheme of formation of residual stresses in the journal with surfacing on internal surface is given on Figure 2. It can be seen from the Figure that internal part *1* drags external

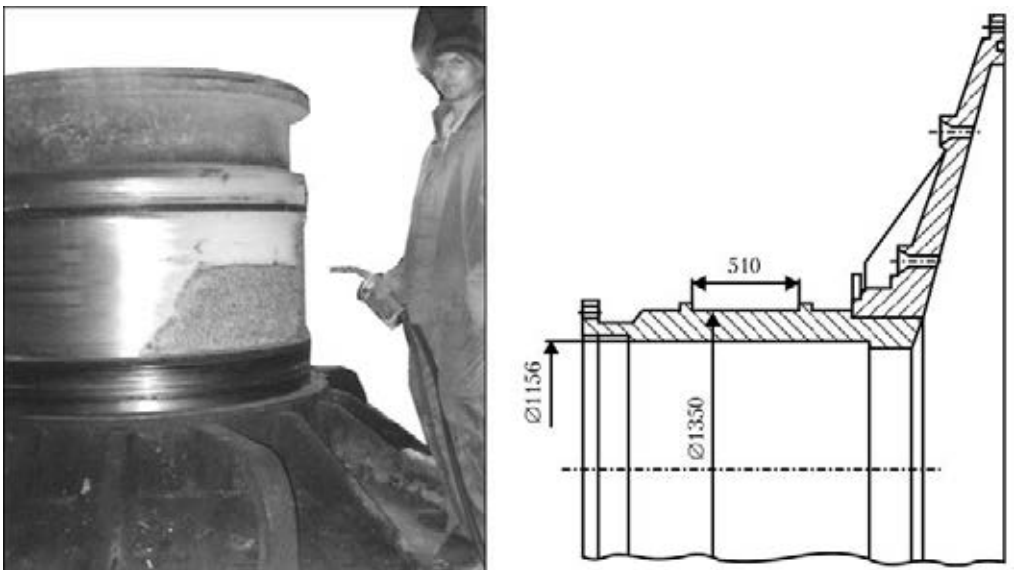

Figure 1. Surfacing of mill journal by semi-automatic welding machine and journal draft

part *2* as a result of heat shrinkage, creating in it the circumferential compression stresses G_t. Formula for the circumferential stresses in elastic region of arbitrary selected hollow cylinder ($a \le r \le b$) according to data of work [7], has the following view:

$$G_t(r) = \frac{G_r(b)b^2(r^2 + a^2) - G_r(a)a^2(b^2 + r^2)}{(b^2 - a^2)r^2}. \quad (1)$$

Let's write expression (1) for external surface ($r = b$) part *2* under the following conditions:

- external surface, being free, has no radial stresses ($G_r(b) = 0$);
- radial stresses $G_r(d) = p$ act on lower boundary of part *2* ($r = d$):

$$G_t(b) = - G_r(d) \frac{2d^2}{b^2 - d^2}, \quad (2)$$

where $G_t(b)$ are the circumferential stresses on external surface ($r = b$) of the journal; $G_r(d)$ are the radial stresses on radius ($r = d$).

Since the radial stresses in hollow cylinders are multiply smaller than the circumferential ones, then talking about autofixing effect of the internal surfacing makes sense only under $\frac{2d^2}{b^2 - d^2} \ge 1$ condition, meeting at

$$d \ge 0{,}6b. \quad (3)$$

It should be considered for estimation of $r = d$ radius that it is located inside HAZ in direction from surfacing. It is shown in works [4–6] that the boundary of plastic compression is located in the range of 100–600 °C isotherms depending on conditions of welding heating and rigidity of the part. In order to reduce the calculations, consideration of HAZ can be omitted and assumed that a force action on the external part of insert is made only by deposited metal. Finally, this approximation reduces the possibility that a calculated autofixing would not proved in reality. Then, value of radius d is found from the expression $d = a + h$, where a is a radius of the internal (worn) surface of insert before surfacing; $h = 4$ mm is a penetration depth at surfacing current 400 A (from calculation of 1 mm per each 100 A of welding current [8]).

Applicable to the journal (Figure 1) of $b = 675$ mm and $a = 578$ mm dimensions, the value of radius d, on which radial stresses are formed, promoting journal autofixing, makes: $d = (578 + 10) + 4 = 592$ mm, where 10 (mm) is a depth of journal wear on the internal surface.

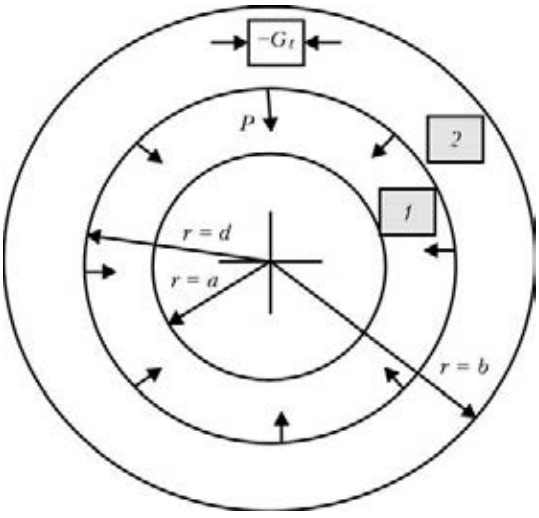

Figure 2. Scheme of formation of residual compression stresses in external part of the journal in surfacing of its internal surface: *1* — zone of deposited metal and high-temperature area of HAZ; *2* — zone of external part of the journal; *P* (arrows) — direction of force action of internal part *1* on external part *2* of the journal

Thus, condition (4) is fulfilled: 592 > > 0.6·675 = 405, that means the possibility of appearance of significant on value circumferential compression stresses on the external surface from single-layer internal surfacing. This, in turn, shows that the internal surfacing is accompanied by autofixing of the journals and can facilitate prevention of crack appearance on their external surface in operation.

Formula from work [9] was used for estimation of the heat radial stresses at $r = d$:

$$G_r(r) = \frac{\alpha E}{r^2}\left[\frac{r^2 - a^2}{b^2 - a^2}\int_a^b T(r)rdr - \int_a^r T(r)rdr\right]. \quad (4)$$

Calculations using it are made with the following assumptions:

- yield strength of the material is constant (G_y = const) at $T < 600$ °C;
- yield strength of the material is negligibly small ($G_y = 0$) at $T > 600$ °C;
- cooling of the deposited layer takes place due to heat exchange with ambient medium, i.e. part 2 on Figure 2 does not increase temperature that means:
- $T(a) = T(d-) = -600$ °C, where $T(d-)$ is a temperature on the boundary of surfacing from internal side;
- $T(d+) = T(b) = 0$ °C, where $T(d+)$ is a temperature on the boundary of surfacing from external side;
- minus mark means that thermal stresses appear at temperature reduction.

Taken assumptions are not original, the similar were used in works on welding stresses and deformations mentioned above. Considering them, expression (6) takes a form:

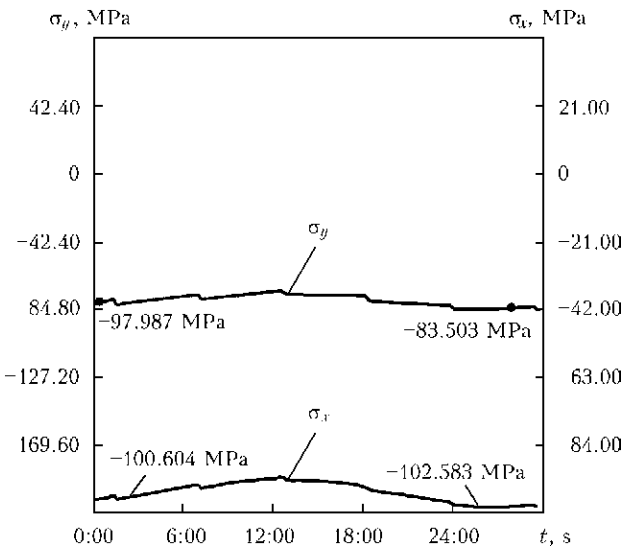

Figure 3. Oscillograms of residual stresses: σ_y in Y direction (axial); σ_x — in X direction (circumferential)

$$G_r(d) = -600\alpha E\left[\frac{(d^2 - a^2)(d^2 - a^2)}{2(b^2 - a^2)d^2} - \frac{d^2 - a^2}{2d^2}\right]. \quad (5)$$

A minuend in square brackets in formula (5) is significantly smaller than deduction that allows omitting it from consideration. Then, the radial stresses at $r = d$ are found from the expression

$$G_r(d) = 600\alpha E\,\frac{d^2 - a^2}{2d^2}, \quad (6)$$

where $\alpha = 14\cdot10^{-6}$ 1/°C is a coefficient of linear expansion; $E = 1.5\cdot10^5$ MPa is an elasticity modulus; values of a and d radiuses are given above.

Calculations on formula (6) show that the radial stresses on the boundary of plastic deformations, creating circumferential autofixing stresses on journal external surface during surfacing, equal $G_r(d) \approx 29$ MPa.

Inserting this value in expression (2), residual circumferential stresses on the journal external surface $G_t(b) \approx -168$ MPa are received.

Their comparability with the yield strength (270 MPa) of journal material (steel 35L) can be noted and a conclusion about significant autofixing effect accompanying surfacing of journals on internal surface can be made.

Experimental check of calculation. Single-layer surfacing on the internal surface of mill journal was carried out on a technology similar to the external surfacing by semi-automatic welding machine.

Calibrated working transducers were preliminary glued to the journal external surface in circumferential and axial directions (plates were welded for force-balance transducers). Resistive-strain sensors of FKPA 10-100 type having 10 mm length base and 91.6–92.0 Ohm resistance were used as transducers. Signal amplifiers, modules for transducer connection and KCKWin software from developer and manufacturer of measuring system CJSC «Teploenergeticheskie tekhnologii» were used.

Balancing of measuring signals from the transducers («0» setting) was carried out after assembly of strain-gauge circuit, but before surfacing of journal on the internal surface. The equipment was switched off before surfacing and switched on again after it performance and the values of stresses in circumferential and axial direction were registered. Figure 3 shows measurement results. It is seen that the residual stresses on external surface of the journal are compression ones. They are on the level of 90 MPa in circumferential direction and 80 MPa in longitudinal.

The experiment justified the calculation prediction of appearance of compression stresses on the journal external surface. The experimental values appeared to be two time lower than the calculation ones (similar accuracy is typical for calculations in welding), but at that, they make around 30 % of yield strength of the journal material (steel 35L; $\sigma_{0.2}$ = 270 MPa) and, therefore, can be considered as a significant factor, increasing crack resistance in operation. Thus, surfacing of internal surface of the journal can simultaneously repair its wear (from contact with the charging spout) and perform fixing role, increasing journal resistance to operating loads.

It should be noted in the conclusion that the calculation analysis and experimental check of the stressed state, forming in surfacing of the mill journal on internal surface, showed formation of the residual compression stresses, significant on value and creating autofixing effect, which increases the journal resistance effect to crack formation from operating loads.

1. Korotkov, V.A., Zamotin, V.A. (2001) Repair of mine equipment parts. *Gorny Zh.*, **8**, 53–56.
2. Smirnov-Alyaev, G.A. (1940) *Theory of autofastening of cylinders*. Moscow: Oborongiz.
3. (1971) Control of strength of press-fit connections in the presence of residual stresses. *Izv. Vuzov. Mashinostroenie*, **8**, 29–33.
4. Bakshi, O.A. (1953) Strains and stresses at local heating of steel sheet. *Avtogen. Delo*, **2**, 1–6.
5. Talypov, G.P. (1957) *Approximate theory of welding strains and stresses*. Izd-vo LGU.
6. Korotkov, V.A. (1996, 1997) Study of thermal deformations of sleeves at local heating. *Izv. Vuzov. Mashinostroenie*, **10–12**, 90–98; **1–3**, 96–103.
7. Ilyushin, A.A., Ogibalov, P.M. (1960) *Elastic-plastic strains of hollow cylinders*. Moscow: Izd-vo MGU.
8. (1975) *Handbook of welder*. Ed. by V.V. Stepanov. Moscow: Mashinostroenie.

Received 26.06.2013

MANUFACTURE OF RESISTANCE ELECTRICAL HEATER BY MICROPLASMA CLADDING PROCESS

Yu.S. BORISOV, S.G. VOJNAROVICH, A.N. KISLITSA, S.M. KALYUZHNY and **E.M. KUZMICH-YANCHUK**
E.O. Paton Electric Welding Institute, NASU
11 Bozhenko Str., 03680, Kiev, Ukraine. E-mail: office@paton.kiev.ua

Attempts to develop flat electrical heating elements with application of the technology thermal spraying of electrically insulating and resistive layers were made several times, in order to improve heating effectiveness and save electric power. This work is a study of the process of manufacturing flat electrical heaters by microplasma powder spraying. Al_2O_3 was selected as electrically insulating material in view of its high electric strength (3–5 kV/mm). TiO_2 powder of Metachin company was used to form resistive coatings. Analysis of the produced coating microstructure showed that they are uniform, dense and do not contain foreign inclusions. Investigations of model heating properties conducted in an experimental facility showed that maximum heating temperature was equal to 230 °C, and the achieved specific power of the heater was 75 W. 7 Ref., 1 Table, 3 Figures.

Keywords: *microplasma spraying, electrical heater, aluminium oxide, titanium oxide, heating tracks, heating temperature*

Manufacture of flat electrical heating elements (FEH) by thermal spraying involves several technological difficulties, including substrate distortion, significant losses of spraying material, unstable resistance value, insufficient heat resistance and mechanical strength of the coating, leading furtheron to overheating and destruction of the resistive layer in service [1].

E.O. Paton Electric Welding Institute (Department 73) conducted research on manufacture of FEH heaters by microplasma spraying. This method allows application of a sound coating of various kinds, both from metal and ceramic materials on small-sized parts with minimum losses of spraying material [2–4]. Al_2O_3 aluminium oxide powder (MRTU 6-09-3916–75) with –40 μm particle size was selected as electrically-insulating material owing to its high dielectric strength (3–5 kV/mm) [5]. TiO_2 of Metachin (15–40 μm particle size) was used to form resistive coatings. This material was selected proceeding from the fact that titanium oxide has semi-conductor properties with specific electrical resistance of $(0.42–0.55)\cdot10^{-6}$ Ohm·m and thermal expansion coefficient of $8.6\cdot10^{6}$ °C^{-1} that allows this material to be used for coatings in the form of heating paths, produced by thermal spraying [6]. MPN-004 system, the general view of which is shown in Figure 1, was used for coating application.

Unit specification is as follows:

Working gas	argon
Shielding gas	argon
Power, kW	up to 2.5
Current, A	10–60
Voltage, V	20–40
Working gas flow rate, l/min	0.5–5
Shielding gas flow rate, l/min	1–10

Figure 1. General view of MPN-004 system

Modes of microplasma coating deposition

Parameters	Al_2O_3	TiO_2
Current, A	45	40
Voltage, V	30	28
Spraying distance, mm	150	150
Working gas flow rate Ar, l/min	1.3	1.3
Shielding gas flow rate Ar, l/min	4	4
Coating thickness, μm	300	100
Efficiency, g/min	1.2	2

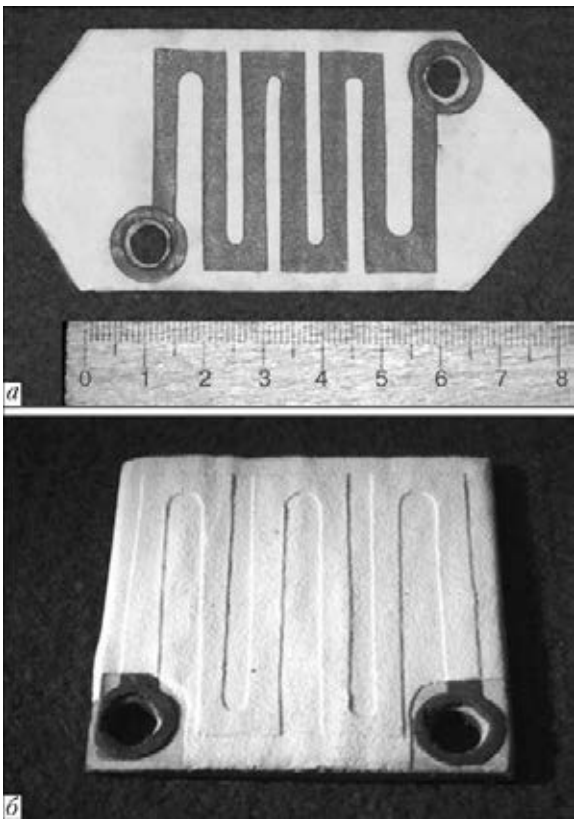

Figure 2. Models of electrical heating elements with two- (*a*) and three-layer (*b*) coatings

Efficiency, kg/h	0.1–2.5
Coefficient of material utilization, %	0.6–0.9
Overall dimensions, mm	500 × 360 × 650
Weight, kg	38.2

Coatings were applied on samples from St3 steel of 70 × 45 × 1 mm (No.1) and 50 × 50 × 2 mm (No.2) dimensions. Modes of deposition of coatings from Al_2O_3 and TiO_2 are given in the Table.

Produced models of heating elements were zigzag paths of 312 and 294 mm length for samples Nos.1 and 2, respectively, of 4 mm width with electrical heating layer thickness (TiO_2) of 100 μm. Figure 2 gives the general view of samples of electrical heating elements. Analysis of coating microstructures showed that the produced coatings are uniform, dense and do not contain any foreign inclusions (Figure 3).

Investigations of model heating properties conducted in the experimental facility showed that TiO_2 path was heated under the impact of 0.3 A current and applied voltage of 250 V. Maximum heating temperature was 230 °C, and specific power of the heater was 75 W. Further increase of temperature leads to loss of the path electrical conductivity, and interruption of the heating process for the reason of polymorphous transformation of TiO_2 from anatase structure into rutile [7]. At heating up to 230 °C no coating delamination was found, path electrical conductivity was preserved. Thus, the possibility of manufacturing FEH operating up to the temperature of 200 °C by microplasma spraying with application of TiO_2 as resistive material, was demonstrated.

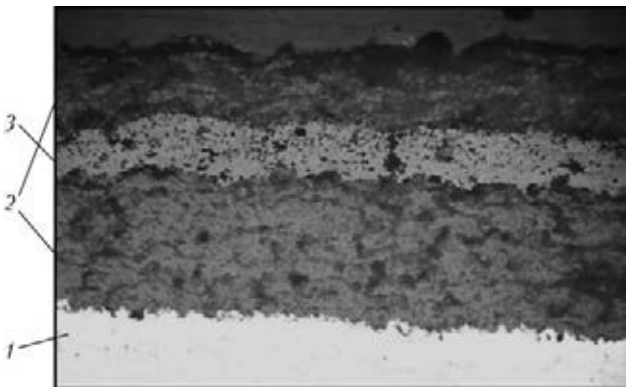

Figure 3. Microstructure (×100) of three-layer coating of a heating element: *1* — base metal; *2* — Al_2O_3 layer; *3* — TiO_2 layer

1. Baranovsky, N.D., Savitsky, V.E., Sapozhnikov, Yu.L. (1989) *Increase in reliability of thermal apparatuses using surface electric heater based on organic-silicate materials*. Leningrad: Znanie.
2. Borisov, Yu., Borisova, A., Pereverzev, Yu. et al. (1997) Microplasma spraying. In: *Proc. of 5th Europ. Conf. on Advanced Material and Processes* (Netherlands, 1997).
3. Borisov, Yu.S., Pereverzev, Yu.N., Bobrik, V.G. et al. (1999) Deposition of narrow band coatings by microplasma spraying. *Avtomatich. Svarka*, **6**, 53–55.
4. Kislitsa, A.N., Kuzmich-Yanchuk, E.K., Kislitsa N.Yu. (2009) Producing of narrow strips by microplasma spraying with Ni–Cr wire. In: *Abstr. of Papers of Sci.-Techn. Conf. of Young Scientists and Specialists on Welding and Related Technologies* (Kiev, 27–29 May, 2009). Kiev, 2009.
5. Vashkevich, F.F., Spalnik, A.Ya., Pluzhko, I.A. (2009) Electrothermic isolation of inductors for interior heating of tubular billets. In: *Construction, materials science, machine building*. Dnepropetrovsk: PGASA.
6. Scheitz, S., Toma, F.-L., Berger, L.-M. et al. (2011) Thermally sprayed multilayer ceramic heating elements. *Thermal Spray Bul.*, **2**, 88–92.
7. Mitrev, P., Benvenuti, J., Hofman, P. (2005) Phase transitions in titanium oxide thin films under action of excimer laser radiation. *http://*journals.ioffe.ru/pjtf /2005/21/p17-23.pdf

Received 12.07.2013

PATON PUBLISHING HOUSE

www.patonpublishinghouse.com

SUBSCRIPTION

«The Paton Welding Journal» is Published Monthly Since 2000 in English, ISSN 0957-798X.

«Avtomaticheskaya Svarka» Journal (Automatic Welding) is Published Monthly Since 1948 in Russian, ISSN 005-111X.

«The Paton Welding Journal» is Cover-to-Cover Translation of Avtomaticheskaya Svarka» Journal into English.

If You are interested in making subscription directly via Editorial Board, fill, please, the coupon and send application by Fax or E-mail.

The cost of annual subscription via Editorial Board is $348 for «The Paton Welding Journal» and $180 for «Avtomaticheskaya Svarka» Journal.

«The Paton Welding Journal» can be also subscribed worldwide from catalogues subscription agency EBSO.

SUBSCRIPTION COUPON

Address for journal delivery _____

Term of subscription since _____ **20** **till** _____ **20**

Name, initials _____

Affiliation _____

Position _____

Tel., Fax, E-mail _____

Subscription to the electronic version of «The Paton Welding Journal» and «Avtomaticheskaya Svarka» can be done at site: URL: www: rucont.ru

We offer the subscription all issues of the Journal in pdf format, starting from 2009. You can subscribe to individual issues or to the entire archive including all issues over a period of 2011–2013. The archives for 2009–2010 are free of charge on www.patonpublishinghouse.com site.

ADVERTISEMENT

in «Avtomaticheskaya Svarka» and «The Paton Welding Journal»

External cover, fully-colored:
First page of cover (190×190 mm) — $700
Second page of cover (200×290 mm) — $550
Third page of cover (200×290 mm) — $500
Fourth page of cover (200×290 mm) — $600

Internal cover, fully-colored:
First/second/third/fourth page of cover (200×290 mm) — $400

Internal insert:
Fully-colored (200×290 mm) — $340
Fully-colored (double page A3) (400×290 mm) — $500

- Article in the form of advertising is 50 % of the cost of advertising area
- When the sum of advertising contracts exceeds $1001, a flexible system of discounts is envisaged

Size of journal after cutting is 200×290 mm

Editorial Board of Journal «Avtomaticheskaya Svarka» and «The Paton Welding Journal»
E.O. Paton Electric Welding Institute of the NAS of Ukraine
International Association «Welding»
11, Bozhenko Str., 03680, Kyiv, Ukraine
Tel.: (38044) 200 60 16, 200 82 77; Fax: (38044) 200 82 77, 200 81 45
E-mail: journal@paton.kiev.ua; www.patonpublishinghouse.com